AEROSOL CONDENSATIONAL GROWTH IN CLOUD FORMATION

A Dissertation

by

JUN GENG

Submitted to the Office of Graduate Studies of
Texas A&M University
in partial fulfillment of the requirements for the degree of

DOCTOR OF PHILOSOPHY

August 2010

Major Subject: Nuclear Engineering

Aerosol Condensational Growth in Cloud Formation

AEROSOL CONDENSATIONAL GROWTH IN CLOUD FORMATION

A Dissertation

by

JUN GENG

Submitted to the Office of Graduate Studies of
Texas A&M University
in partial fulfillment of the requirements for the degree of

DOCTOR OF PHILOSOPHY

Approved by:

Chair of Committee,	William H. Marlow
Committee Members,	Yassin Hassan
	Sarah Brooks
	Zhengdong Cheng
Head of Department,	Raymond Juzaitis

August 2010

Major Subject: Nuclear Engineering

ABSTRACT

Aerosol Condensational Growth in Cloud Formation. (August 2010)
Jun Geng, B.S., Huazhong University of Science and Technology;
M.S., Huazhong University of Science and Technology;
M.S., Texas A&M University
Chair of Advisory Committee: Dr. William H. Marlow

A code for the quasi-stationary solution of the coupled heat and mass transport equations for aerosols in a finite volume was developed. Both mass and heat are conserved effectively in the volume, which results in a competitive aerosol condensation growth computational model.

A further model that couples this competitive aerosol condensation growth computational model with computational fluid dynamics (CFD) software (ANSYS FLUENT) enables the simulation of the realistic atmospheric environment. One or more air parcels, where the aerosols reside, are placed in a very big volume in order to mimic the large atmospheric environment. Mass (water vapor) and heat transportat between the air parcels and the environment facilitates the growth and prevents the parcels from unrealistically overheating.

The suppression of cloud condensation nuclei (CCN) growth by high number densities was quantified by our model study. Model study with organic particles (L-malic acid and maleic acid) indicates that when these organic species and ammonium sulfate are internally mixed, the particles can grow much more than if they are separately associated with distinct particles. Moreover, by using more multiple air parcels, which are randomly assigned with different initial relative humidity values according to a power law distribution, we studied the effects of atmospheric stochastic RH distribution on the growth of CCN.

To my parents

ACKNOWLEDGEMENTS

I would like to thank my committee chair, Dr. Marlow, for his guidance and support all through these two years. His insights on the subject and many stimulating discussions have been a source of inspiration and encouragement for me. Without his patience and help, this work could not have been done.

I also thank my committee members, Dr. Brooks, Dr. Hassan and Dr. Cheng, for their guidance and support throughout the course of this research.

I thank the department for the financial support in the form of a graduate assistantship.

Thanks also go to department faculty and staff for making my time at Texas A&M University a great experience.

Thanks to my coworker and friend, Dr. Chu Nie, for his contributions and suggestions, which always helped.

Finally, thanks to my mother and father for everything they have given to me.

TABLE OF CONTENTS

CHAPTER Page

LIST OF FIGURES

FIGURE Page

FIGURE Page

FIGURE Page

FIGURE Page

FIGURE Page

FIGURE Page

LIST OF TABLES

TABLE Page

CHAPTER I

INTRODUCTION

1. Atmospheric aerosol particles

Aerosol refers to a suspension of solid or liquid particles in a gas. Aerosol particles, also called particulates, particulate matter (PM) or fine particles, are the suspended particles. The sizes of aerosol particles can range from nanometers to hundreds of micrometers in diameter. They can be divided as PM10 which is used to describe particles with diameters of 10 micrometers or less and PM2.5 representing particles less than 2.5 micrometers in aerodynamic diameter; other numeric values may also be used depending upon specific need. The classification of free-molecule regime, transition regime and continuum regime based upon particle Knudsen number is also often used. For standard atmospheric conditions, the free-molecule regime denotes small particles with aerodynamic diameters of several nanometers while the continuum regime is for the relatively large particles whose aerodynamic diameters are in the range of micrometers (0.1's micrometers and larger).

Atmospheric aerosol particles come from both natural and human sources. The ocean is a large source of particles. In ocean regions where wind speeds are high and/or other aerosol sources are weak, sea salt may be the dominant contributor to CNN (O'Dowd and Smith 1993; Murphy et al. 1998; Quinn et al. 1998; Gong et al. 2002; Shinozuka et al. 2004). Combustion sources contribute most to the anthropogenic part, namely the burning of fossil fuel in internal and external combustion engines in automobiles and power plants, and the dust blown from construction and agricultural sites and other land areas where the water or vegetation has been removed. Some of these particles are emitted directly to the atmosphere (primary emissions) and some are

---

This dissertation follows the style of *Journal of Atmospheric and Ocean Science.*

emitted as gases and form particles in the atmosphere (secondary emissions).

The compositions of aerosol particles depend on their sources. Wind-blown mineral dust mainly consists of mineral oxides and other material from the earth's crust; this aerosol is light absorbing. Sea salt (Lave and Seskin 1973) is considered the second largest component of the global aerosol budget, and consists mainly of sodium chloride originating from sea spray; other constituents of atmospheric sea salt reflect the composition of sea water, and thus include magnesium, sulfate, calcium, potassium, etc. In addition, sea spray aerosols may contain organic compounds, which influence the chemistry of those aerosols.

Secondary particles derive from the oxidation of primary gases such as sulfur and nitrogen oxides into sulfuric acid (liquid) and nitric acid (gaseous). The precursors for these aerosols, i.e., the gases from which they originate, may have anthropogenic origins (from fossil fuel combustion) and natural biogenic origins. In the presence of ammonia, secondary aerosols often form ammonium salts, i.e., ammonium sulfate and ammonium nitrate, both of which could be dry or in aqueous solution; in the absence of ammonia, secondary compounds take an acidic form as sulfuric acid (liquid aerosol droplets) and nitric acid (atmospheric gas). Secondary sulfate and nitrate aerosol are strong light scatters (Paredes-Miranda, G. et al. 2009) because the presence of sulfate and nitrate causes the aerosols to grow by water absorption, or condensation, to a size that can scatter light effectively.

Organic matter (OM) can be either primary or secondary, with the latter part derived from the oxidation of volatile organic compounds (VOCs). Organic material in the atmosphere may either be biogenic or anthropogenic. Organic matter influences the atmospheric radiation field by both scattering and absorption. Organic matter usually can be divided as water-soluble organic carbon (WSOC) and water-insoluble organic carbon (WISOC). Another important aerosol type is constituted of elemental carbon (EC, also known as black carbon, BC). This aerosol type contains strongly light absorbing materials and is thought to yield large positive radiative forcing. Organic matter and elemental carbon together constitute the carbonaceous fraction of aerosols (Mokdad

2004). Organic compounds comprise typically 10%-50% and EC 5%-20% of fine particle mass (Park et al. 2005). EC is produced only in the combustion process and is therefore always associated with primary particles. OM can be either primary or secondary particles. Typically, a significant part, 10%-70% of the OM in the atmospheric aerosols is WSOC (Jaffrezo et al. 2005).

The chemical composition of the aerosol directly affects how it interacts with solar radiation and is not the focus here, though its effects on cloud nucleation will be treated.

Air pollution aerosols refer to ambient aerosols arising from both natural processes and human activity. They have been receiving more attention by countries all over the world since they are closely related to the human health and the environment.

2. Aerosols and precipitation

The formation of precipitation involves several complex processes. In meteorology, precipitation is any product of the condensation of atmospheric water vapor deposited on the earth's surface. When the partial pressure of water in the atmosphere rises, it selectively deposits on the condensation nuclei (CN), which are very small particles. This process is called condensation nucleation. Since ice nucleation is not our consideration now, here we limit this discussion to only wet condesation. CN capable of condensational growth to 5μm to 10μm size range under the low supersaturation condition of the atmosphere are called cloud condensation nuclei (CCN). When these small particles grow bigger, the process of coagulation dominates. Aerosol particles suspended in a fluid may come into contact and merge because of their Brownian motion or as a result of their motion produced by hydrodynamic, electrical, gravitational or other forces; this process is called coagulation (J. H. Seinfeld and S. N. Pandis, 2006). There are several kinds of coagulation for the atmospheric aerosol: Brownian coagulation which is caused by the Brownian diffusion of particles; coagulation in laminar shear flow which is induced when the velocity gradients in the air cause relative motion; coagulation in turbulent flow which is a very complicated process

and is not well understood yet; and gravitational coagulation, which is caused by the differential gravitational motion of the particles. These are the routes through which cloud droplets form. When those cloud droplets grow big enough, they start to precipitate. It is how precipitation, like rainfall, snow and so on, comes.

The first step for the generation of precipitation is that water vapor condenses on the cloud condensation nuclei. So, it is not hard to see that aerosol properties, such as concentration, size distribution and composition, are very important for the formation of precipitation. Many different types of atmospheric particles can serve as CCN. The particles may be composed of dust, clay, soot and black carbon, which come from grassland or forest fires. Sea salt from ocean wave spray, soot from factory smokestacks and internal combustion engines may also contribute to form these particles. Moreover, sulfate from volcanic activity and phytoplankton or the oxidation of sulfur dioxide and secondary organic matter formed by the oxidation of volatile organic compounds also provide raw material for the formation of these particles. The ability of these different types of particles to form cloud droplets vary according to their size and their exact composition since the hygroscopic properties of their different constituents vary. Sulfate and sea salt, for instance, readily absorb water while soot, WISOC and mineral particles do not. This situation is further complicated by the fact that many chemical species may be mixed within the particles (particularly the sulfate and organic carbon). Additionally, while some particles (such as soot and minerals) do not make very good CCN, they are very good ice nuclei in colder parts of the atmosphere.

3. Effects of high number density pollutant aerosols on precipitation

It is impossible for us to look into the effects of all of these properties on precipitation. Our focus here is on how the concentration and chemical composition of air pollution aerosols affect the condensational growth of CN to become cloud particles and hence affect the amount of tropical precipitation. As mentioned above, many pollution aerosols, especially the small ones that are present in the atmosphere, can serve as condensation nuclei. Let us assume that there is a very clean place with no particles

in the sky. It is obvious that the water vapor has nowhere to condense because there are no CCN available. That place would not have precipitation unless clouds from somewhere else migrated here somehow. Again, if there is a highly polluted place and the concentration of aerosols in the sky is high, it is fairly reasonable to conclude that there would hardly have any precipitation. Why? Twomey (1974) suggested that increasing aerosols leads to an increase of CCNs; more CCNs will increase the number concentration of cloud droplets. The increase in cloud droplets leads to an increase in particles' competition for the water vapor in the cloud. But the amount of water vapor will not increase with the concentration of particles; in other words, the amount of water is limited. There will not be enough water vapor for these small particles to grow big enough, as cloud nuclei, to participate in the subsequent coagulation processes that generate precipitation. Actually they could hardly grow big enough to start the process of coagulation in a limited period of time. In such a place, you can see gray sky, but it seldom rains; and no washing out either. This is the reason why we suspect that high concentration air pollution particles can suppress rainfall.

Many previous field (Rosenfeld 1999; Rosenfeld, Rudich and Lahav 2001; Givati and Rosenfeld 2004; Jirak and Cotton 2005) studies have mentioned this phenomenon. From the satellite visualization of NOAA (National Oceanic and Atmospheric Administration) AVHRR (Advanced Very High Resolution Radiometer) images, Rosenfeld (2000) found that there were many more small drops in the clouds above the polluted areas compared to the clouds above clean areas. The AVHRRA is a space-borne sensor deployed on the NOAA family of polar orbiting platforms. AVHRR instruments measure the reflectance of the Earth in 5 relatively wide spectral bands. The analysis of the observed data from the Tropical Rainfall Measuring Mission (TRMM) showed clearly that the cloud particle effective radii are much smaller in the polluted area at the same temperature and the precipitation echos are less intense (Rosenfeld 2000) when compared to their values in clean areas. Givati and Rosenfeld (2004) suspected that ideally the effect of precipitation suppression would be most pronounced downwind of coastal cities with hills inland that receive precipitation mainly during the winter in

maritime onshore flow from shallow convective clouds. This is because these regions are dominated by relatively short-lived clouds that are more sensitive to the slowing of the conversion of cloud water to precipitation. However, long-lived clouds would eventually convert their water into precipitation regardless of the conversion rate. So, the main effect would be the suppression of the orographic components of the precipitation, which would be manifested as a reduction in the orographic enhancement factor Ro. Orographic precipitation, also known as relief precipitation, is precipitation generated by a forced upward movement of air upon encountering a physiographic upland. The orographic enhancement factor Ro is defined as the ratio of the precipitation amounts at hills and at the upwind lowland. Their underlying assumption is that small-particle air-pollution emissions have increased with the growth of urban areas, resulting in a decrease in Ro with time. So they studied several such cases both in California, USA and Israel. They found a significant reduction of Ro in the polluted area. Furthermore they noticed that this kind of effect was more obvious when the temperature was relatively low (Givati and Rosenfeld, 2004). Following this paper, Jirak and Cotton (2005) investigated the effect of air pollution on the precipitation at elevated sites downwind of urban areas along the Front Range of Colorado. They found that when only upslope precipitation was considered, the evidence of precipitation suppression is strongest. This is because that upslope winds carry the pollution up to the terrain and thus affects the formation of clouds and precipitation (Jirak and Cotton, 2005).

4. Numerical studies of aerosol droplet condensational growth

Numerous investigators have examined the theoretical description of the droplet growth process, the earliest description having been the analysis of the stationary growth of a single droplet in an infinite and uniform medium by Maxwell (1877). The steady state theory of droplet growth has been improved by accounting for the effect of latent heat of condensation (Fuchs 1959) and the effect of curvature and solution concentration (Mason 1971) on the droplet growth rate. A review of theory and experiments relating

to single particle growth by Wagner (1982) surveyed the approximations made to the full-coupled nonstationary mass and heat transfer equations in obtaining the droplet growth equations. Wagner's quasistationary description of single droplet growth was based on the full first order phenomenological equations of mass and heat transport. The first order effects, the mutual interactions of mass and heat flux in the vicinity of the droplets, were in the form of diffusion and thermal corrections to the zeroth order Maxwellian fluxes. Analytical solutions for growth rates in the continuum have also estimated the effect of radiation heat transfer on the droplet growth (Barrett and Clement 1988). Kulmala and Vesala (1991) not only investigated the effect of Stephan flow and thermal diffusion on the mass flux but also included the temperature dependence of the transport coefficients. The effect of composition and temperature dependence of the transport coefficient on the mass and heat fluxes have been analyzed by Heidenreich (1994) while neglecting radiative heat transfer and the effect of droplet curvature.

The common approach in droplet growth analysis is to assume that the growth process can be approximated to be quasistatic. As a result, the mass and heat flux correspond to the steady state vapor concentration and temperature profiles. Also the boundary conditions are assumed to be constant at the droplet surface and at large distances from the droplet surface. The constant interfacial conditions of droplet surface temperature and vapor pressure assumes that the temperature difference between the droplet and the ambient medium is negligible. Such an assumption overpredicts the growth rates for large supersaturations and heats of vaporization, which are encountered in many practical cases like in a condensation nucleus counter. While steady state approximations have been appropriate for a range of calculations involving small supersaturations and growth rates, they fail to describe the competitive condensation kinetics of volatile aerosols involving high supersaturations and large heats of vaporization, or when the temperature differences between the droplet surfaces and the surrounding medium are not negligible.

Kulmala et al. (1989), also show a comparison between the various static and quasistatic analytical and numerical results for a single particle growth of water, n-

butanol and methanol. In this paper, Kulmala et al. (1989) found that for a comparatively low vapor pressure liquid (n-butanol), all the models considered yield nearly identical results; For an intermediate vapor pressure liquid (water), agreement was obtained only for low supersaturations. In the case of the condensation of methanol, a high vapor pressure volatile liquid, the nonisothermal, steady state models showed significant discrepancies in the predicted growth rates even at low supersaturation. When the latent heat of vaporization is large, as in the case of water and methanol, the accepted quasistatic solutions over-predict the mass flux and therefore the droplet growth rates. A linear quasistatic theory of droplet growth shows good agreement with experimental results reported only for nonvolatile organic compounds and low supersaturations.

5. Numerical studies of interactions of aerosols and clouds

As early as the 1950s, Howell (1949) and Mordy (1959) started to study numerically the effects of aerosols on clouds. In their work, the growth of a population of aerosol particles in a rising parcel of air was considered. From then until now, there have been a number of models developed to address the interactions of aerosols and cloud.

Beginning with the early roots of cloud parcel models that simulated droplet growth by condensation, there have been two parallel and complementary foci (Levin Z. and W. R. Cotton, 2009). One of them addresses mainly the cloud physics problems and they have expanded the original parcel models to one-dimension, two-dimension and three-dimension models. The other focuses address the cloud chemistry problem and they mainly study the effects of aerosol composition on cloud characteristics.

Cloud microphysics is a major part of cloud modeling that has gained increasing attention in recent years. Cloud microphysics deals with the dynamic and kinetic process cloud aerosols are involved in, such as nucleation, condensation, coagulation, transportation, etc. Depending on the way the aerosol distribution is treated, there are two major branches of cloud microphysics models. One is called bulk microphysics and the other one is size-resolved microphysics (Z. Levin and W. R. Cotton, 2009).

Models using moment methods represent size distributions of hydrometeors by one or more of its moments (e.g. number concentration, surface area and etc.). This kind of model has the advantages of high efficiency and can easily trace the broad features of the particle distribution. But usually, the size distribution needs to be prescribed as a basic function, such as lognormal and Gaussian. Also, since the particles are treated as a "bulk", more detailed information for the particles cannot be obtained. There are many examples of such models, e.g. Clark 1976, Nickerson et al. 1986, Feingold et al. 1998, 2002, McGraw 1997, Seifert and Beheng 2006 a, b.

The other branch is called size-resolved or explicit bin microphysical methods. Instead of looking at the bulk information of particle size distribution, models in this branch treat the particle sized distribution in more detail. The first of such models is the Lagrangian method. These models represent particles at discrete sizes and allow each particle to grow by condensation on a moving mass grid. Such an approach enables detailed presentation of aerosol sizes and compositions to be included (eg. Facchini et al. 1999; Kulmala, M. 1993). However, it also has the disadvantages that it is not easy to adept for some process such as coagulation and not suitable for Eulerian dynamical models. Fortunately, Eulerian microphysics models can fill this need. Eulerian models, also called fixed bin models, are most useful for the collision-coalescence calculation. In this kind of model, numerical diffusion is associated with the mass-grid resolution. More recent bin models, such as those used by Tzivion et al. (1987), Hounslow et al. (1988), and Chen and Lamb (1994), use a multi-moment representation of the cloud microphysics in each individual drop bin; this significantly reduces numerical diffusion and has the added benefit of conserving more than one moment of the size distribution. Following these efforts, numerical methods that include a bin representation of aerosol in each individual hydrometeor size-bin (Bott et al. 1990; Chen and Lamb 1994; Kerkweg et al. 2003; Leroy et al. 2006) have been developed. Such methods are very accurate but are too computationally intensive to be included in 3-D models.

6. Our focus

Our previous study has quantitatively shown that in selected urban settings, decreasing concentrations of air pollution aerosol particles are correlated with increasing local rainfall (*in preparation*). Following that study, here we numerically study the relationship of air pollution aerosol properties and cloud nuclei condensational growth. Unlike previous model studies, in the current study we treat the water vapor depletion and latent heat effects caused by aerosol condensational growth as a promoter of turbulence and as it affects the evolution of this turbulence. Because of what we anticipate, if a quasi-balance has been reached between a cloud and the outside environment, after the aerosols take up a certain amount of water vapor inside the cloud, this quasi-balance will be destroyed. To reach a balance again, there will need to be vapor diffusion from outside to inside across the boundary of the cloud. Since most of the time, clouds have large dimensions, like thousands of cubic meters, the diffusion will certainly result in turbulence. We investigate how this turbulence evolves when the aerosols take up water over a sufficiently long time period to reach equilibrium. Furthermore, we expect that it is this kind of mechanism, which restricts water vapor inside the clouds leading to a higher relative humidity inside the clouds than the outside and this will affect the growth of aerosol particles also.

To serve this purpose, we couple a model of time dependent condensational aerosol growth (Kalyanasundaram, M. 1999) with ANSYS FLUENT software. A simple demonstration is as Figure 1.1:

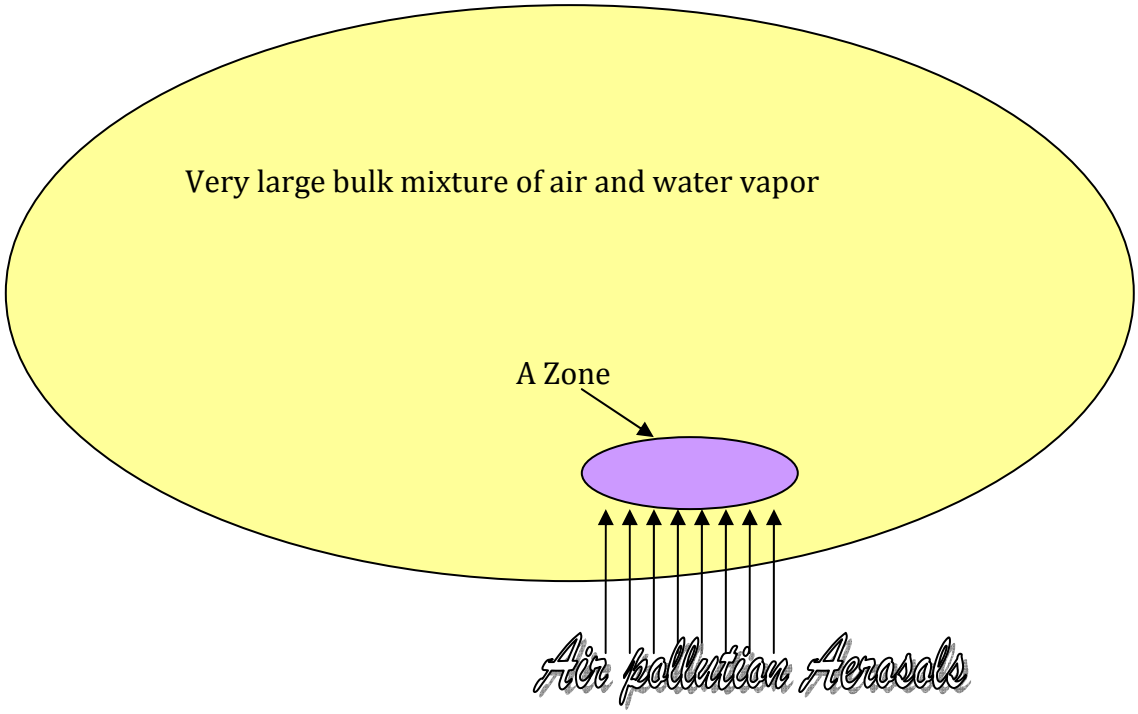

Fig. 1.1 Demonstration of the situation to be considered

There is a very large bulk mixture of air and water vapor in the atmosphere; inside it, there is a comparatively small volume (A zone), like 10^3 m^3. When we introduce a certain amount of aerosols into A zone, heat will be released and water vapor will be taken up (or released) because of growth (or evaporation, depending on the relative humidity of A zone) of these particles. Then heat and mass will transfer between A zone and the large volume. Every time step, we use aerosol condensational growth model calculating the heat release and water vapor depletion amount in A zone and pass these two variables to ANSYS FLUENT. Then ANSYS FLUENT software will simulate the interaction between A zone and the large volume. When a new equilibrium is reached, the relative humidity and temperature of all zones will be reset and the next time step starts.

The first part of our study is to run the time dependent condensational aerosol growth model with different cases. These cases will differ in particle number concentration, initial supersaturation and aerosol composition.

Secondly, we consider the simplest case in which there is only one A zone. We redo all the cases in the previous part and compare the differences of the results. Then, we look at the more complicated cases that there are more than one such A zones and these A zones will interact with each other if they are close enough. With such a model setup, we will also explore the effects of stochastic supersaturations in the atmosphere on aerosol particle growth.

The final part of our study is to use external and internal mixtures of organic compounds with inorganic compounds into our model. It has been proved that the hydroscopic character will change much when organic species and inorganic species are mixed together (Cruz and Pandis, 2000; Dick et al, 2000; Ming and Russel, 2002). We will study how this can affect the cloud nuclei condensational growth.

CHAPTER II

MODEL DESCRIPTION

1. Introduction

The formation of precipitation involves several complex processes. In meteorology, precipitation is any product of the condensation of atmospheric water vapor deposited on the earth's surface. When supersaturation conditions arise, the water vapor in the atmosphere starts to deposit on the cloud condensation nuclei (CCN), which are very small particles. This process is called cloud condensation nucleation. When these small particles grow bigger, the process of coagulation dominates. The first step for the generation of precipitation is that water vapor condenses on the cloud condensation nuclei. This process is critical to the generation of rainfall since only when CCN are big enough can the follow-on processes, like coagulation, take place. Here, we develop a model that couples time dependent condensational aerosol growth (Kalyanasundaram, M. 1999) with bulk air transport via ANSYS FLUENT software to simulate the scenario for the first stage of CCN's growth. We take into account only condensation because we intentionally focus on this specific process and because the time scale in our study is no more than 3 seconds, which is far less than required for the coagulation process to become important.

2.Time dependent condensational aerosol growth model

a. Description

A system consisting of a carrier gas and condensable vapor is considered. The gas and vapor are assumed to behave as ideal gases as the vapor concentration is sufficiently dilute compared to the concentration of the carrier gas. The system volume is assumed to be much larger than that of the droplet, and the droplets are randomly

distributed in the volume of the system. Also, only diffusive heat and mass transfer are considered while radiative heat transfer is assumed negligible and convective mass and heat transfer to the droplet are disregarded. The vapor pressure at the droplet surface is assumed to be the equilibrium vapor pressure for the surface conditions and is corrected for curvature and solution concentration effects. The changed vapor phase concentration and temperature due to water vapor uptake (release) and heat release (absorption) by the aerosol condensational growth are determined throughout the growth.

Condensational growth of aerosol particles is a central feature of aerosol dynamics in general and many aerosol measurement devices. Here, we treat growth by condensation of CCN as the first stage of cloud formation. Physically and chemically realistic computational simulations of this process will advance detailed understanding of how aerosols can facilitate or suppress precipitation.

Condensational growth and evaporation of aerosol particles are described by the fully coupled, nonstationary equations for heat and mass transport to the droplet aerosol. We adapt a time dependent model to simulate the competitive condensational growth kinetics of sub-micron volatile aerosol (Kalyanasundaram, 1999). The gross description of the model follows.

Initially in this description, the droplet aerosol is assumed to be in the continuum regime where the mean free path of the gas is neglected compared to be the droplet radius. Later, this assumption is corrected by modifying the continuum mass and heat fluxes by semi-empirical interpolation formulas to encompass the full range of particle sizes. The diffusive mass and heat fluxes to a droplet are obtained from the mass and energy conservation equations for a binary mixture of carrier gas and vapor, coupled with the phenomenological equations describing mass and heat transport in the binary mixture. The equations are as follows:

The conservation of mass in the binary mixture of carrier gas and vapor:

$$\frac{\partial \rho}{\partial t} + divj = 0 \qquad (2.1)$$

where $\rho = \rho_v + \rho_g$ is the total mass concentration of the binary mixture and *j* is the total mass flux density. ρ_v and ρ_g are the partial densities of the vapor and the carrier gas respectively.

The conservation of energy in the binary mixture:

$$\frac{\partial}{\partial t}(\rho_v c_{v,v} + \rho_g c_{v,g})T + divq = 0 \tag{2.2}$$

where $c_{v,v}$ and $c_{v,g}$ are the specific heat capacities at constant volume and T is the absolute temperature of the gas respectively. q is the heat flux density.

Commonly, in droplet growth theory, the mass and heat fluxes to the droplet are calculated independently, being described by Fick's law of mass diffusion and Fourier's law of heat conduction. However, Fourier's law of heat conduction only applies in the absence of diffusive mass transport. Similarly, Fick's law of diffusion is valid only when there are no temperature gradients (isothermal) in the carrier gas mixture. Wagner (1982) considered the mutual interaction of mass and heat fluxes by means of the first order phenomenological equation for mass and heat transport in a binary mixture. Starting with the first order phenomenological equation for mass transport in a binary mixture of a condensable vapor and background gas, in the absence of external forces and pressure gradients (Hirschfelder et al. 1954), Wagner obtained an accurate expression for the diffusive mass flux modified by first order correction factors. Assuming that the vapor and gas behave as ideal gases, the mass flux density obtained from the first order phenomenological equations can be expressed as:

$$\vec{j}_v = -D\left[grad\rho_v + \frac{\rho_v + \rho k_T^v}{T} gradT \right] + \rho_v \cdot \vec{V} \tag{2.3}$$

where *D* is the modified binary diffusion coefficient, and k_T is the thermal diffusion ratio defined as

$$k_T = \alpha X_v X_g \tag{2.4}$$

where α is the thermal diffusion factor and X_v and X_g are the mole fractions of the vapor and gas respectively.

In the present estimation of the vapor mass flux density, the thermal diffusion factor is assumed to be zero and the convective Stefan flow is neglected since the enhancement of the mass flux due to these two factors is less than a 1%, as shown by the numerical experiments of Kulmala and Vesala (1991).

Following a similar definition as the mass flux density, the expression for the heat flux density $\vec{q}$ can be rigorously obtained from first order phenomenological equation. An approximate form of the heat flux density can then be expressed as

$$q = -KgradT + h_v j_v + e_{duf} \tag{2.5}$$

where K is the thermal conductivity of the binary mixture and

$$h_v \approx c_{pv} T \tag{2.6}$$

is the enthalpy carried by the diffusing molecules. e_{duf} is the heat flux density due to thermal diffusion, or the Dufour effect (Hirschfelder et al. 1954). The radiative contribution to the heat flux is neglected here.

The temperature and vapor concentration profiles are obtained by solving the mass and energy conservation equations for the system along with the transport fluxes and a set of boundary conditions at the droplet surface and infinity. The mechanism of these transfer processes on submicron aerosol particles depend on the Knudsen number (Kn), which is defined as a ratio of the mean free path λ of the vapor molecules to the radius r of the aerosol particle (Hidy and Brock 1970). In the continuum regime (Kn->0), the transfer processes are purely diffusive and represented by equations of heat conduction and mass diffusion. In the free molecular regime (Kn->∞), the particle is assumed not to disturb the velocity distribution function of the molecules, which strike the particle. According to the kinetic theory of gases, the number of binary collisions between vapor and particle is proportional to the condensation flux. When the radius of the aerosol particle is of the order of the mean free path of the gas molecules, or in the transition regime (intermediate values of Kn), the transfer process cannot be expressed

as for the free molecular and continuum regimes. Transition regime condensation fluxes are hence semiemperical in nature. A number of investigators starting with Langmuir (1915) have calculated the transitional fluxes by equating the stationary continuum and free molecular fluxes at the droplet surface. A review of improvements to Langmuir's theory by matching fluxes at different jump distances outside the droplet can be found in Wagner (1982). In this study, the transitional correction factors obtained by Fuchs and Sutugin's interpolation formula (Fuchs and Sutugin 1971) are used to compute the noncontinuum mass and heat fluxes.

In addition to the Knudsen number, the heat and mass transfer processes are also characterized by mass and thermal accommodation coefficients β_T and β_M respectively. The thermal accommodation coefficient is the ratio of the actual heat transfer to that predicted if every molecule thermally accommodates at the surface of the particle. The mass accommodation coefficient, or sticking coefficient, is the fractions of molecules that strike the surface of the particle that adhere to it. These accommodation coefficients take a range of values for different liquids from different investigations based on a comparison of theoretical and experimental droplet growth theory. The mass and energy accommodation coefficients were chosen to be unity based on an experimental results for water droplets by Sageev et at. (1986).

The transitional correction factors to the mass and heat fluxes applied in this study are

$$\beta_T = \frac{1 + Kn_g}{1 + 1.71Kn_g + 1.33Kn_g^2} \tag{2.7}$$

where

$$Kn_g = \frac{\lambda_g}{r} \tag{2.8}$$

$$\beta_m = \frac{1 + Kn_v}{1 + 1.71Kn_v + 1.33Kn_v^2} \tag{2.9}$$

where

$$Kn_v = \frac{\lambda_v}{r} \tag{2.10}$$

and where Kn_v is the Knudsen number with respect to the vapor molecules and Kn_g is the Knudsen number with respect to the gas molecules.

The droplet temperature is obtained by equating the change in the energy of the droplet to the difference in the heat flux to and from the droplet.

$$\frac{d}{dt}\left[\rho_1 c_1 \frac{4\pi}{3} a^2 T(t,a)\right] = LI - Q \tag{2.11}$$

The total heat flux due to conduction to the droplet Q is given by

$$Q = -4\pi a^2 K grad T \beta_T(Kn_v) \tag{2.12}$$

where I is the total mass flux toward the droplet, c_1 is the specific heat capacity of the droplet. L is the latent heat of condensation of the liquid at the droplet temperature given by

$$L(T_a) = h_v(T_a) - h_1(T_a) \tag{2.13}$$

where $h_1(T_d)$ is the liquid enthalpy at the droplet temperature.

The interfacial equilibrium relation is calculated from Kohler theory and definition of water activity,

$$P_{v,a} = P_S(T_a) a_W \exp\left(\frac{2M_W \sigma_{1v}}{RT_a \rho_1}\frac{1}{a}\right) \tag{2.14}$$

Finally, the rate of droplet growth is obtained from a mass balance equation where $P_s(T_a)$ is the equilibrium vapor pressure at the droplet temperature T_a. The droplet equilibrium vapor pressure is corrected for solute and Kelvin effect. a_w is the activity of water in the solution droplet. n_s is the moles of solute.

$$\frac{dm}{dt} = 4\pi a^2 D \frac{\partial \rho_v}{\partial r}(t,a) \tag{2.15}$$

where a is the droplet radius, and D is the binary diffusion coefficient.

In order to account for the competitive condensation kinetics, the time dependent bulk parameters for the vapor concentration and ambient temperature are obtained considering the vapor depletion and production of latent heat in the system. From conservation of total mass of vapor in the system, an expression for the time dependent vapor density is obtained as

$$\rho_{v,\infty} = \frac{(T_\infty)_0}{T_\infty}\left[(\rho_{v,\infty}) - \frac{4\pi}{3}\rho_1 \sum_i C_{i,o}(a_i^3 - a_{i,o}^3)\right] \tag{2.16}$$

where the subscript "0" stands for the initial concentration. The index "i" expresses the polydispersity of the aerosol. The particles are classified into i bins based on their composition and initial radii. $C_{i,0}$ represents the initial particle number concentration of the ith class. a_i represents the instantaneous radius of the aerosol particle of class I while $a_{i,0}$ represents the initial particle radius.

Similarly the time dependent bulk temperature of the gas is calculated as:

$$T_\infty = (T_\infty)_0 + \frac{\rho_1 L(T_a)}{(\rho_{g,\infty})_0 c_{p,g} + (\rho_{v,\infty})_0 c_{p,v}} \frac{4\pi}{3} \sum_i C_{i,0}(a_i^3 - a_{i,0}^3) \tag{2.17}$$

where $c_{p,g}$ and $c_{p,v}$ are the specific heat capacities at constant pressure of the gas and vapor respectively.

b. Solution method

The above set of time dependent equations can only be solved numerically to obtain the droplet growth rates. The coupled heat and mass transport equations with the appropriate boundary (initial value) conditions at the droplet surface and at infinity were solved using a finite difference scheme. The spherically symmetric equations were first transformed to another coordinate system h by the following expression,

$$\eta = \frac{r - r_s}{r_\infty - r_s} \tag{2.18}$$

so that, $\eta = 0.0$ always corresponded to the droplet surface, r_s, and $\eta = 1.0$ to r_∞, infinity,. The discretized equations for the system of coupled nonlinear equations were obtained by a Taylor series expansion. The discretized equations for the above one-dimensional problem, which are fully implicit in time, display a tridiagonal pattern. The tridiagonal system of equations was solved by an efficient algorithm-- the tridiagonal matrix algorithm or Thomas algorithm (Patankar 1980).

At every time step the coupled finite difference approximation equations are solved to obtain the temperature and density gradients around the droplet. The mass flux to the droplet is calculated from the density gradient and the corresponding increase in the droplet radius is computed. The energy balance equation at the droplet surface and the equation describing the interfacial vapor pressure as a function of temperature are iteratively solved at the new droplet radius to find the change in the droplet temperature due to phase change. The droplet vapor pressure is calculated at the new surface temperature and solute concentration. The time dependent bulk parameters, the vapor density, temperature and supersaturation are evaluated by balancing the amount of vapor condensed by all the droplets and the increase in the temperature due to latent heat of condensation. With the new set of boundary (initial) conditions, the calculations are repeated for the next time.

c. Calculational results

Here, we will use this time dependent condensational aerosol growth model to numerically study the relationship of air pollution aerosols and cloud condensation nucleation inducing growth to sizes where inertial coagulation is possible. Additionally, we use this model to study the condensational growth of a $(NH_4)_2SO_4$-H_2SO_4-H_2O system. In all the calculations of this chapter, the particles were all initially equilibrated at 85% relative humidity (RH). The water activity cofficient data was from the experiment data (Tang 1997) and thermodynamic model (Clegg and Brimblecombe, 1994).

Calculational results for single species of aerosol

For convenience, we choose $NaNO_3$ as the example for our calculations of single species. We assume an initial log-normal size distribution of mean radius of 0.2 micrometer and the standard derivation of 2.1. We divide this log-normal size distribution into size bins of 0.025 micro meter radius and assume the smallest particles have radius of 5 nanometer and the largest particles have radius of (mean radius + 3 standard derivation). First, we calculated 30 cases with 6 different total number concentrations, 1.0E10/m^3, 2.5E10/m^3, 5.0E10/m^3, 7.5E10/m^3, 1.0E11/m^3, and 2.5E11/m^3, and 5 different initial supersaturations, 0.1, 0.5, 1.0, 2.0 and 3.0.

Figures 2.1 to 2.5 represent the computational results by giving the changes of size distributions at selected initial supersaturations, for 1 second of growth.

Figures 2.6 to 2.11 represent the results by the views of change of total number concentration at fixed initial RH, respectively.

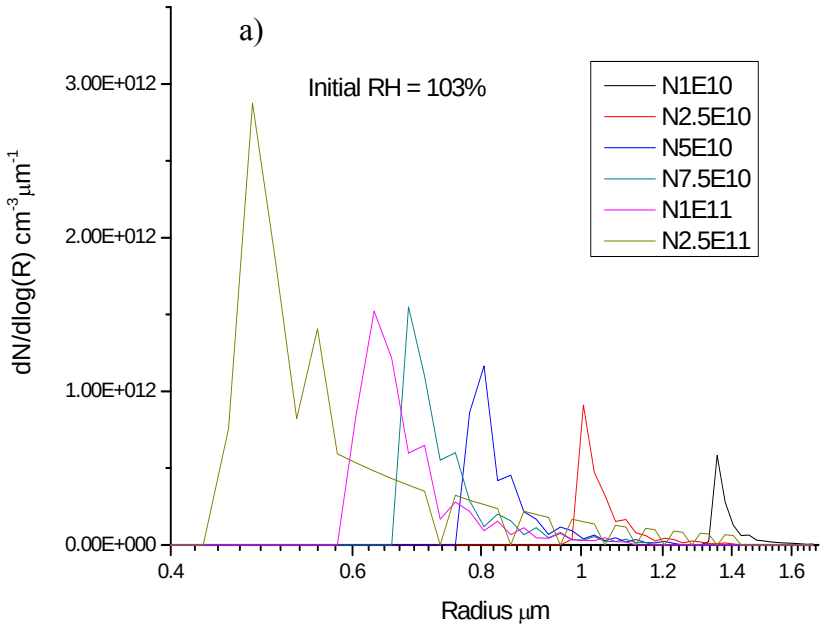

Fig. 2.1 Size distribution of different total number concentrations after 1s calculation for the case of initial supersaturation = 3.0%. a) normal view b) magnified view for details

b)

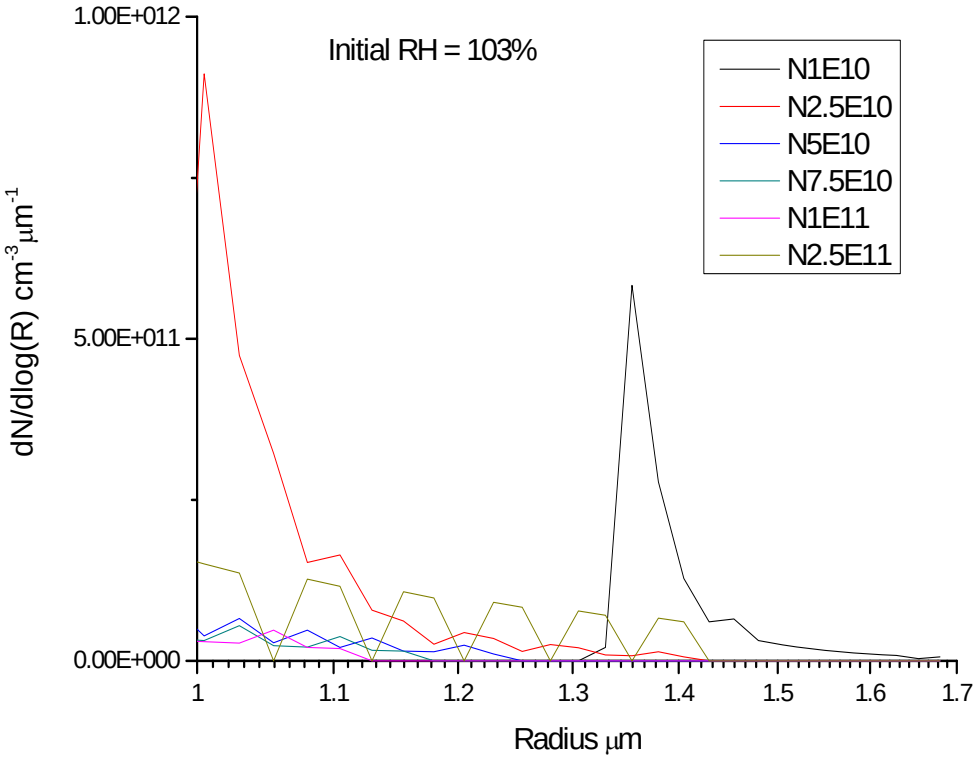

Fig. 2.1 Continued

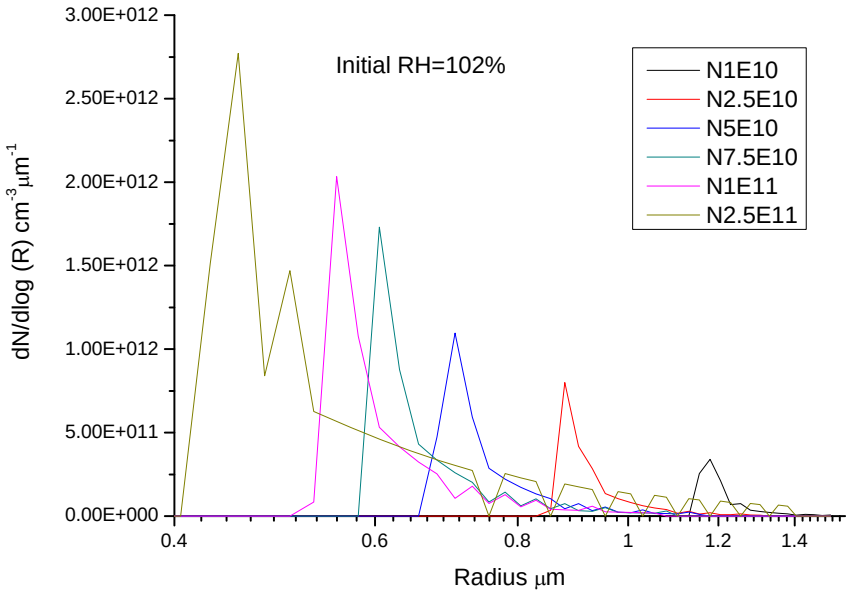

Fig. 2.2 Size distribution of different total number concentrations after 1s calculation for the case of initial supersaturation = 2.0%

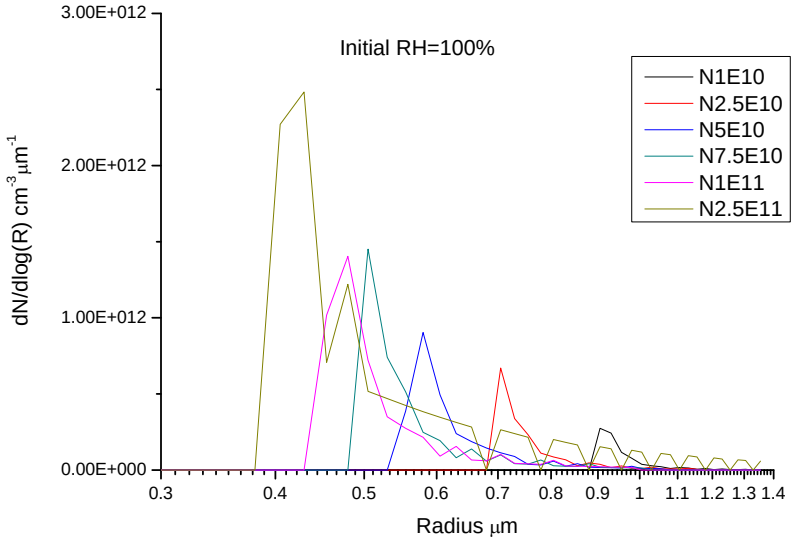

Fig. 2.3 Size distribution of different total number concentrations after 1s calculation for the case of initial supersaturation = 0%

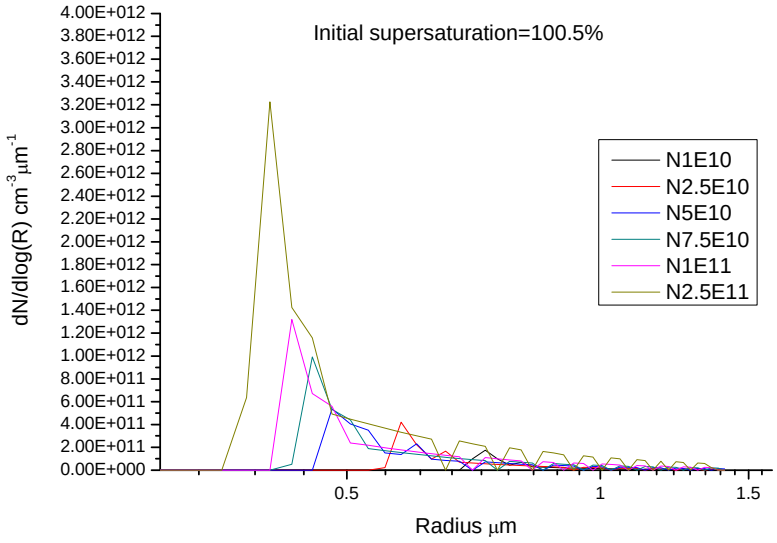

Fig. 2.4 Size distribution of different total number concentrations after 1s calculation for the case of initial supersaturation = 0.5%

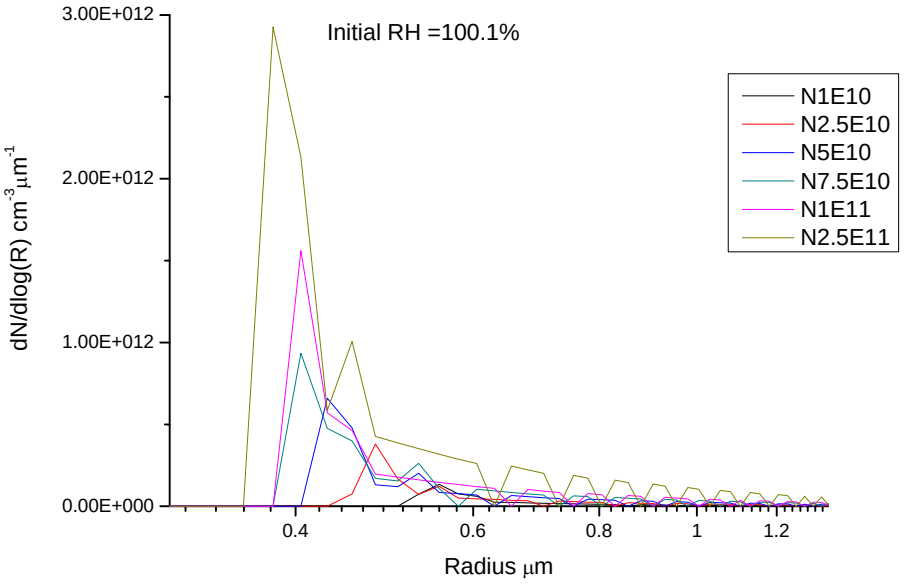

Fig. 2.5 Size distribution of different total number concentrations after 1s calculation for the case of initial supersaturation = 0.1%

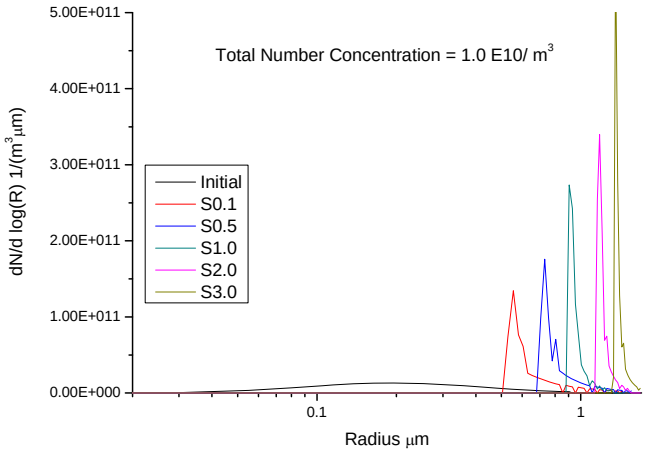

Fig. 2.6 Size distribution of different initial supersaturations after 1s calculation for the case of total number concentration = 1E10/m^3

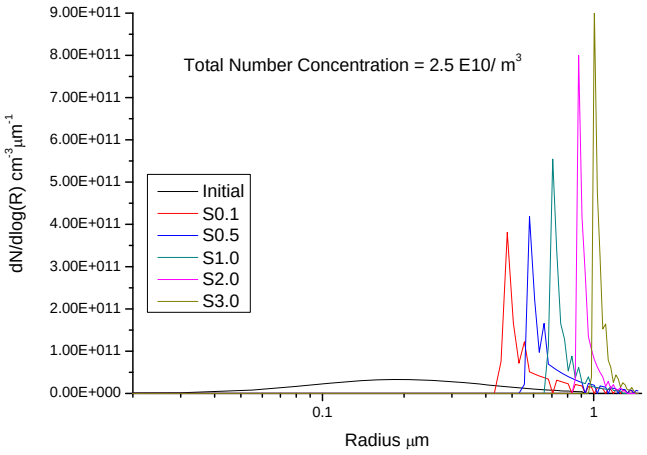

Fig.2.7 Size distribution of different initial supersaturations after 1s calculation for the case of total number concentration = 2.5E10/m^3

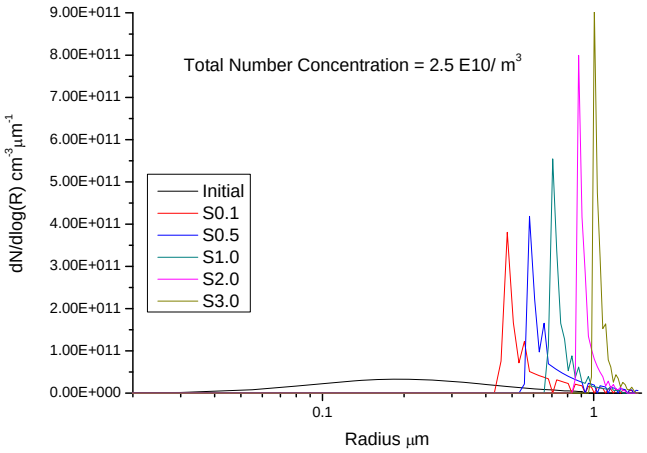

Fig. 2.8 Size distribution of different initial supersaturations after 1s calculation for the case of total number concentration = 5.0E10/m^3

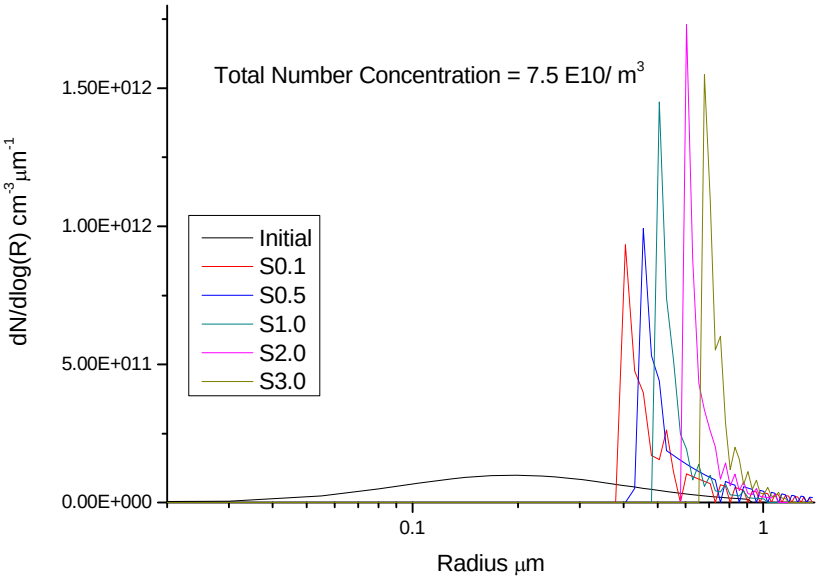

Fig. 2.9 Size distribution of different initial supersaturations after 1s calculation for the case of total number concentration = 7.5E10/m^3

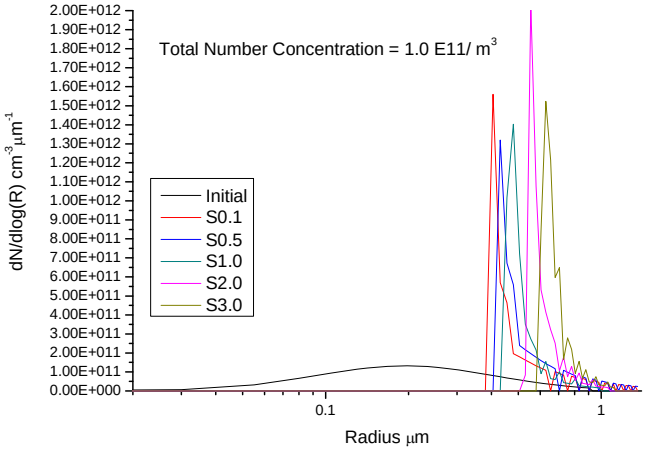

Fig. 2.10 Size distribution of different initial supersaturations after 1s calculation for the case of total number concentration = 1.0E11/m^3

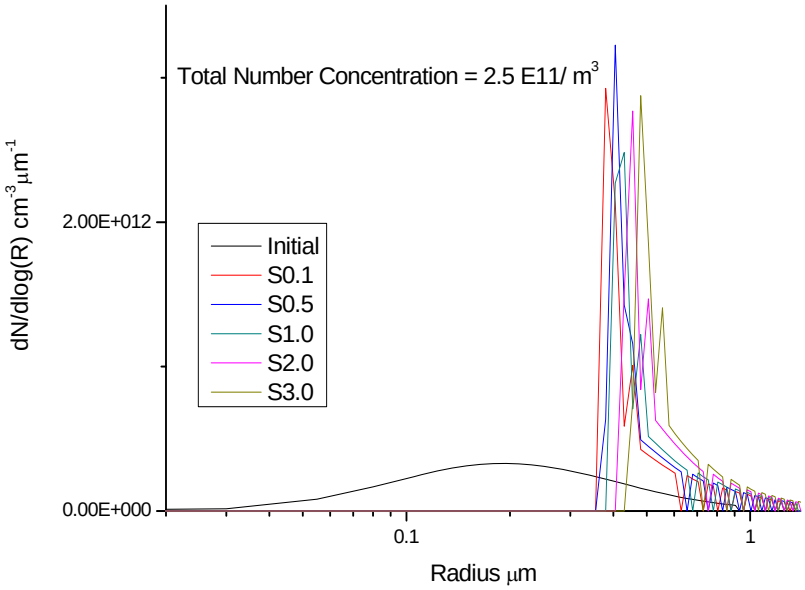

Fig. 2.11 Size distribution of different initial supersaturations after 1s calculation for the case of total number concentration= 2.5E11/m^3

From all these results, we can clearly see the dependency of aerosol condensational growth on the total number concentrations and initial supersaturations. Moreover, the effects of these parameters on the computational results are not independent. We can see from figures 2.1 to2.5 that higher number concentration leads to narrower size distribution and smaller mean radius and, with lower number concentration, the largest particle can grow more. However, comparing these 5 figures shows that with the decrease of initial supersaturation, this trend becomes less obvious and the importance of the effect of total number concentration is weakened. From figures 2.6 to 2.10, we observe that the higher the initial supersaturation, the more the particles can grow. Also, with the increase of total number concentration, this trend becomes less obvious and the importance of the effect of initial supersaturation is weakened.

We also traced the change of relative humidity, temperature, total particle surface areas and volume and size evolution of each size bin with time. Figures 2.12 to 2.15 show the calculational results for 4 cases with total number concentration of 2.5E11/m^3 and initial supersaturation of 0.1, total number concentration of 2.5E11/m^3 and initial supersaturation of 3.0, total number concentration of 1.0E10/m^3 and initial supersaturation of 0.1 and total number concentration of 1.0E11/m^3 and initial supersaturation of 3. 0 respectively.

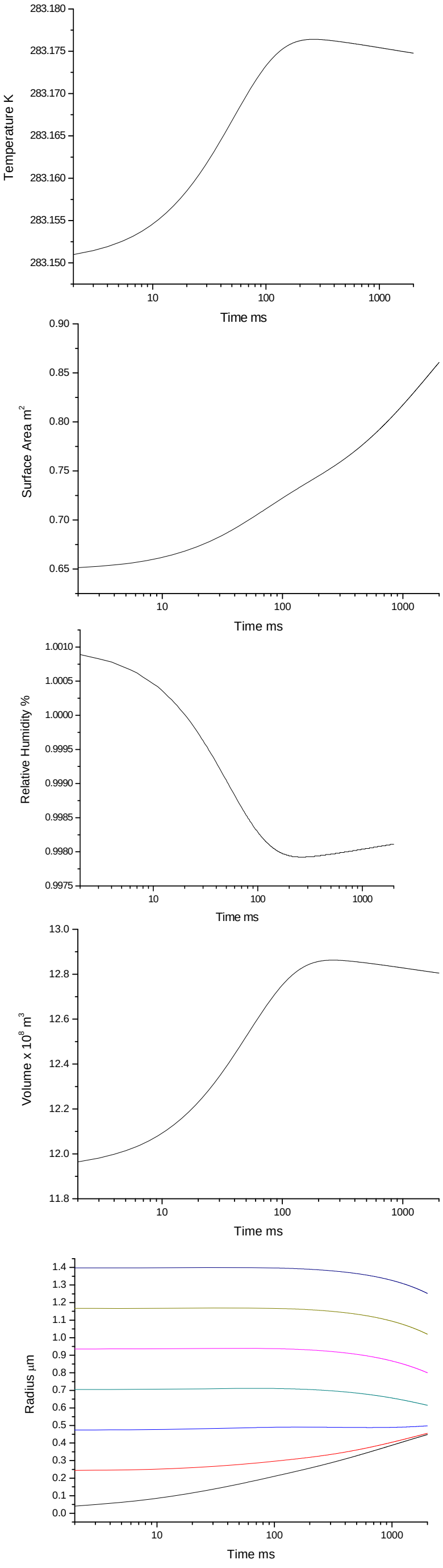

Fig.2.12 Calculated change of relative humidity, temperature, total particle surface areas and volume and size evolution of each size bin with time during aerosol condensational growth for the case N= 2.5E13/m^3 and S= 0.1%

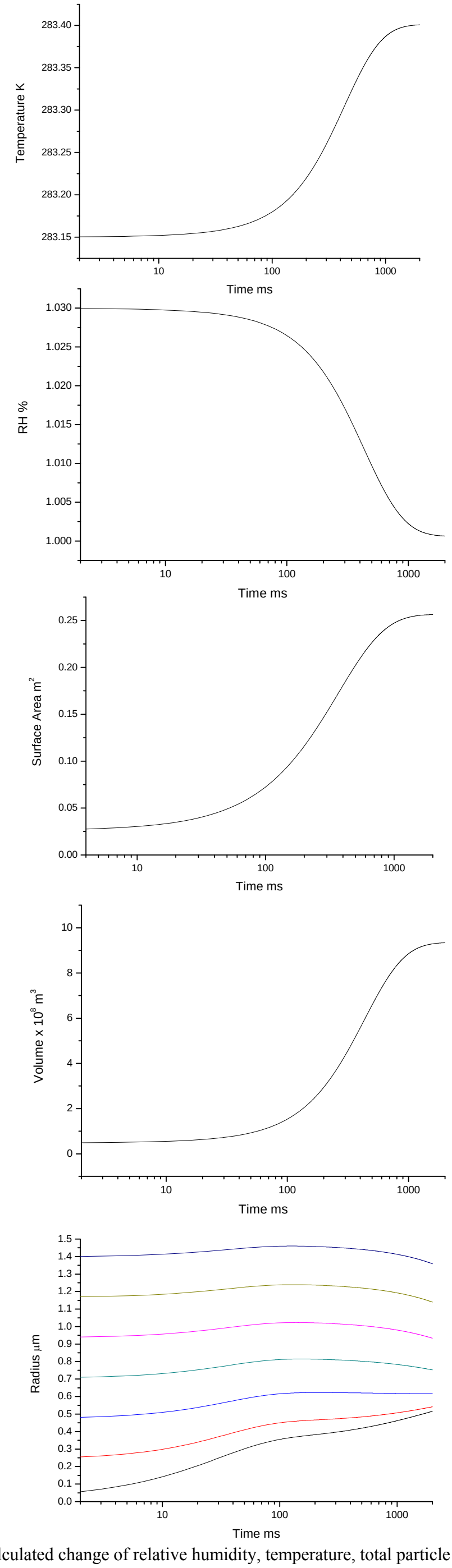

Fig. 2.13 Calculated change of relative humidity, temperature, total particle surface areas and volume and size evolution of each size bin with time during aerosol condensational growth for the case 2.5E13/m^3 and S= 3.0%

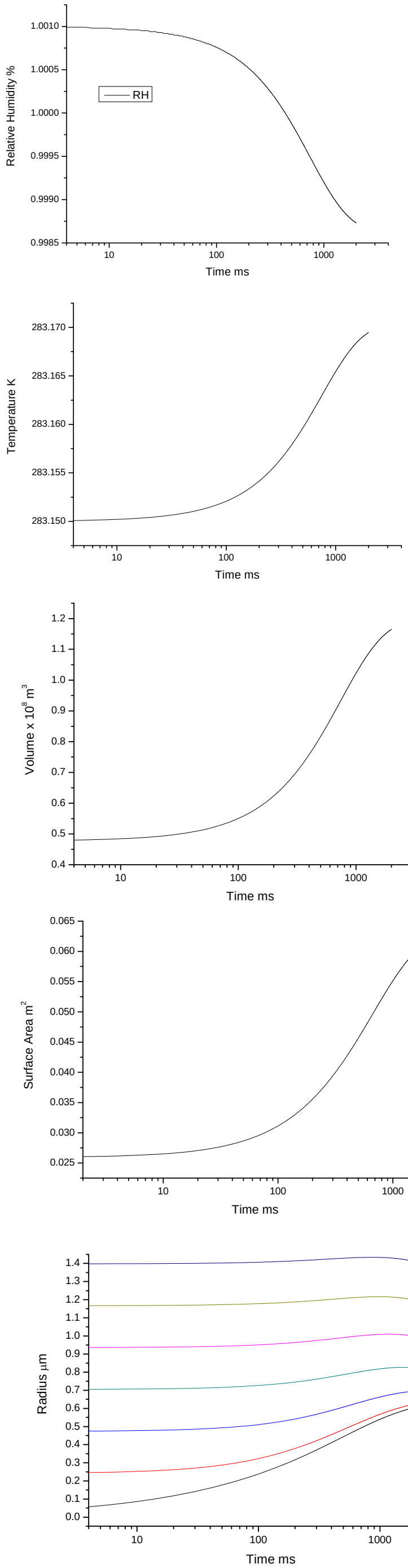

Fig. 2.14 Calculated change of relative humidity, temperature, total particle surface areas and volume and size evolution of each size bin with time during aerosol condensational growth for the case 1.0E10/m^3 and S= 0.1%

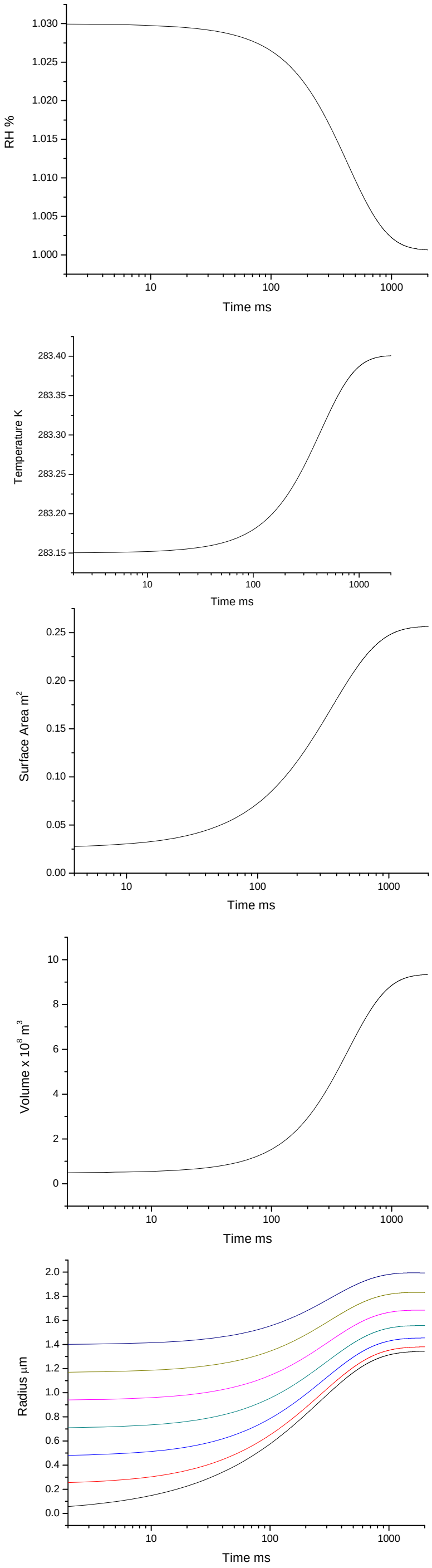

Fig. 2.15 Calculated change of relative humidity, temperature, total particle surface areas and volume and size evolution of each size bin with time during aerosol condensational growth for the case 1.0E10/m^3 and S=3.0%.

Firstly, we can see from the high concentration with low initial supersaturation case (figure 2.12) that relative humidity decreases first, then increases; and temperature and volume finally decrease after increasing for the initial period of time. Then, note in the low concentration with high initial supersaturation case (figure 2.15), there is no such phenomenon. In this case, the relative humidity maintains its decreasing trend of change until the end and the temperature and volume also maintain their increasing trends of change until the end. Finally, observe figures 2.13 and 2.14. These two cases, which can reach a compromise between initial supersaturation and total number concentration, are either high total number concentration with low high initial supersaturation or low total number concentration with low initial supersaturation. Different from figures 2.12 and 2.15, the changes of relative humidity, temperature and volume in these two cases neither keep their original trend nor do they turn to the opposite direction. Instead, they just stop changing or the changes become untraceable if there is any. We can draw a conclusion that this up and down curve in figure 2.12 is because some particles eventually become incapable of competing for water vapor and start to vaporize due to increased temperature and decreased vapor. This vaporization process finally triumphs over the condensational growth process and becomes dominant. While with low number concentration and high initial supersaturation (figure 2.15), particles are able to continue growing; for the intermediate cases (figures 2.13 and 2.14), some particles are not able to continue the high growth and will not vaporize. But unlike the high concentration with low initial supersaturation case (figure 2.13), the vaporization cannot become the dominant process but can only reach an equilibrium with the condensational growth process. The growth history of each size bin confirms the above conclusion. In figure 15, none of the 7 size bins shows the tendency of vaporization. The other three graphs all show some phenomena of vaporization in some of the 7 size bins. These results agree with what we extrapolated from figures 2.1 to 2.12.

Calculation of the $(NH_4)_2SO_4$-H_2SO_4-H_2O system

Here, we employ the thermodynamic model of the of $(NH_4)_2SO_4$-H_2SO_4-H_2O system developed by Clegg et al (Clegg et al. 1995, 1998 and 1999). This time, we only assume monodisperse initial size distribution with initial particle radius equals to 1.0E-6 m. Here we make variables of the ammonium to sulfate ratio (ASR) and total number concentration (con). Three different values of ASR are tested; they are 1.0, 1.5 and 2.0. The water activity values are calculated by Clegg et al's model. 2.5E10/m^3 and 2.5E11/m^3 are used as the number concentration in the calculations. Other initial parameters are all the same: initial relative humidity =100%, temperature =298.150000.

The calculated results are presented in figure 2.16. The 3 graphs show the evolution history of particle radii, system relative humidity and temperature from 1ms to 1000ms, and total amount of condensed water after 1000ms. Again, the total number concentration has great effect on the final particle size. A factor of ten increase in particle number concentration results in about 0.5 micrometer less growth and 1.5 factor more of total condensed water vapor after 1000ms at all three ASR. On the other side, ASR plays its own role on the particle condensational growth; although it is a much less significant one compared to the role that number concentration plays. We can see from the graphs that higher the ammonium ratio, the more the particle can grow and less water vapor was condensed. However, unlike the particle number concentration, which can quantitatively change the growth process, difference in ASR has only a relatively small effect on the final size.

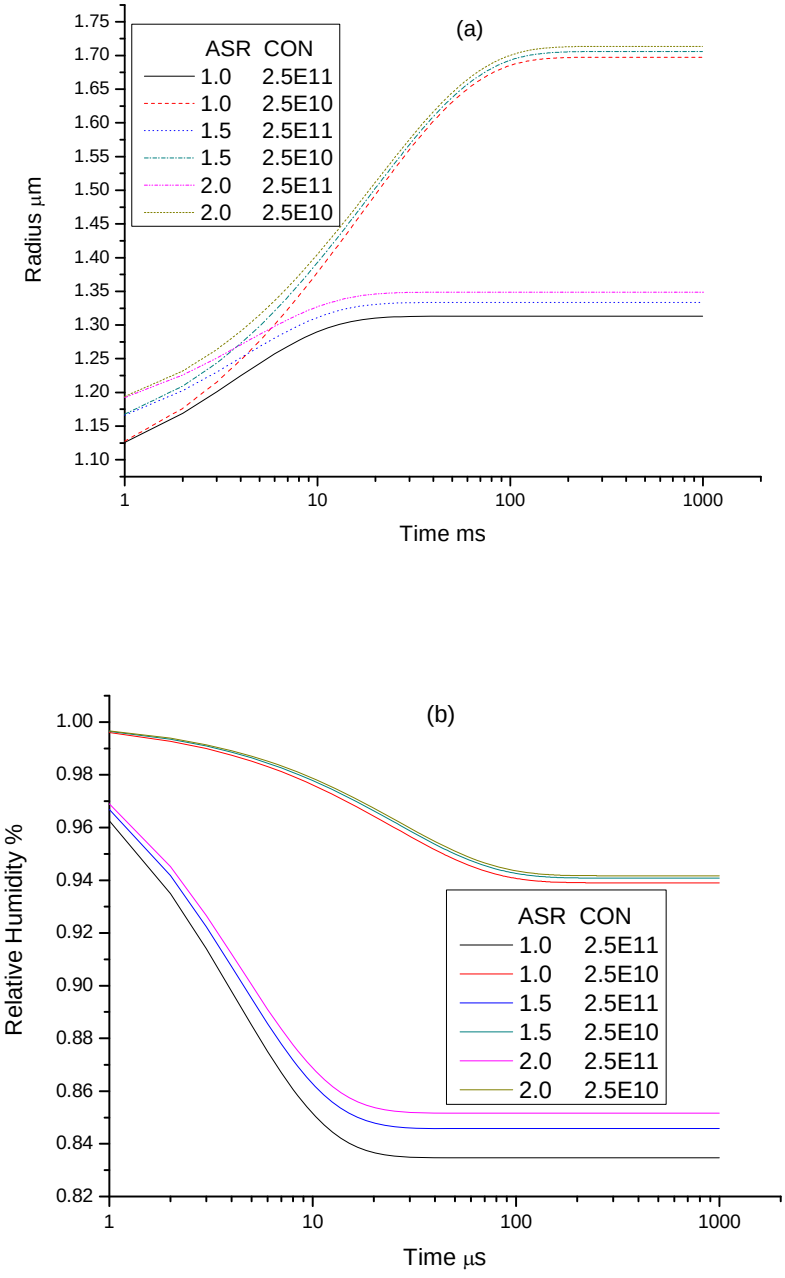

Fig. 2.16 Calculation results for the $(NH_4)_2SO_4$-H_2SO_4-H_2O system. (a) Radius growth with time (b) Change of relative humidity with time(c) Change of temperature with time (d) Total amount of condensed water after 1000ms

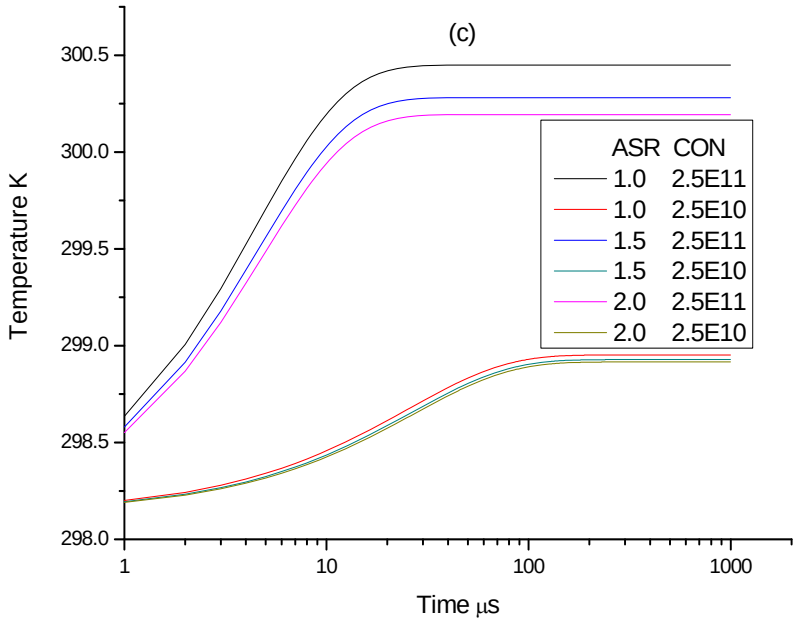

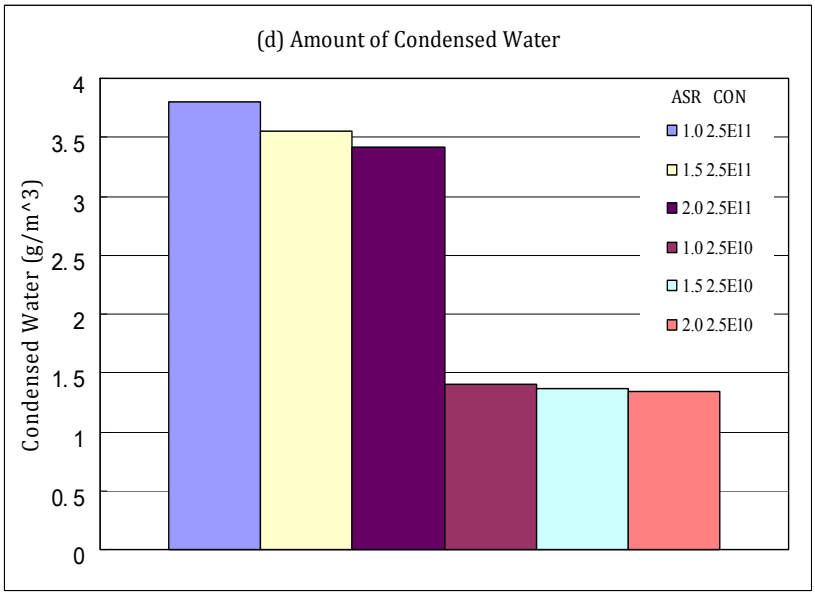

Fig. 2.16 Continued

3.Model coupled time dependent condensational aerosol growth model with ANSYS FLUENT software

Aerosols and clouds together play crucial roles in the earth's climate. Many atmospheric studies and large-scale global climate models focus on aerosol-cloud interactions. The aerosol-cloud-climate interaction is a very complicated one and much of the feedback between aerosols, clouds and climate is yet to be understood and incorporated in climate models.

The heat and mass uptake or release by aerosol condensational growth will absolutely break the equilibrium between the air parcel where the aerosols reside and the environment around it. This kind interaction between cloud and aerosol is obvious but has not received sufficient attention. The time dependent condensational aerosol growth model we introduce here has the ability to calculate the heat release or uptake and water vapor uptake or release every time step. This allows us to simulate the heat and mass flow field caused by aerosols with computational fluid dynamic (CFD) simulation programs.

a. Relatively simple prototype

We begin with a review of the idea of this model mentioned in chapter I. As indicated in figure 2.17, we assume a large volume with a very small ZONE A inside it. In this section, we will assume an initially homogeneous relative humidity distribution everywhere, which means the relative humidity will be the same inside and outside Zone A. Aerosol condensational growth (or evaporation) in Zone A will be allowed depending on the relative humidity of A zone. Here, in order to mimic the real clouds which usually have large areas at the base and smaller areas at the top, we made Zone A a hemispherical volume with diameter r and the bottom is perpendicular to the z direction (actually we do compare the results with hemisphere and sphere Zone A, they are very close and do not have significant differences); the large volume is a rectangle with length and width equal to a in the x and y directions and height equals q/2 in the z

direction. The center the rectangle is also Zone A 's basal center. Aerosols are assumed not to move out of A zone. Since CCN have the tendency of remaining in the same parcel, this assumption is reasonable. As a consequence of the aerosol condensational growth (or evaporation), heat will be released (or absorbed) and water vapor will be absorbed (or released) because of growth of these particles. Then heat and mass will transfer between A zone and the large volume. ANSYS FLUENT allows user to interpolate their codes in C language as User Defined Function (UDF) into ANSYS FLUENT. This enables us to couple our aerosol condensational growth model with ANSYS FLUENT software. As demonstrated in figure 2.18, every time step, we use aerosol condensational growth model calculating the heat release and water vapor depletion amount in A zone and pass these two variables to ANSYS FLUENT. Then ANSYS FLUENT software will simulate the interaction between A zone and the large volume. When a new equilibrium is reached, the relative humidity and temperature of all zones will be reset and then next time step starts.

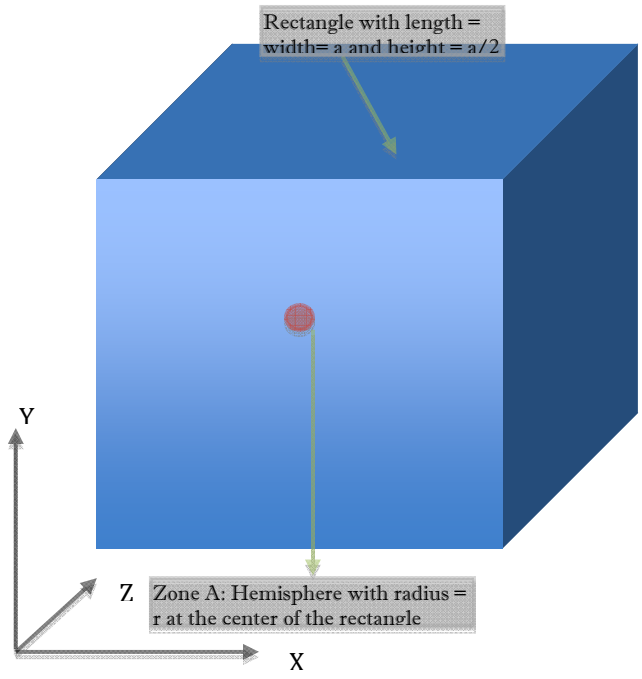

Fig 2.17 Demonstration of the prototype

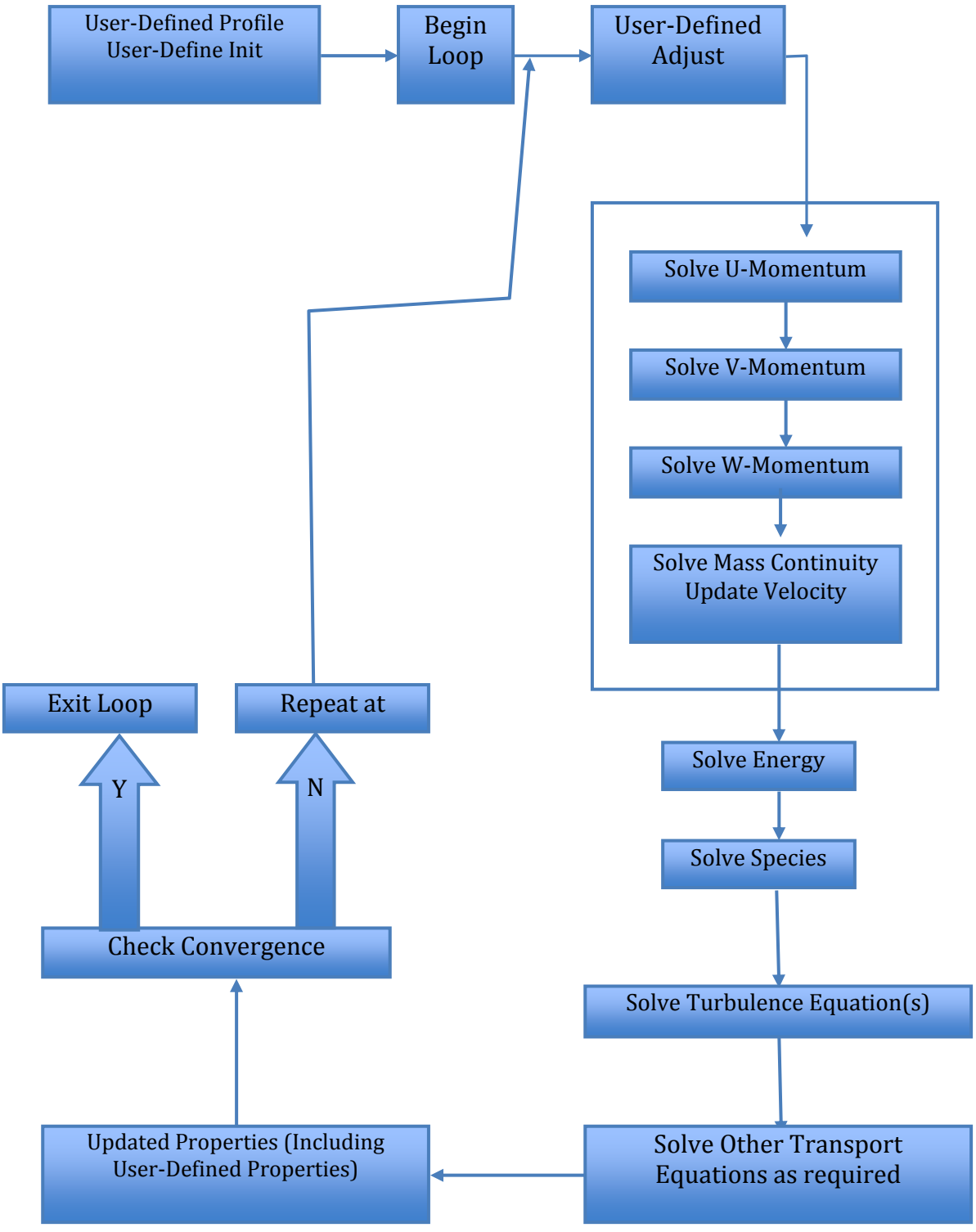

Fig 2.18 Solution procedure for the pressure-based coupled solver in ANSYS FLUENT (ANSYS FLUENT 6.3 UFD manual, 2006)

b. Sensitivity study

Because the limit of the embedding volume should approximate an infinite background, we should make it as large as possible. Also, in the computation, we should make the grid as dense as possible. But, we must consider the cpu time and memory cost; so it is impossible to make the rectangle too large or with too many grids. We must make a compromise between the realism of the model and the computational cost. So, we conducted a sensitivity study first.

We tested 3 cases with different dimensions and grid densities that are listed in Table 2.1. In all these three cases, we mesh the whole computational domain following the same rules. The first one is to mesh the big rectangular solid embedding volume and small hemisphere separately. Also the density of meshes in the small hemisphere should be higher than that in the embedding volume. The highest mesh density appears at the boundary between large rectangle and small hemisphere and a boundary layer is set there. Following are two demonstration graphs. Figure 2.19 is the meshes observed from outside the embedding volume and figure 2.20 is the slice view of the mesh at Z=0.5Ztotal.

Table 2.1 3 cases for sensitivity study

Case No.	Dimension of the Embedding Volume (unit in m)	Number of Meshes of the rectangle	Number of Meshes of Zone A
1	1300*1300*650	135211	8697
2	1300*1300*650	169727	9013
3	650*650*325	95712	9883

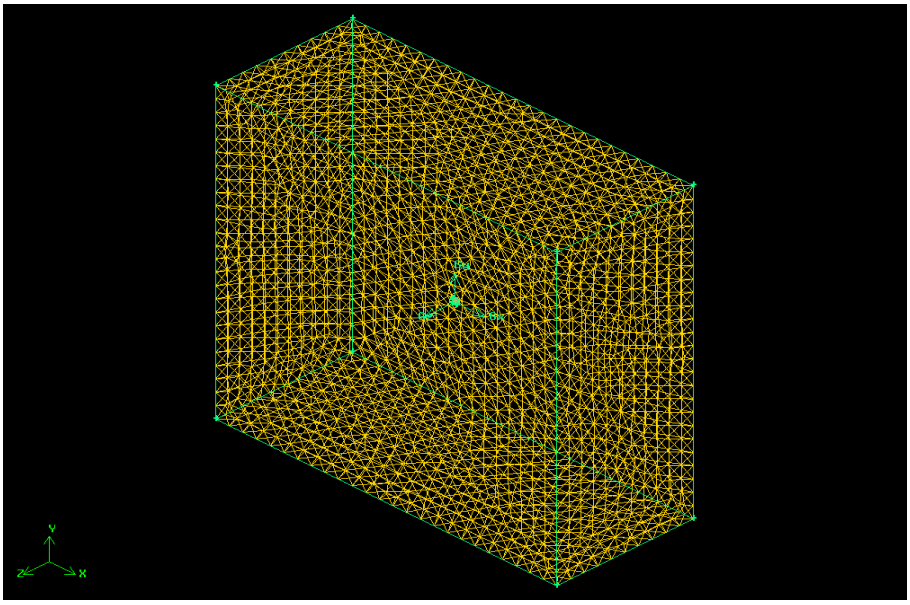

Figure 2.19 Meshes observed from outside the embedding volume

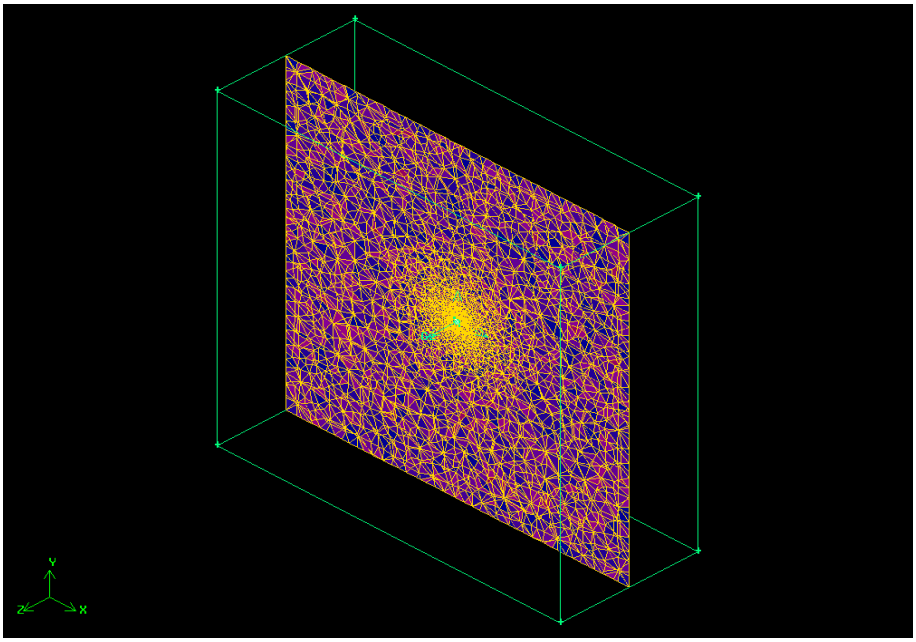

Figure 2.20 Slice view of the into inside mesh at z = 0.5 Ztotal

1st study: case 1 vs. case 2

A monodisperse initial distribution with in radius = 0.1 micrometer and number concentration = 1.0E10/m^3. Initial temperature equals to 298.15K and initial relatively humidity is 101.447%. The results are shown in Figures 2.21, 2.22, and 2.23.

Figure 2.21 is the comparison of particle growth history. Figure 2.22 is the temperature evolution history inside Zone A and Figure 2.23 is the relative humidity evolution history inside Zone A.

There is almost no observable difference except for the temperature, which is still very small. There, the difference in the temperature was very small and no more than 0.001 K, and at the end, this difference vanished.

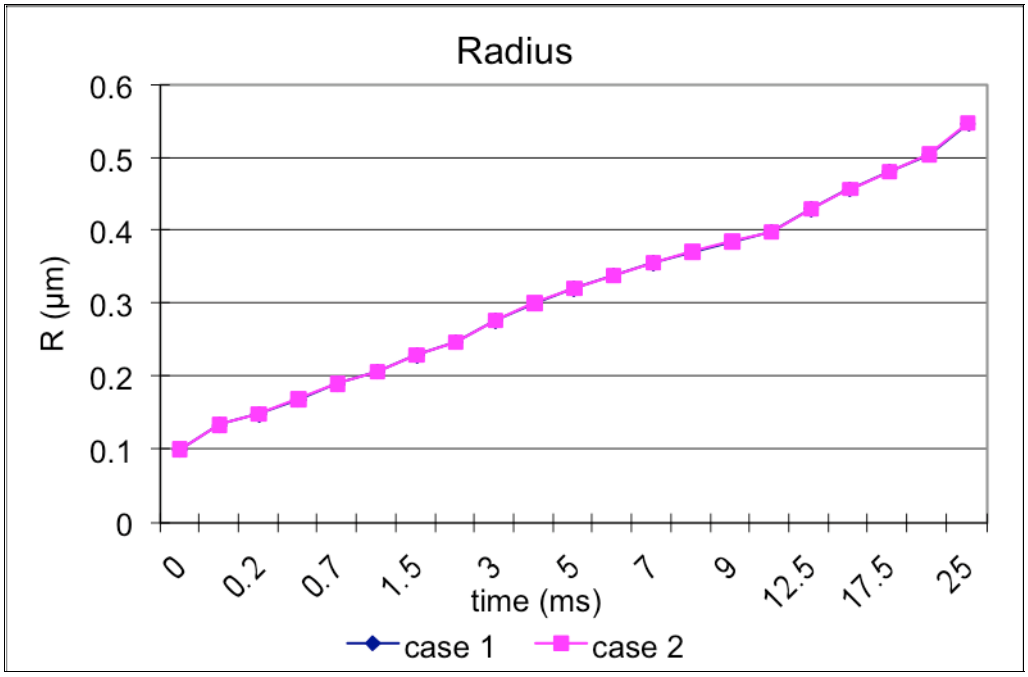

Figure 2.21 Comparison of particle growth history of case 1 and case 2 for the 1st study

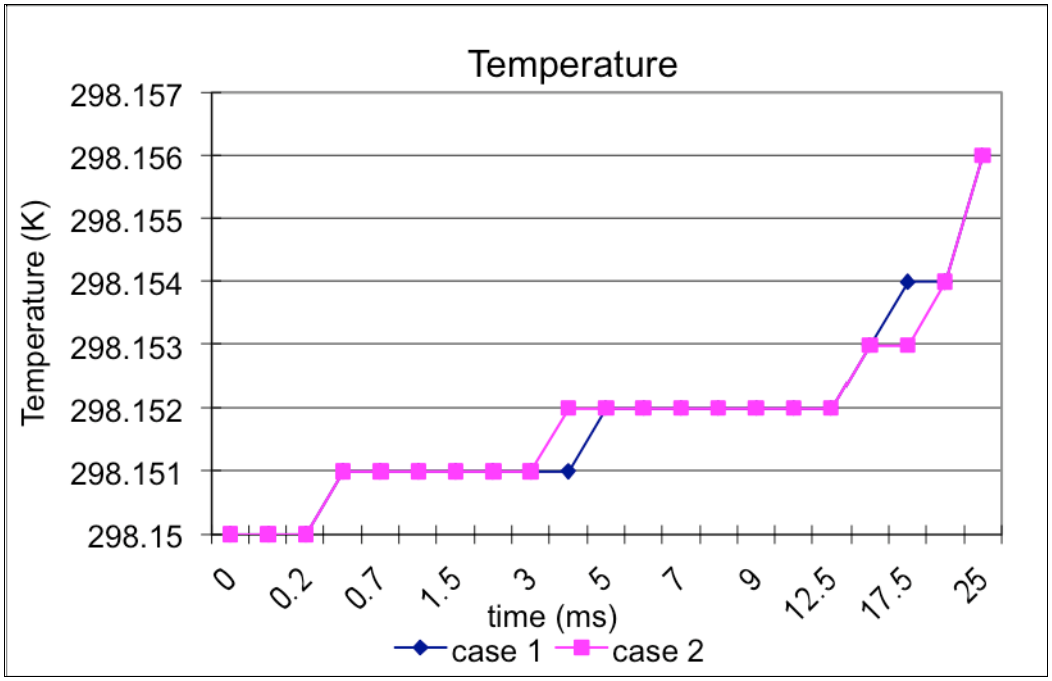

Figure 2.22 Comparison of temperature evolution history inside Zone A of case 1 and case 2 for the 1st study

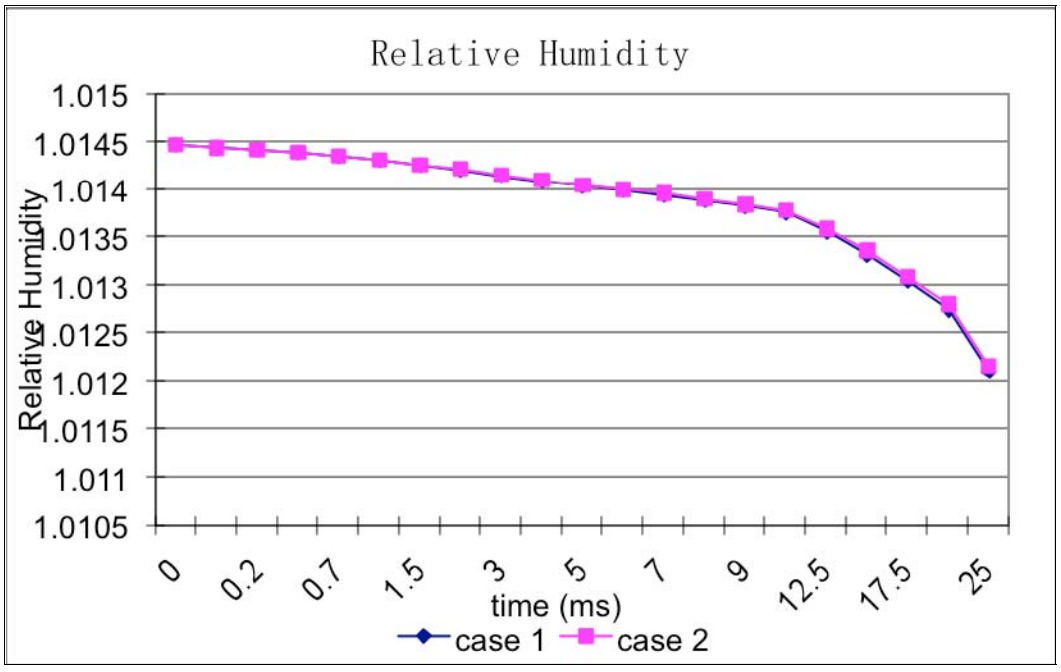

Figure 2.23 Comparison of relative humidity evolution history inside Zone A of case 1 and case 2 for the 1st study

2nd study: case 1 vs. case 2

A monodisperse initial distribution with in radius = 0.25 micrometer and number concentration = 1.0E13/m^3. Initial temperature equals to 298.15K and initial relative humidity is 99.4574%. The results are shown in Figures 2.24, 2.25, and 2.26.

Figure 2.24 is the comparison of particle growth history. Figure 2.25 is the temperature evolution history inside Zone A and Figure 2.26 is the relative humidity evolution history inside Zone A.

This time, there is also no observable difference for the results of radius during the entire simulation period. There is some difference for the relative humidity during the first 0.1-0.2 millisecond; but after that, this difference vanished. The most obvious difference appears in the temperature evolution. The maximum absolute difference is 0.318K and maximum relative difference is 0.6675%. Also, this difference vanished after about 4 ms.

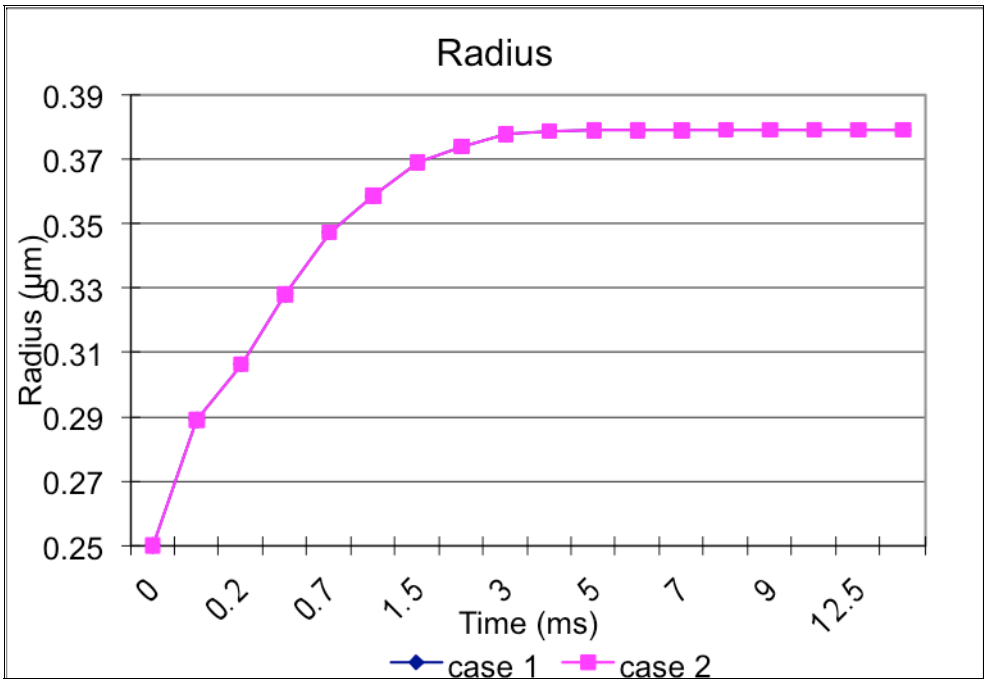

Figure 2.24 Comparison of particle growth history of case 1 and case 2 for the 2nd study

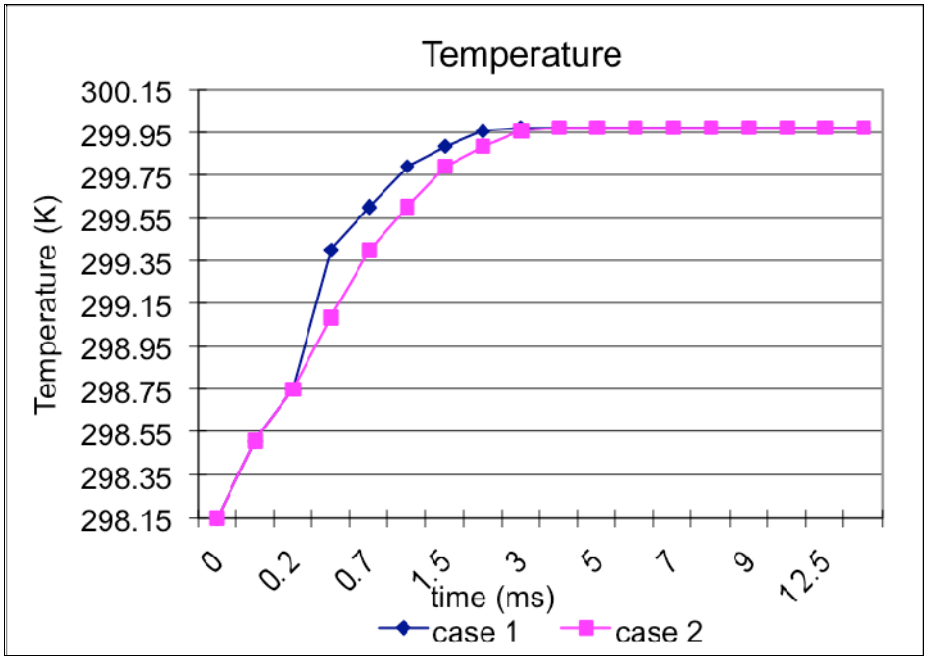

Figure 2.25 Comparison of temperature evolution history inside Zone A of case 1 and case 2 for the 2nd study

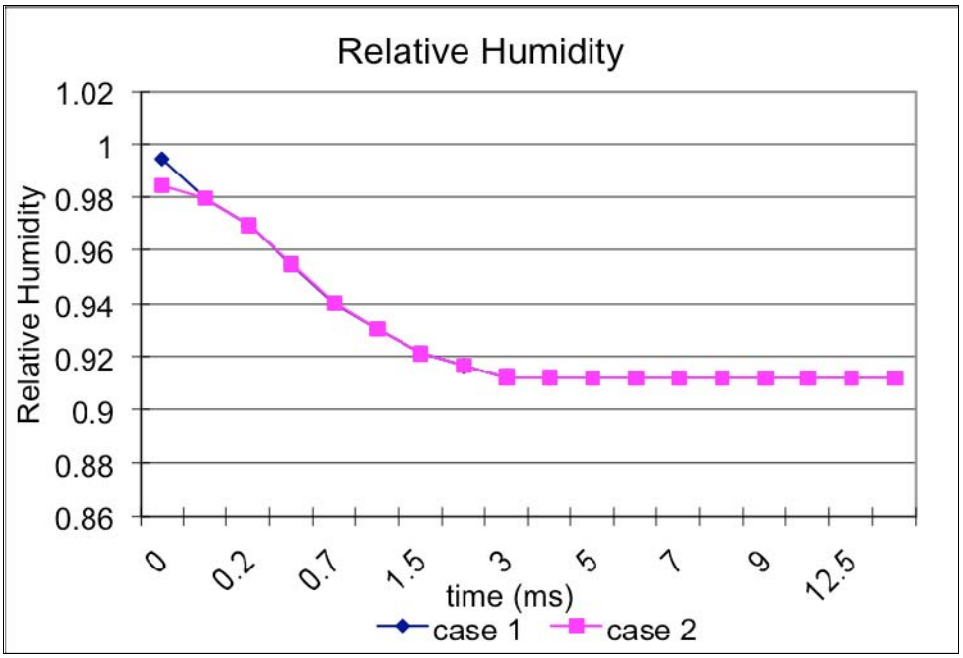

Figure 2.26 Comparison of relative humidity evolution history inside Zone A of case 1 and case 2 for the 2nd study

3rd study: case 1 vs. case 3

A monodisperse initial distribution with in radius = 0.1 micrometer and number concentration = 1.0E11/m^3. Initial temperature equals to 298.15K and initial relatively humidity is 99.4574%. The results are shown in figures 2.27, 2.28, and 2.29.

Figure 27 is the comparison of particle growth history. Figure 2.28 is the temperature evolution history inside Zone A and Figure 2.29 is the relative humidity evolution history inside Zone A.

This time, the same as the 1st study, there is almost no noticeable difference. Although it looks like that there is some discrepancy during 1-2ms for the radius, this discrepancy soon disappeared.

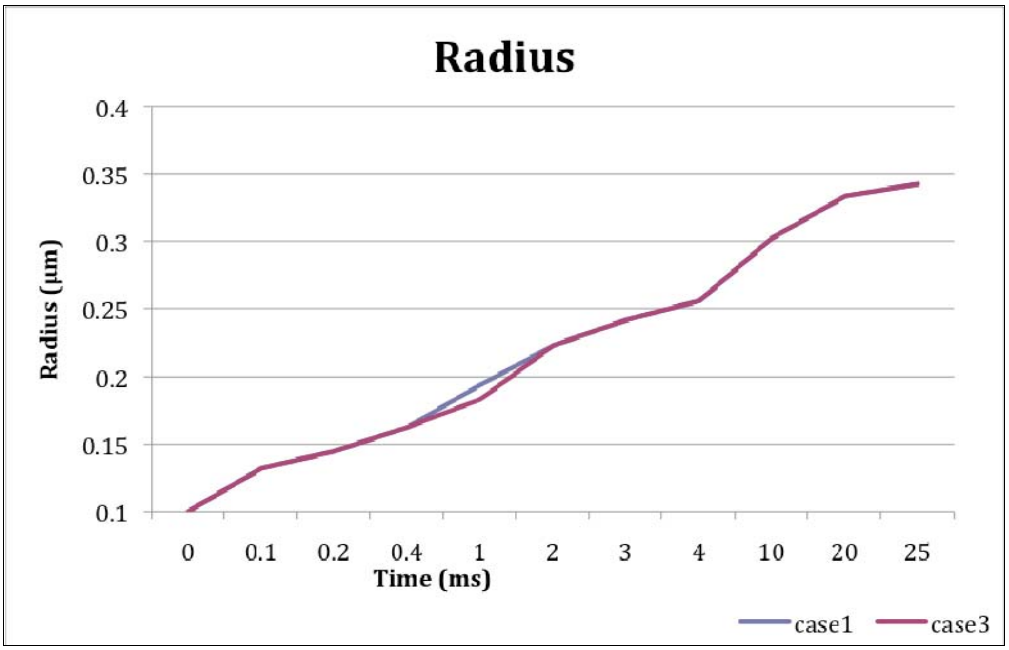

Figure 2.27 Comparison of particle growth history of case 1 and case 3 for the 3rd study

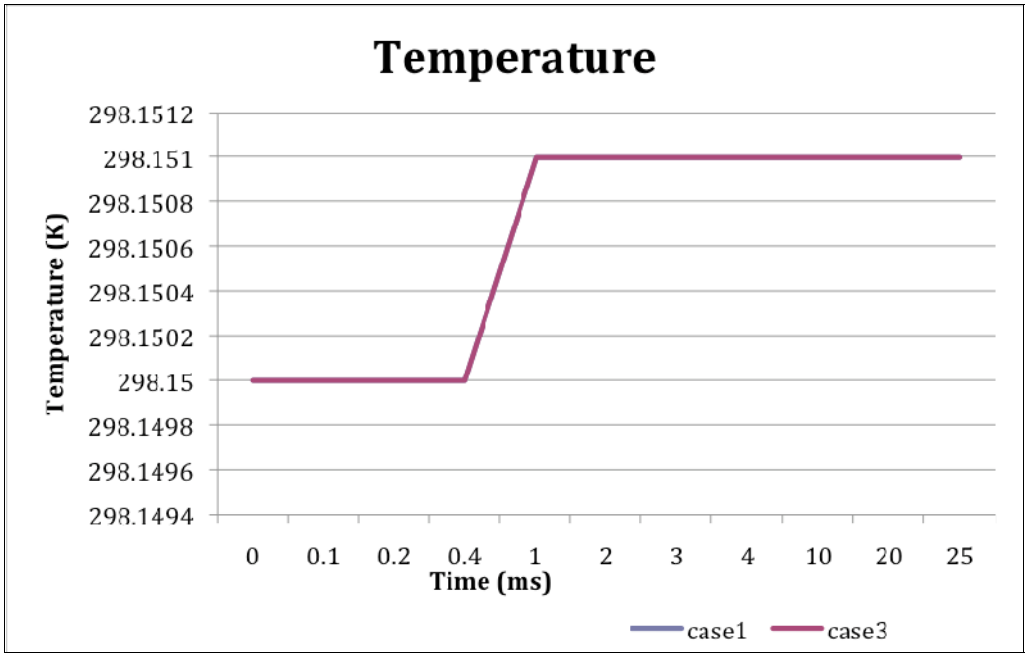

Figure 2.28 Comparison of temperature evolution history inside Zone A of case 1 and case 3 for the 3rd study

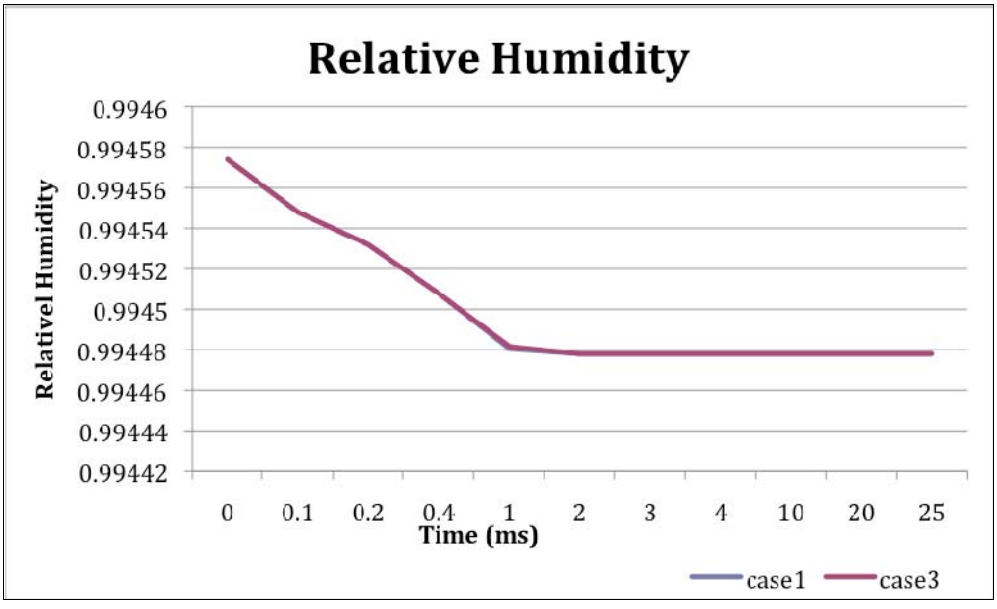

Figure 2.29 Comparison of relative humidity evolution history inside Zone A of case 1 and case 3 for the 3rd study

4th study: case 1 vs. case 3

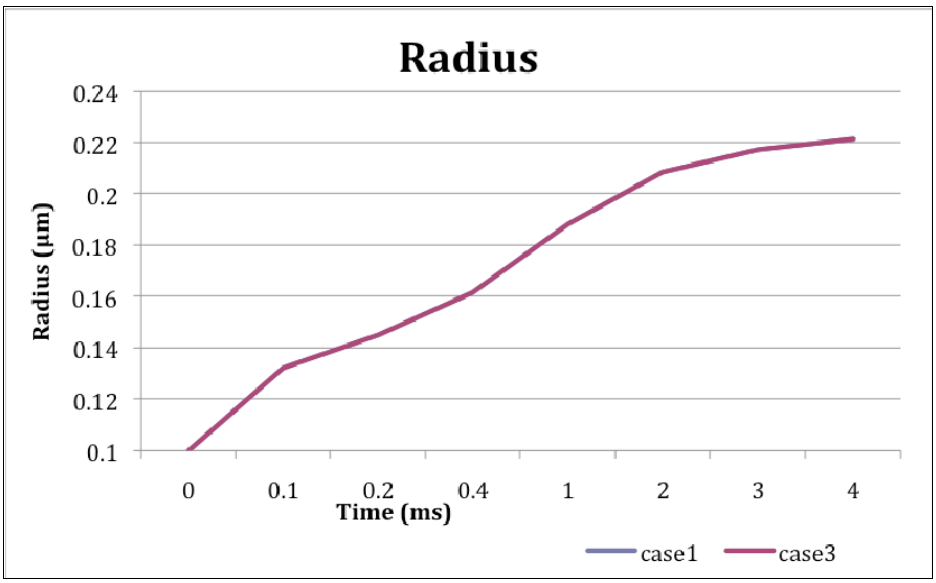

Figure 2.30 Comparison of particle growth history of case 1 and case 3 for the 4th study

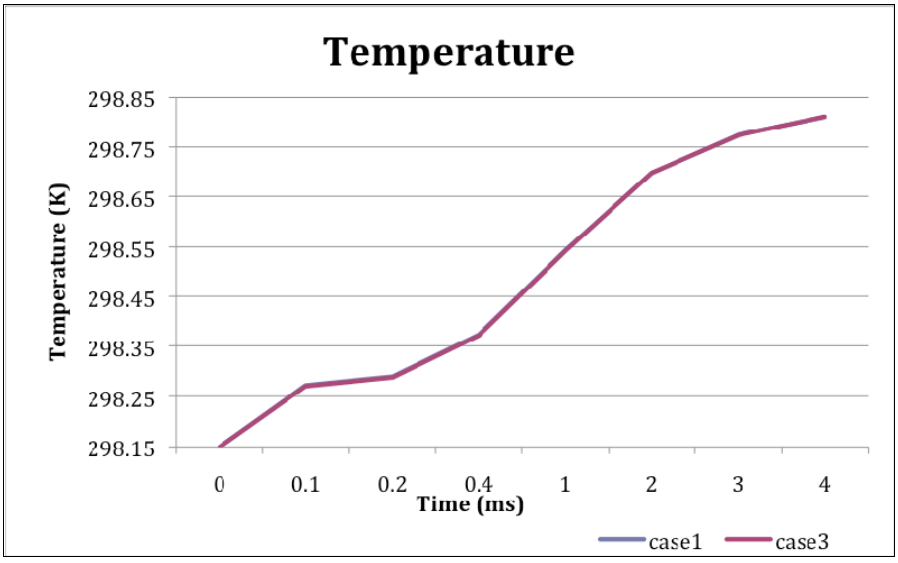

Figure 2.31 Comparison of temperature evolution history inside Zone A of case 1 and case 3 for the 4th study

A monodisperse initial distribution with in radius = 0.1 micrometer and number concentration = 1.0E13/m^3. Initial temperature equals to 298.15K and initial relatively humidity is 99.4574%. The results are shown in figures 2.30 and 2.31.

Figure 2.30 is the comparison of particle growth history. Figure 2.31 is the temperature evolution history inside Zone A.

As we can see, for both particle radius and temperature in Zone A, there is no noticeable difference.

The results of study 1 are that at low number concentration and high relative humidity, changes of 34000 meshes do not make a significant difference. In study 2, although there is some observable difference during the temperature evolution for high number density and low relative humidity, this difference is temporary and vanishes after 4s calculation. Considering the computational expense, we think this is acceptable. From study 3 and 4, no matter for high number density or low number density, there is no observable difference whether a=10*r or a=20*r.

These cases were tested on a X86 platform. CPU is premium 512 and total memory is 3.2GB. With 0.1 μs time step, it took about 30 hrs for case 1, more than 40 hrs for case 2 and less than 24 hrs for case 3 to do a 1s simulation. Since it is concluded that these three cases makes no significant difference in the results, in the future simulations, the way we set up the dimensions and mesh the simulation domain will be the same as case 3.

c. Results-comparison with Model without ANSYS FLUENT

In the following, some demonstration results are given. The aerosol density is 1E13/m^3 consisting of monodisperse 0.1 micro meter sodium nitrate particles. The initial relative humidity is 99.4574%.

Figure 2.32 is the particle growth history. It shows the same characteristics as results simulated by the time dependent aerosol condensational growth model, which was introduced in the previous section.

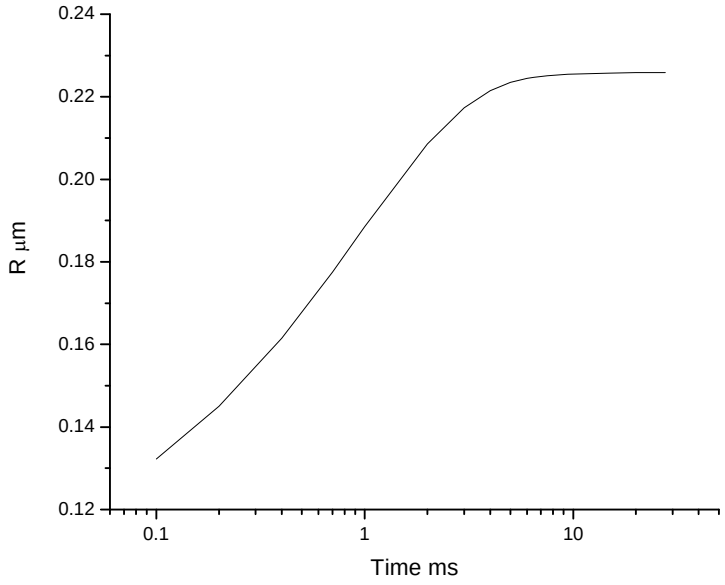

Figure 2.32 Particle growth history

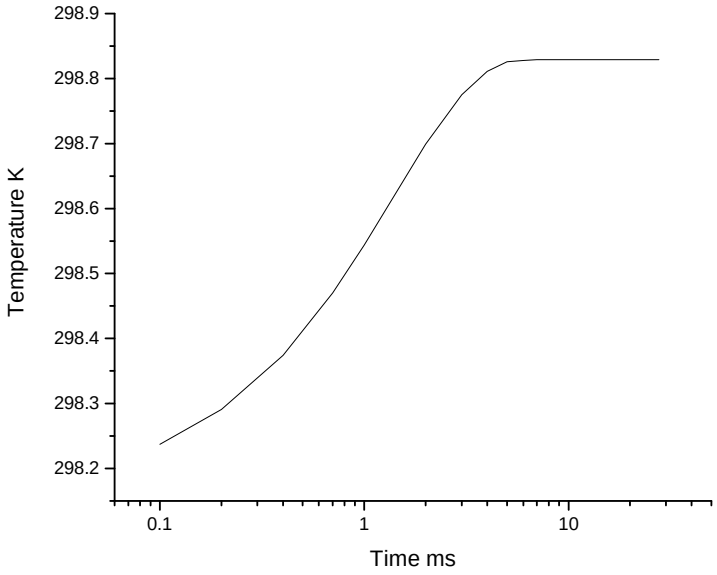

Figure 2.33 Temperature evolution of ZONE A

Figure 2.33 shows the temperature evolution of ZONE A. Again, as what we expect, it keeps the same characters as results simulated by the aerosol condensational growth model.

Figures 2.34 are the contours of turbulent kinetic energy of ZONE A looking in –z direction at 0.1 ms, 0.2 ms, 0.7 ms, 1ms, 2 ms, 3ms, 5ms, 9 ms and 28 ms respectively. As can be seen in the group, the turbulence is relatively more intense at the beginning. This is because of the introduction of the aerosol particles caused a sudden release of heat and depletion of water vapor in ZONE A by their condensational growth. This forces the heat and mass to be transported from the large rectangle into ZONE A. With time, the speed of particle growth slows down and so does the speed of heat release and water vapor depletion. This makes the transportation of heat and mass slow down and the turbulence less intense. Eventually, the rate of particle growth will remain at a very low level (in any) and the turbulent kinetic energy will also be very low and has a tendency to be homogenous distributed.

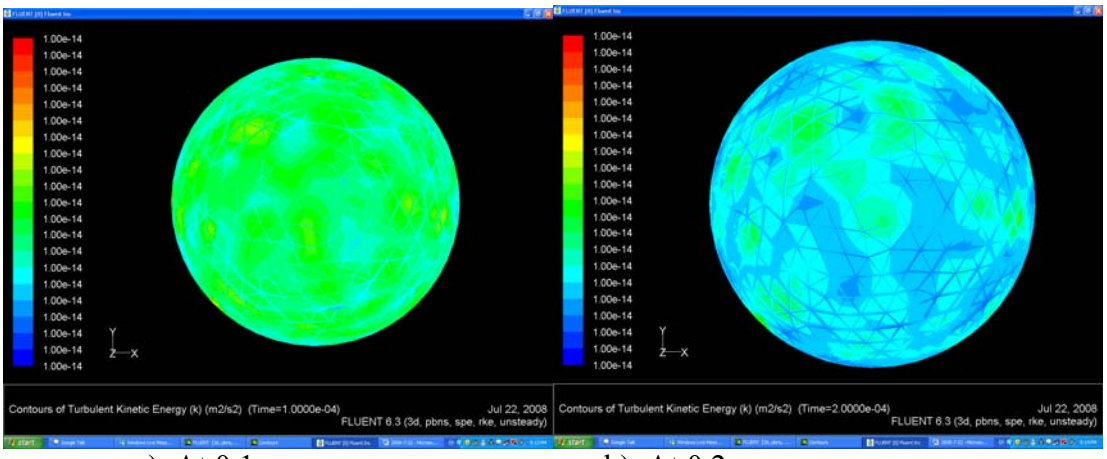

a). At 0.1ms b). At 0.2ms

Figure 2.34 Contours of turbulent kinetic energy of ZONE A looking in –z direction. at a). 0.1 ms, b). 0.2 ms, c). 0.7 ms, d). 1ms, e). 2 ms , f). 3ms, g). 5ms, h). 9 ms and i). 28 ms respectively

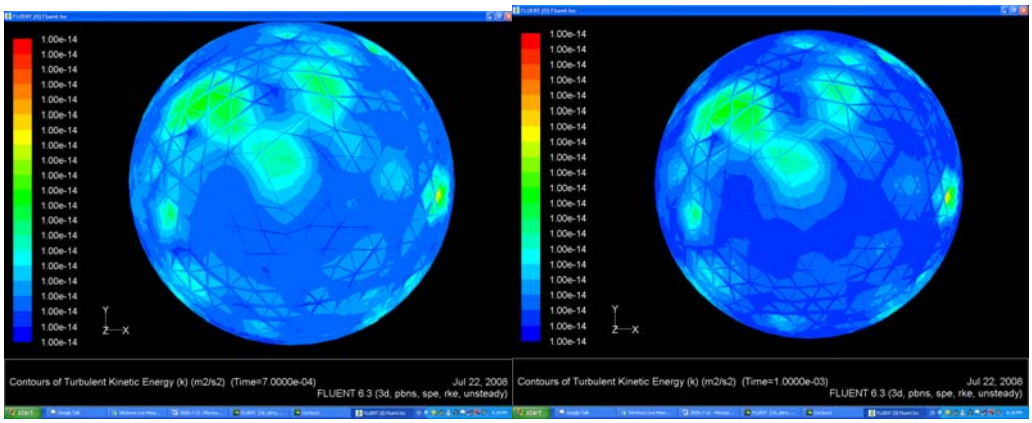

c). At 0.7ms d). At 1.0ms

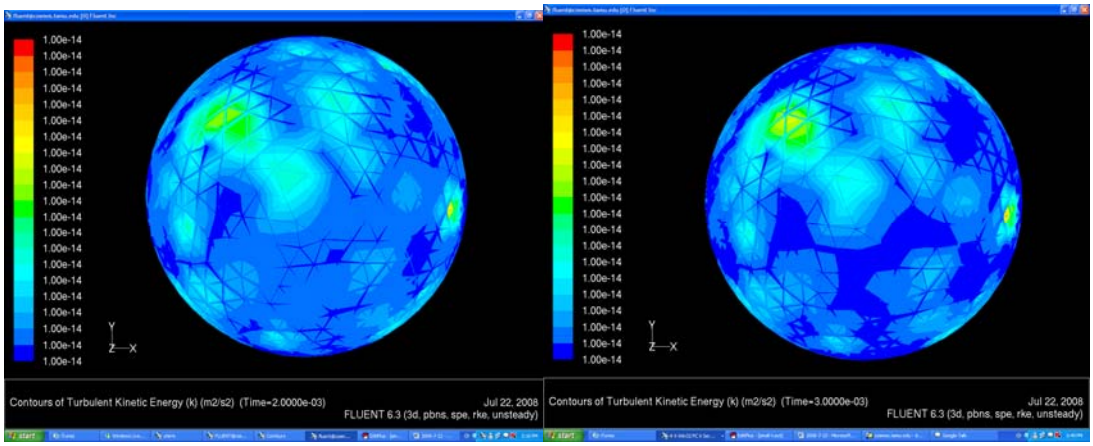

e). At 2.0 ms f). At 3.0 ms

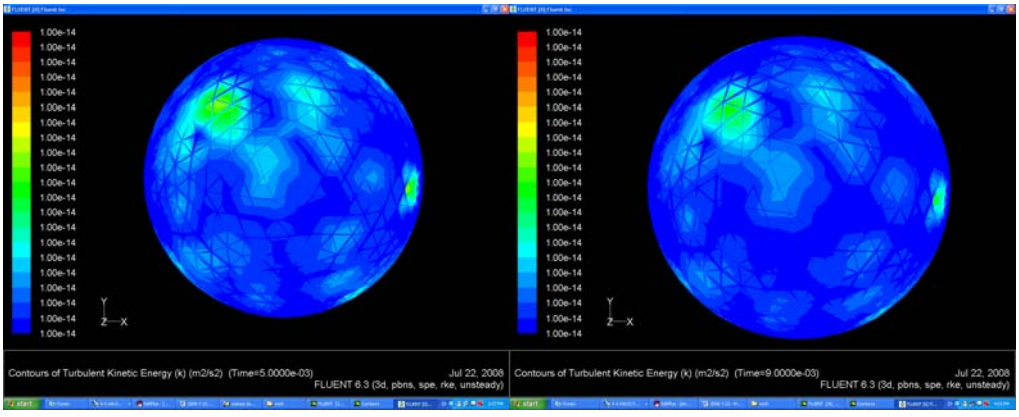

g). At 5.0 ms h). At 9.0 ms

Figure 2.34 Continued

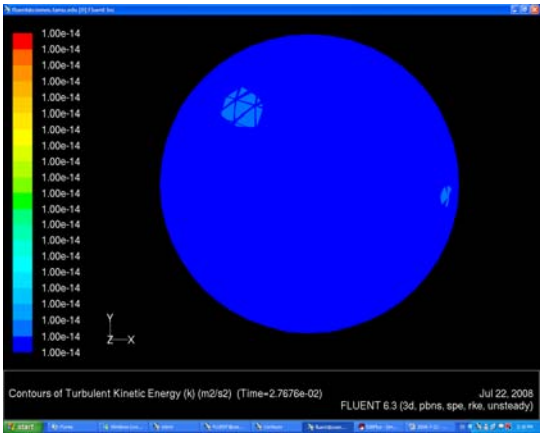

i). At 28.0s

Figure 2.34 Continued

The next step is to compare the simulation results of this prototype model to the results of section 1 of this chapter, from the aerosol condensational growth model alone without ANSYS FLEUNT, to see the effects of introduction of turbulent transport.

To serve this purpose, we compared the results for 4 different initial setups. The details of these four setups are presented in Table 2.2. For all the setups, the initial temperatures are 298.15K and particles are monodisperse.

Table 2.2 Four different initial setups

Setup No.	Particle Radius (μm)	Relative Humidity (%)	Particle Density
1	0.1	99.5	1E11
2	0.1	101.4	1E13
3	0.1	99.5	1E13
4	0.1	101.4	1E11
5	0.25	101.4	1E13

Some of the results of the comparison are presented as below in figures 2.35 to 2.38.

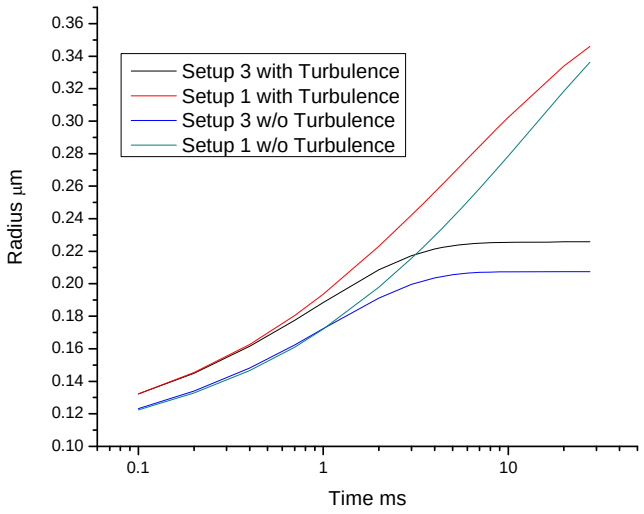

Figure 2.35 Comparison of particle growth for setup 1 and 3

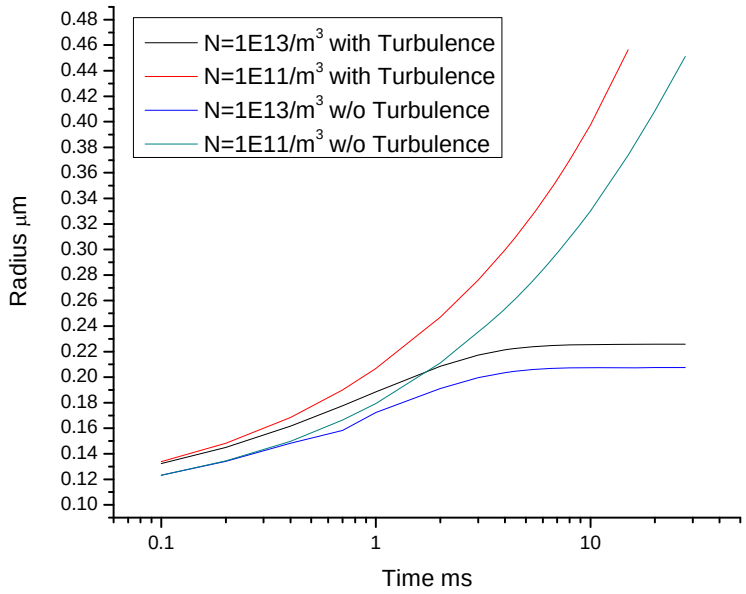

Figure 2.36 Comparison of particle growth for setup 2 and 4

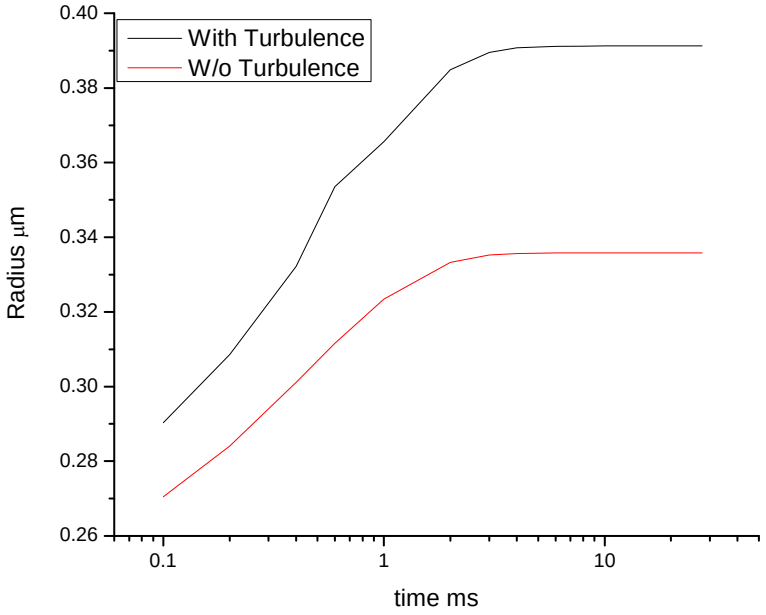

Figure 2.37 Comparison of particle growth for setup 5

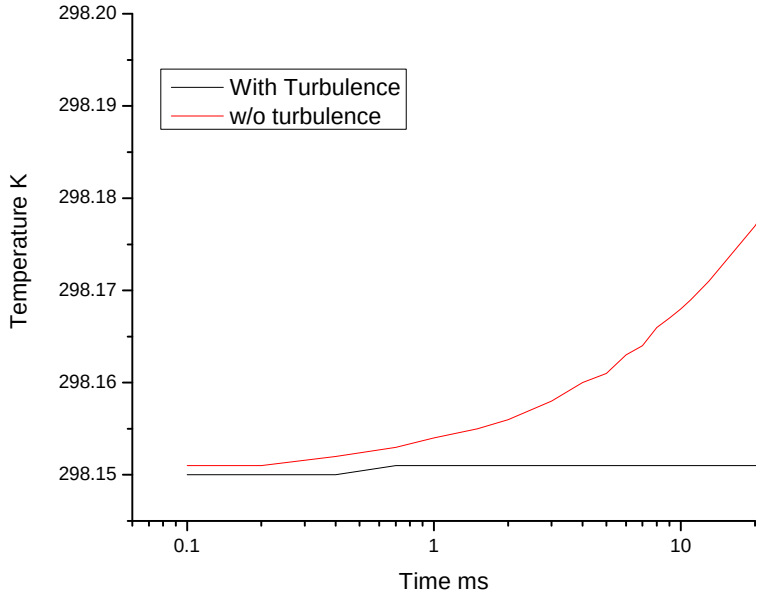

Figure 2.38 Comparison of temperature evolution for setup 1

We can see from all the results above, the introduction of fluid dynamic simulation materially changes the results. Compared to the results without turbulence simulation involved, with the presence of turbulence, particles grow more and temperatures stay more stable. The reason for this is because the transport from outside ZONE A into inside ZONE A keeps the relative humidity inside ZONE A higher than without this transport and consequently makes the particle grow more; similarly, the transport of heat from inside ZONE A to outside ZONE A keeps the temperature inside ZONE A lower than that without this heat transportation.

We did not test more setups because these results are completely in agreement with what we have expected and should be enough to justify the validity for this part of this model.

d. Results-comparison of different number density

Next we tested the effect of number density on particle growth in this model. We tested 3 initial setups with 5 different number densities, which are 1E11/m^3, 5E11/m^3, 1E12/m^3, 5E12/m^3 and 1E13/m^3. Particles are monodisperse. The details of the 3 initial setups are listed in Table 2.3.

Table 2.3 Three different initial setups

Setup No.	Particle Radius (μm)	Initial Relative Humidity (%)
1	0.1	101.4
2	0.25	99.5
3	0.1	99.5

Figures 2.39 – 2.47 are the plots of particle growth history, temperature evolution history and relative humidity evolution history for these three setups, respectively.

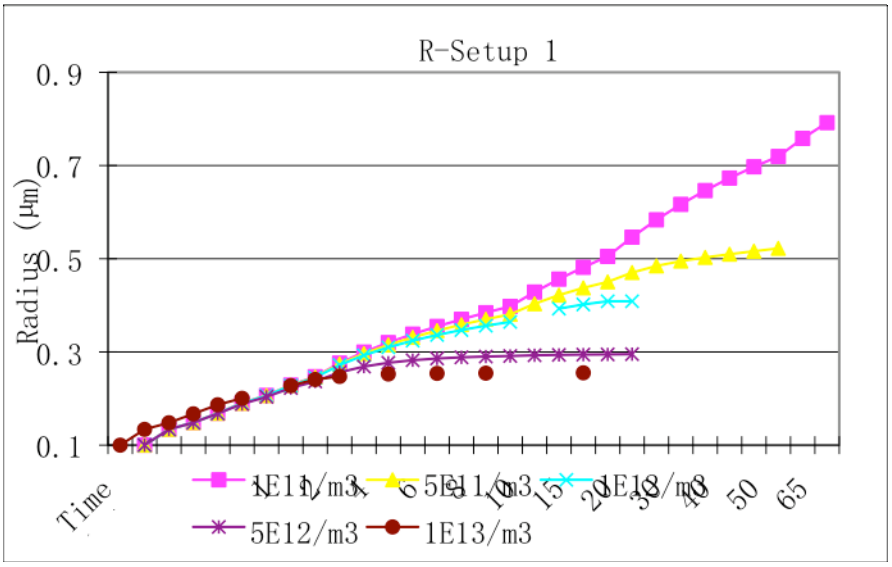

Figure 2.39 Comparison of particle growth history of different number concentration for the 1st setup

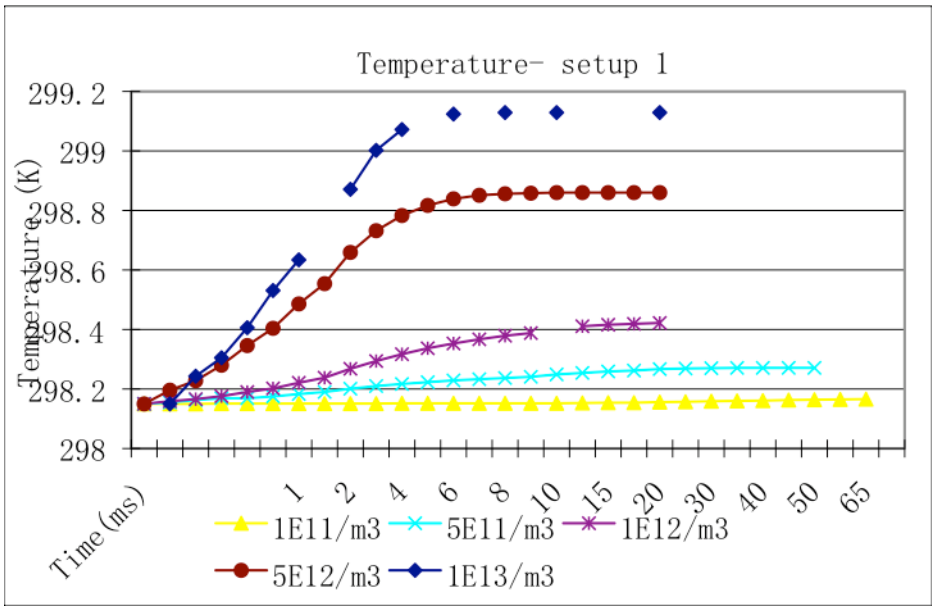

Figure 2.40 Comparison of temperature evolution history inside Zone A of different number concentration for the 1st setup

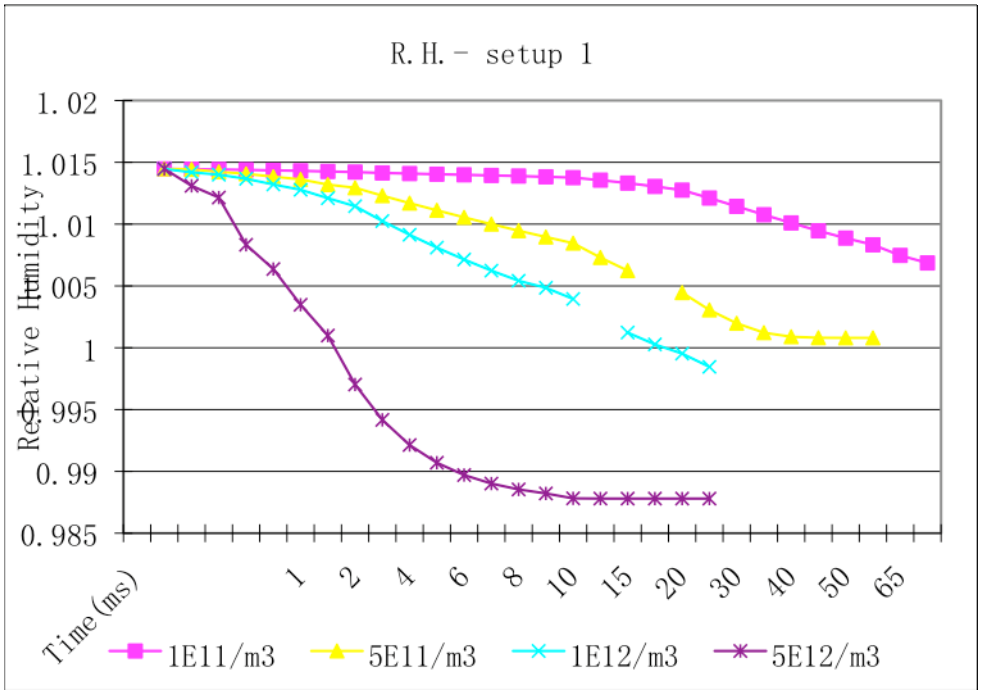

Figure 2.41 Comparison of relative humidity evolution history inside Zone A of different number concentration for the 1st setup

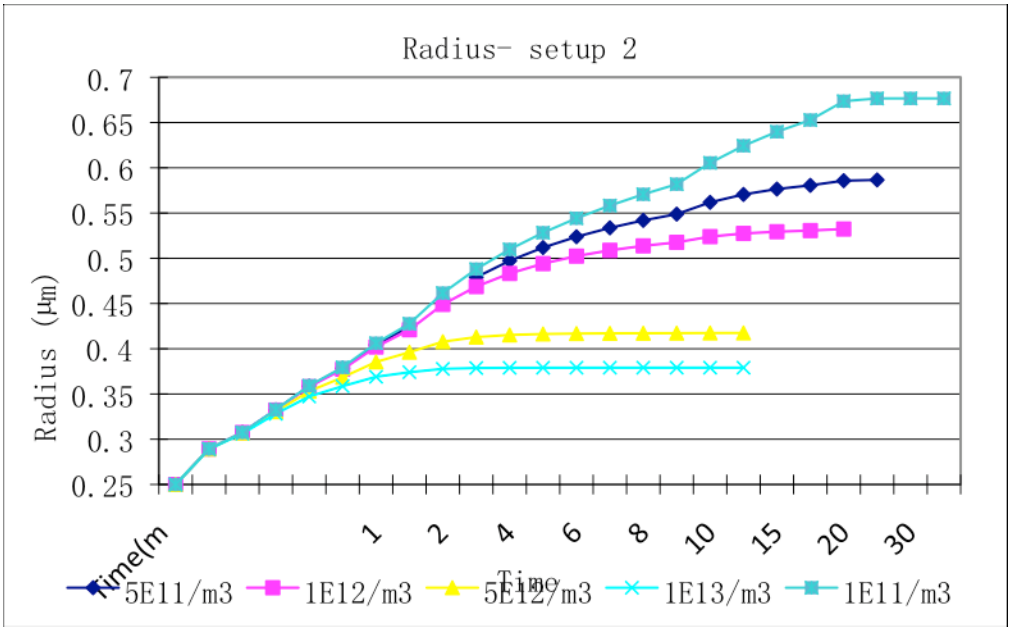

Figure 2.42 Comparison of particle growth history of different number concentration for the 2nd setup

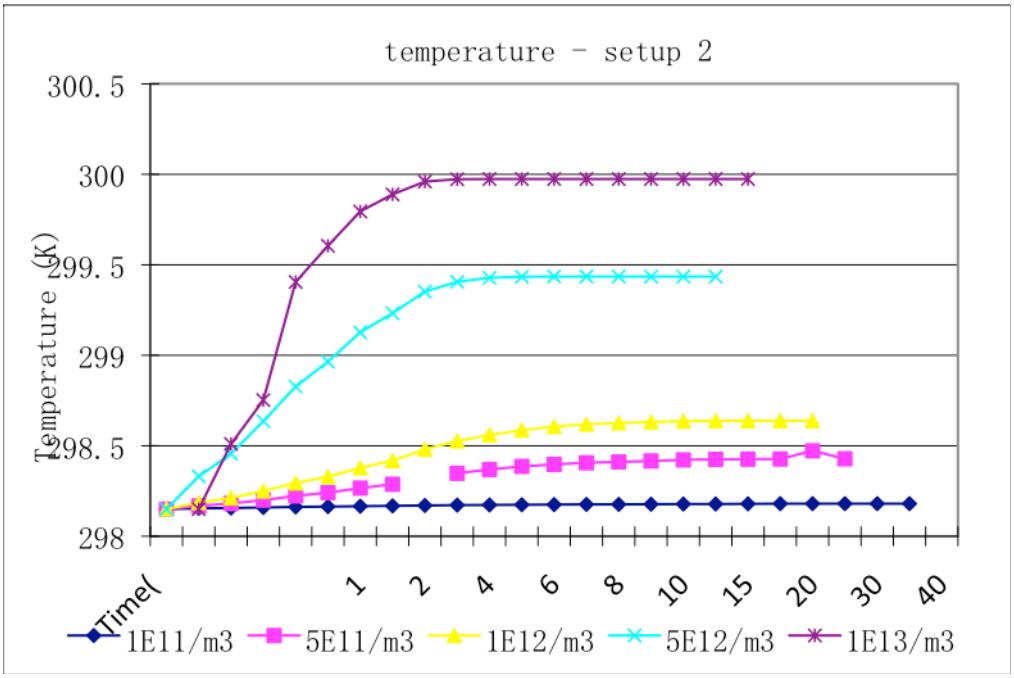

Figure 2.43 Comparison of temperature evolution history inside Zone A of different number concentration for the 2nd setup

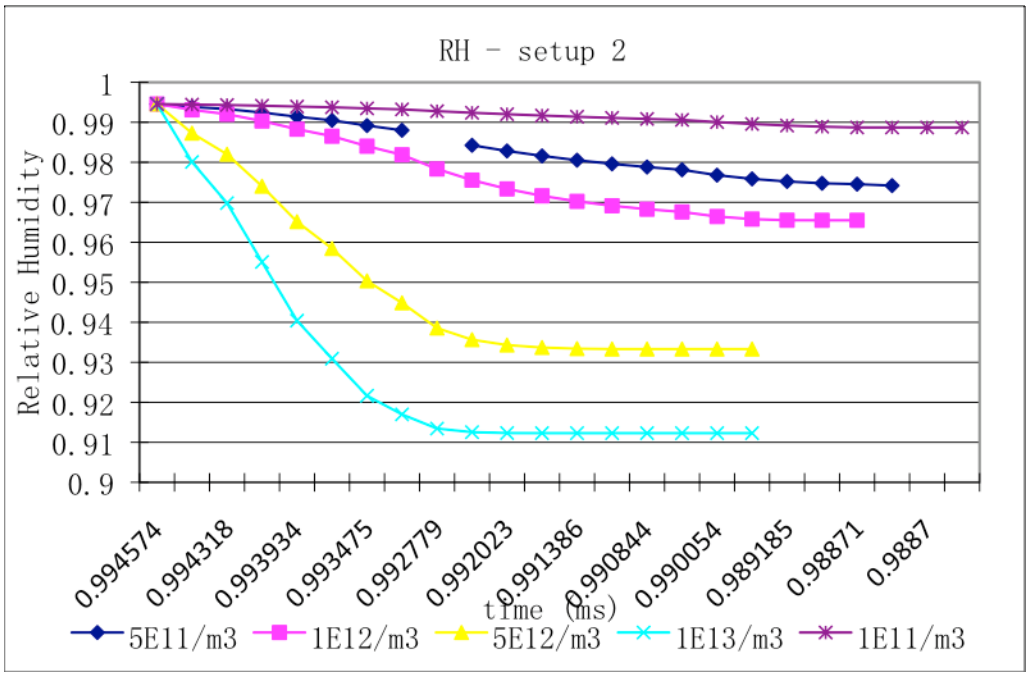

Figure 2.44 Comparison of relative humidity evolution history inside Zone A of different number concentration for the 2nd setup

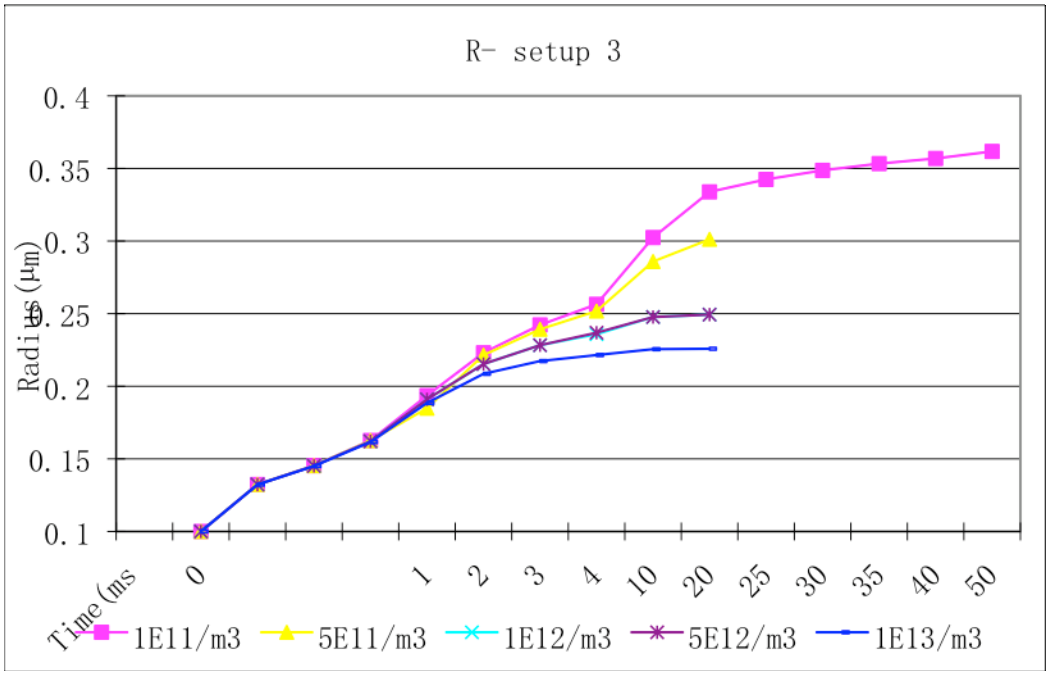

Figure 2.45 Comparison of particle growth history of different number concentration for the 3rd setup

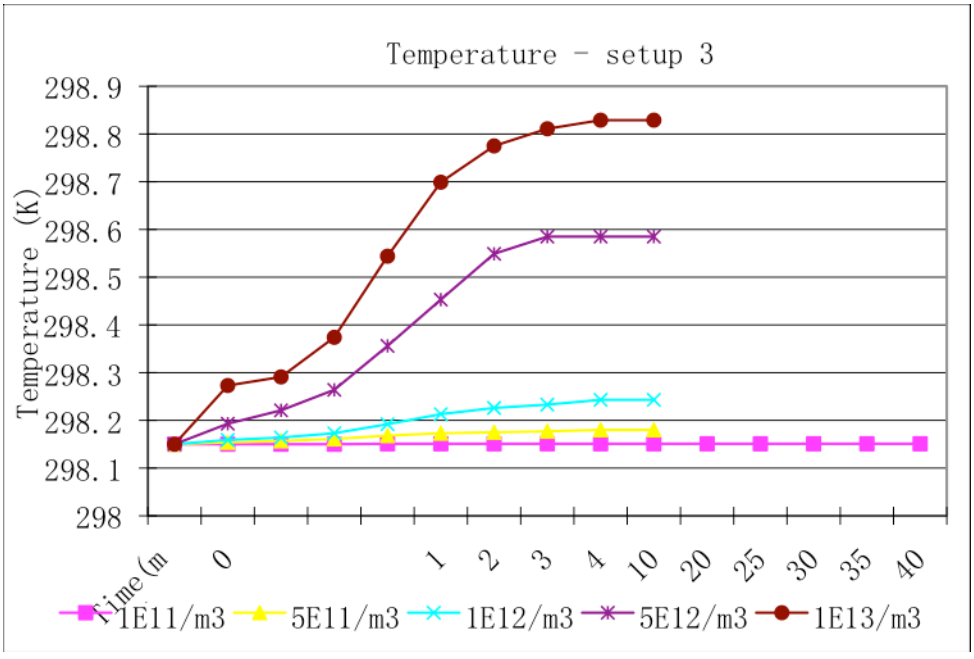

Figure 2.46 Comparison of temperature evolution history inside Zone A of different number concentration for the 3rd setup

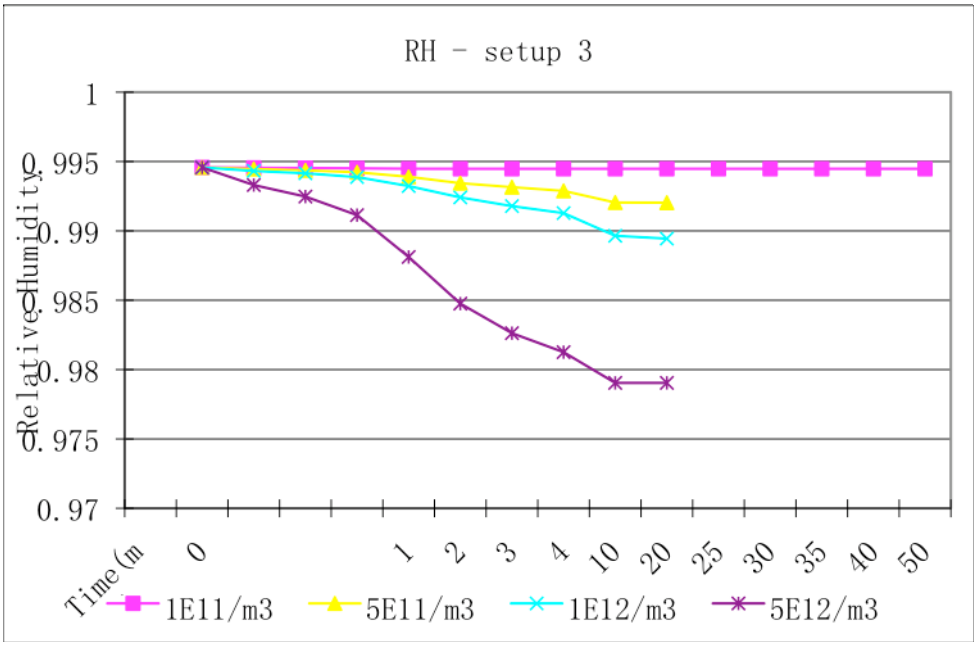

Figure 2.47 Comparison of relative humidity evolution history inside Zone A of different number concentration for the 3rd setup

These results are similar to those from calculations without ANSYS FLUENT, that is when everything else is the same, with lower number density, particles get more growth, less heat releases and less water vapor is depleted. This is exactly what we expected to see based on the results of the aerosol condensational growth model without CFD.

4. Conclusions

In this chapter, firstly an aerosol condensational growth model was introduced. This model is capable of coupling heat and mass equations when calculating the growth of aerosol particles. The simulation results have shown the dependency of particle growth on the number concentration and initial environmental relative humidity. Then a model combined this aerosol condensational growth model with fluid dynamic simulation by ANSYS FLUENT was developed. This model permits simulating the

more realistic situation in which cloud aerosol particle grow. It allows the heat and mass transport between the inside and the outside of the air parcel in which the aerosol particles reside. A sensitivity study was done and some example results were presented.

The importance of involving of ANSYS FLUENT is that it can simulate an environment that is very similar to the real atmosphere where the CNs grow. The heat and mass are transferring between the outside and inside of the air parcel, in which the aerosols reside, while the process of aerosol condensation is absorbing (releasing) heat and water vapor; this is exactly what happens in the real atmosphere. Without the contribution of ANSYS FLUENT, the air parcels is more likely to become isolated and no vapor will be provided to facilitate the growth, which is critical to the growth of aerosols in the atmosphere. Moreover, the transfer of heat prevents the parcel from being unrealistically overheated, and hence has a significant effect on the aerosol growth. From all these points, it is not hard to see that the combination of aerosol heat and mass transfer with fluid dynamic simulation by ANSYS FLUENT would both quantitatively and qualitatively change the results.

In the next chapter, we will use a more sophisticated version of this model to explore the impact of RH distribution and number concentration on cloud inorganic aerosol condensational growth.

CHAPTER III

CNN CONDENSATIONAL GROWTH WITH STOCHASTIC SUPERSATURATIONS

1. Introduction

Water vapor is not homogeneously distributed in the atmosphere. Even more, its detailed distribution is largely stochastic. The water vapor content differs from one position to another and this is the reason why clouds always appear randomly in the sky and the distribution of cloud droplets within clouds is anything but uniform. As summarized by Pruppacher and Klett (1997), the relative humidity of clouds usually remains close to 100%, although considerable departures from this value have been observed. It is said relative humidity in cloud both as high as 107% and as low as 81% has been observed.

Considerable work (eg. Twomey 1959, Fitzgeral 1972, Ji and Shao 1998, and Kulmala et al. 1997) has been devoted to studying the relationship of atmospheric water vapor content and size distribution of CCN. Twomey (1959) proposed the power law relationship between the number concentration of CCN and supersaturation S. This power law relationship has been widely accepted and expanded. Fitzgerald proposed an exponential relationship in 1972. Ji and Shaw (1998) studied this relationship experimentally. None of these studies addressed the stochastic problem, so a single value of supersaturation S is always assumed. Kulmala et al. (1997) studied the effect of fluctuation of saturation with time on droplet growth. But the spatial stochastic distribution problem is still left addressed.

The practical problem for cloud measurements is, usually, that in-flight measurements from airplane platforms traversing clouds can only determine an average relative humidity over a certain sampling path. An average value cannot accurately describe the detailed relative humidity distribution within that distance. For example, two totally different distributions of relative humidity can result in the same average

value. What we propose here is to quantitatively study this stochastic effect of relative humidity on the CNN condensational growth, which is complementary to the previous study.

Unlike the previous work, we simultaneously simulate the aerosol growth in multiple air parcels with different initial relative humidities. These humidities are randomly distributed according to a power law distribution derived by Sherwood et al. (2006) based upon atmospheric measurements. Separated air parcels with different relative humidities, in which aerosols reside, are exposed to the same environment. Heat and mass are allowed to transfer among the air parcels and between the air parcel and environment. Then, although the aerosols reside in different air parcels, they are not isolated from each other. More details of the model are given below.

2. Model description

The main idea of this model is to adapt the methodology of the prototype introduced in Chapter II to aerosol systems distributed in space. First, as demonstrated in Figure 3.1, we make small, hemispherical zones with radius of r and the embedding volume is a cube with dimension of (110r+10m) instead of an a*a*a/2 rectangular solid. Second, we build in the model 19 small zones instead of only 1 zone A in the prototype; and since these 19 hemispheres are identical, they are all still called Zones A. In this model, we will randomly assign relative humidity to these 19 hemispheres according to a power law distribution. The mean value of the power law distribution, which is the average value that is generally cited, will be assigned to the cube. Initially, in the 19 hemispheres there are aerosols with identical size distributions. Aerosol condensational growth (or evaporation, depending on the relative humidity of the certain zone A) is allowed to happen in all 19 zones A simultaneously. The positions of the 19 hemispheres are demonstrated in figure 3.2, if we take the center the cube as the origin, the coordinates of the 19 hemispheres are (0, 0, 0), (3r, 0, 0), (-3r, 0, 0), (0, 3r, 0), (0, -3r, 0), (0, 0, 3r), (0, 0, -3r), (6r, 0, 0), (-6r, 0, 0), (0, 6r, 0), (0, -6r, 0), (0, 0, 6r), (0, 0, -6r), (9r, 0, 0), (-9r, 0, 0), (0, 9r, 0), (0, -9r, 0), (0, 0, 9r) and (0, 0, -9r). Aerosols are assumed

not to move out of the specific zone A where they initially reside. As a consequence of the aerosol condensational growth (or evaporation), heat will be released (or absorbed) and water vapor will be absorbed (or released). Then heat and mass transfer among the 19 zones A and the large volume.

Similarly as in the prototype, at every time step we use the aerosol condensational growth model introduced in the last chapter to calculate the heat release and water vapor depletion in the 19 A zones and pass these two variables to ANSYS FLUENT. Then ANSYS FLUENT software simulates the interaction between zones A and the embedding volume. When a new equilibrium is reached, the relative humidity and temperature of all zones will be updated and then next time step starts.

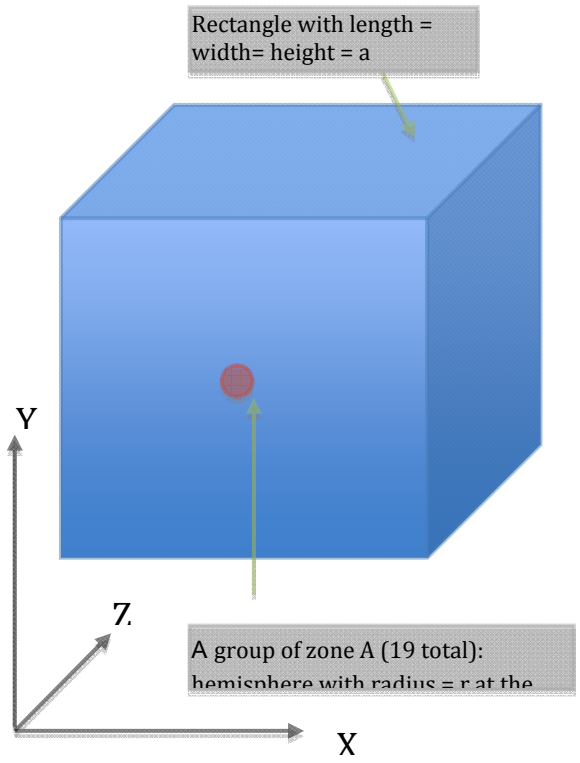

Figure 3.1 Demonstration of the model

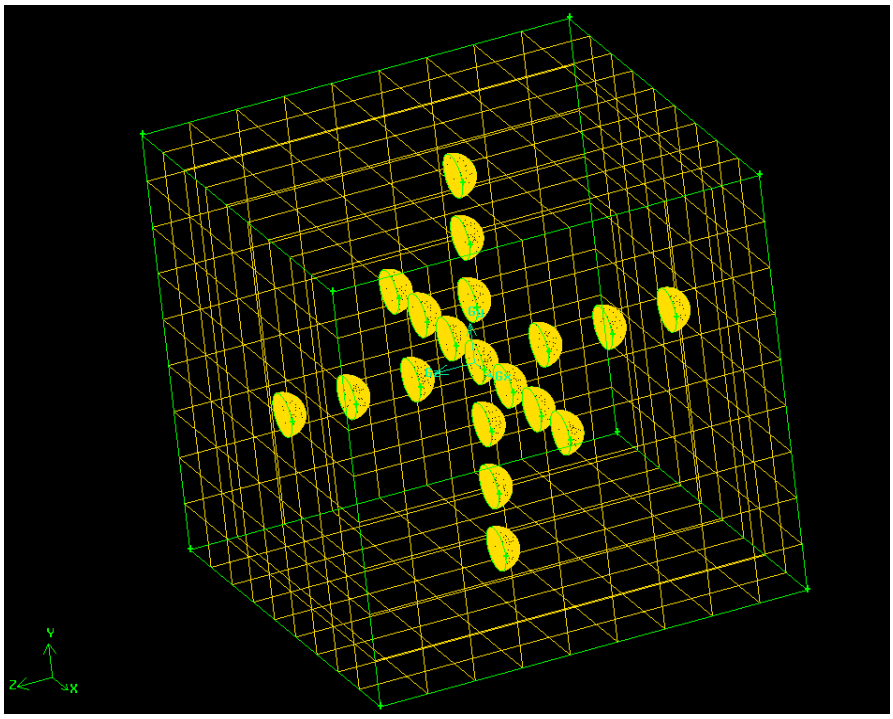

Figure 3.2 Detailed position of the 19 A Zones

3. Power law distribution of relative humidity

Equation 3.1 is the power law distribution (Sherwood et al. 2006) will be used here. Although this distribution was derived for atmospheric date< 100% relative humidity, we are assuming it can be extended to these slightly higher value of RH for lack of a better model.

$$P_R(R) \propto R^{r-1} \tag{3.1}$$

Here R is the relative humidity and r is a constant from observation, which we choose to be 0.67 from three candidates that are given in Sherwood et al. (2006) paper. So the actual distribution equation is:

$$P_R(R) = AR^{r-1} \tag{3.2}$$

Here A is a constant decided by the upper and lower limit of the relative humidity distribution, which are chosen by the interest of the study. Suppose we will

use a distribution with upper limit b and lower limit a, then the distribution can be written as below:

$$P_R(R) = AR^{-0.33}$$
$$R \in (a,b) \tag{3.3}$$

The cumulative possibility from a to b should be 1, so we have:

$$\int_a^b P_R(R)\,dR = 1 \quad \Rightarrow \int_a^b AR^{-0.33}\,dR = 1 \tag{3.4}$$

$$\Rightarrow \frac{A}{0.67} R^{0.67}\Big|_a^b = 1 \;\Rightarrow A = \frac{0.67}{b^{0.67} - a^{0.67}} \tag{3.5}$$

The mean value $\tilde{R}$ is derived as below:

$$\tilde{R} = \int_a^b R_R(R) \times R\,dR \Rightarrow A\int_a^b R^{0.67}\,dR \Rightarrow \frac{A}{1.67}(b^{1.67} - a^{1.67}) \tag{3.6}$$

In this chapter, 7 different distributions will be used. We name them case 1 to case 7. The details of these 7 cases are listed in Table 3.1.

Table 3.1 Upper limit and lower limit of the relative humidity for cases 1-7

Case No.	Lower Limit a	Upper Limit b	$\tilde{R}$
1	65%	110%	86.9%
2	70%	100%	84.7%
3	91%	110%	100.4%
4	70%	101%	85.2%
5	70%	102%	85.7%
6	70%	104%	86.6%
7	70%	106%	87.6%

4. Results and discussion

Here we take ammonium sulfate, which is commonly found in the atmosphere, as the representative aerosol material for the calculations. The initial temperature is 298.15k for all cases. The activity data was taken form Tang (1997). The change in water activity with temperature was ignored because the temperature remains pretty stable in most cases. When the number density is lower than 1E12/m^3, the fluctuations

of temperature are always within the range of -+ 3K. The largest temperature change happens when the number density equals to 1E13/m^3, and it is about 10K, which is not small any more. But 1E13/m^3 is a very high number density and we do not expect to see that number much in the real atmosphere.

The same lognormal distribution with mean value of 0.2 micrometer and geometric standard deviation of 0.15 micrometer will be used for the initial particle distribution in all the calculations. We divide this lognormal size distribution into size bins of 0.025-micrometer radius and assume the smallest particles have radius of 5 nanometer and the largest particles have radius of mean radius + 3 standard deviations (0.65μm here). Particles were initially equilibrated at $\widetilde{R}$, except case 3 at 99% relative humidity.

For every case 1-5, 7 different particle number concentrations are calculated separately; they are 1.8E7/m^3, 1.8E8/m^3, 1.8E9/m^3, 1.8E10/m^3, 1.8E11/m^3, 1.8E12/m^3, and 1.8E13/m^3. Since during the process of calculations, we found particles always do not grow with high densities, for our cases 6 and 7, only the lower 5 densities are used. The total calculation time is 3.0 s for all cases. The calculational results are shown in Figures 3.3(a)-(f) through 3.9(a)-(f).

Case 1 for NH_4SO_4

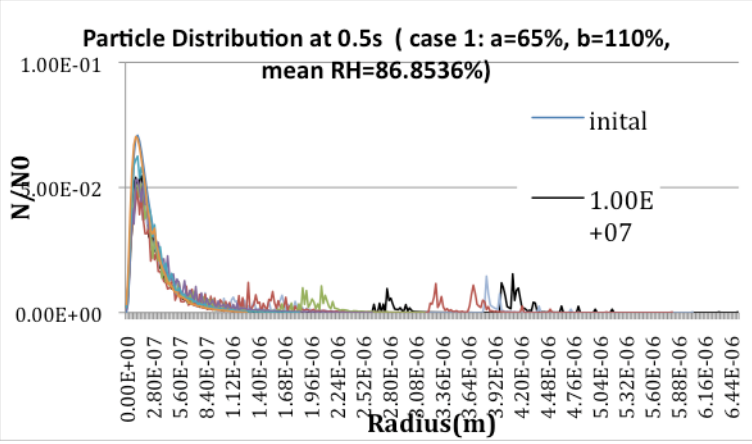

Figure 3.3(a) Calculation results at 0.5s of case 1 for NH_4SO_4

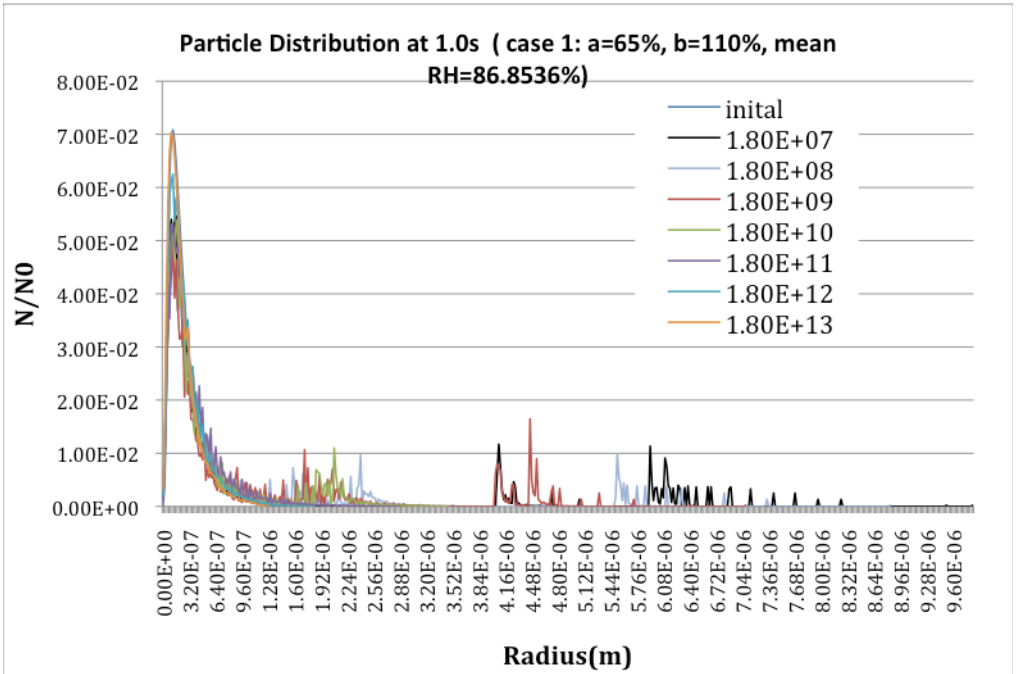

Figure 3.3(b) Calculation results at 1.0s of case 1 for NH_4SO_4

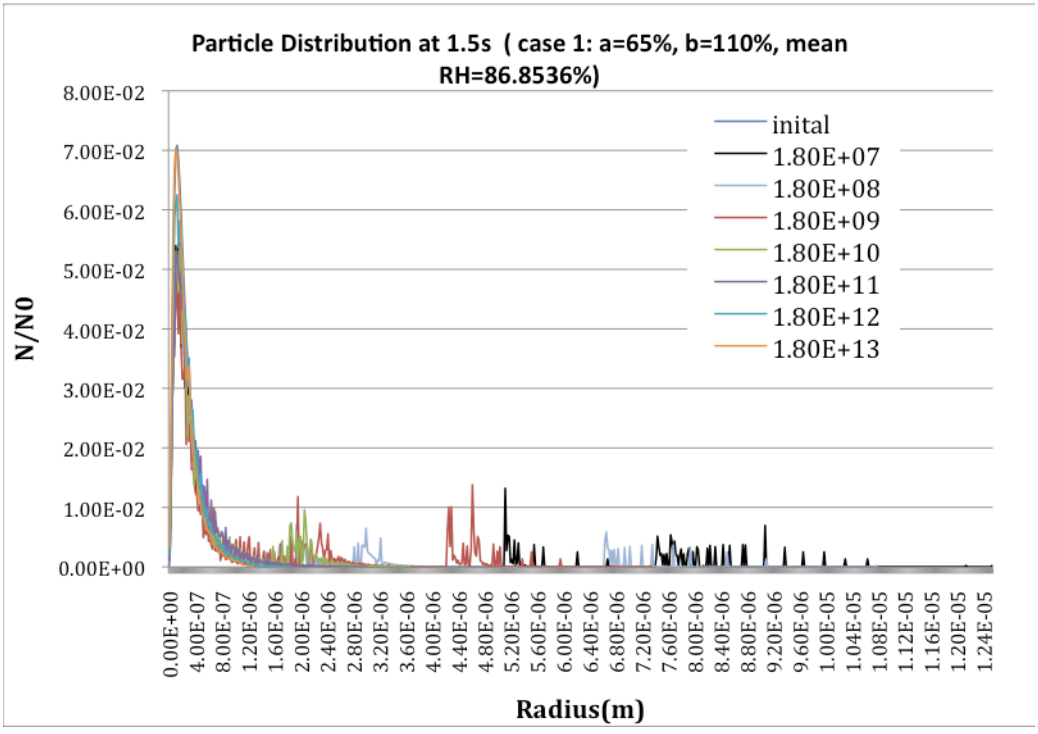

Figure 3.3(c) Calculation results at 1.5s of case 1 for NH_4SO_4

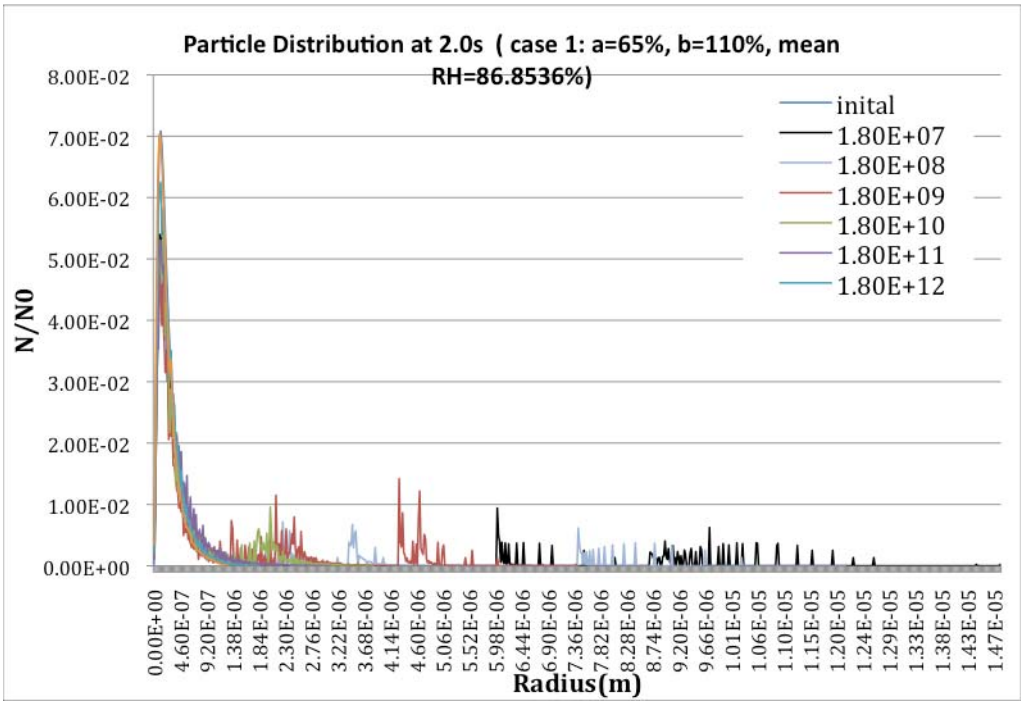

Figure 3.3(d) Calculation results at 2.0s of case 1 for NH_4SO_4

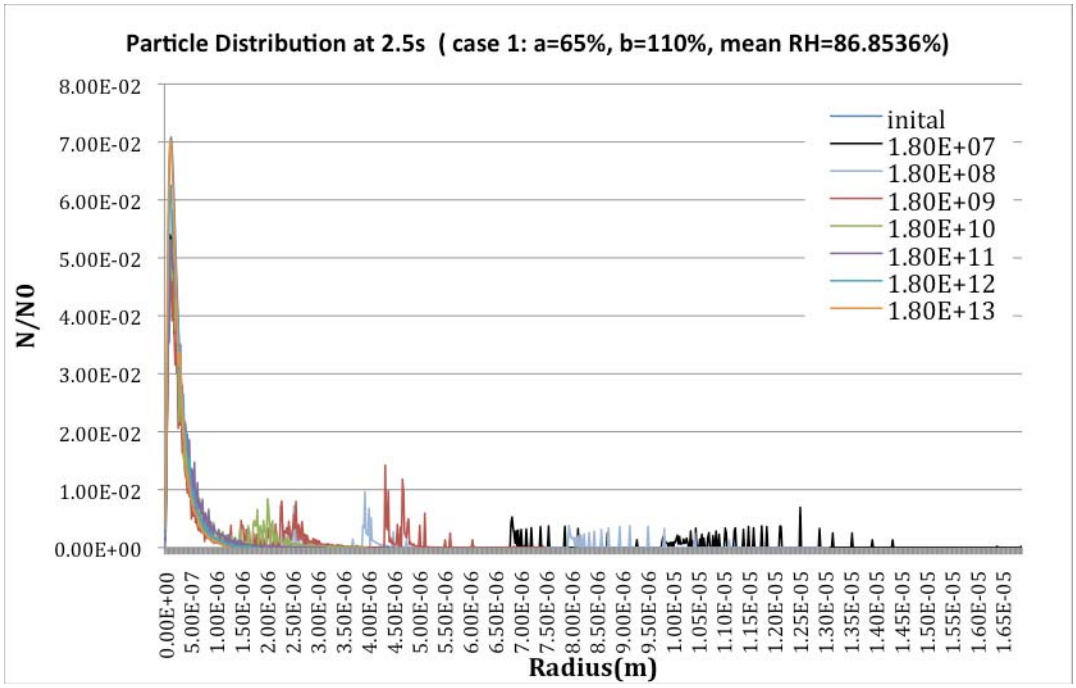

Figure 3.3(e) Calculation results at 2.5s of case 1 for NH_4SO_4

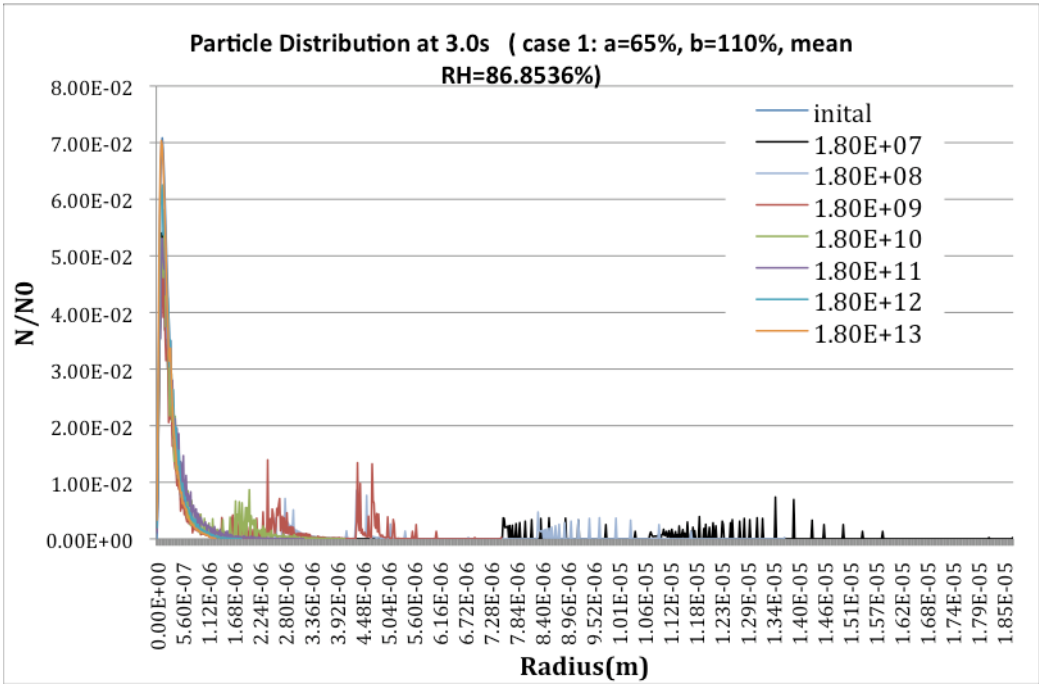

Figure 3.3(f) Calculation results at 3.0s of case 1 for NH_4SO_4

From Figures 3.3(a) - 3.3(f), we can see that in this case, when particle number density is higher than 1.8E10/m^3 (1.8E11/m^3, 1.8E12/m^3, 1.8E13/m^3), the particles hardly grow from the very beginning. When the number density is equal to or lower than 1.8E10/m^3, the lower the density, the more the particles grow. At 0.5s, there is little difference among the particle distribution of 1.8E7/m^3, 1.8E8/m^3 and 1.8E9/m^3 and they all have two groups of peaks; one is around 1µm to 2µm and another at 3.6µm ~ 4.2µm. The discrepancy of particle size among different number densities increases along with time. After 3.0s, we can see peaks between 11µm – 14µm for number density of 1.8E7/m^3, between 8µm – 11µm for 1.8E8/m^3 and between 4.3µm – 4.8µm for 1.8E9/m^3. For density of 1.8E10/m^3, it looks like the peaks remain about 2.0 µm, which means after 0.5s, the particles have lost the ability to grow due to water vapor depletion. According to Rosenfeld and Gutman (1994), particles can be considered as activated when their radii reach 7µm. According to these results, a fraction of particles with density of 1.8E7/m^3 and 1.8E8/m^3 have already grown beyond 7µm in radius by 3s;

although none of the particles with density of 1.8E9/m^3 have reached this criterion after 3μm, we can still speculate that it is possible for the some of these particles to continue growing and reach a 7μm radius if there is sufficient time. So, we can conclude that at this relative humidity condition, particles can be activated only when the number density is lower than 1.8E10/m^3.

Case 2 for NH_4SO_4

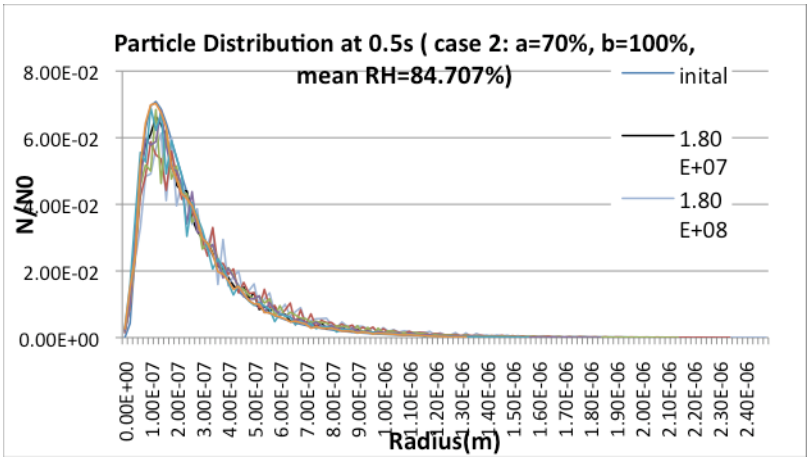

Figure 3.4(a) Calculation results at 0.5s of case 2 for NH_4SO_4

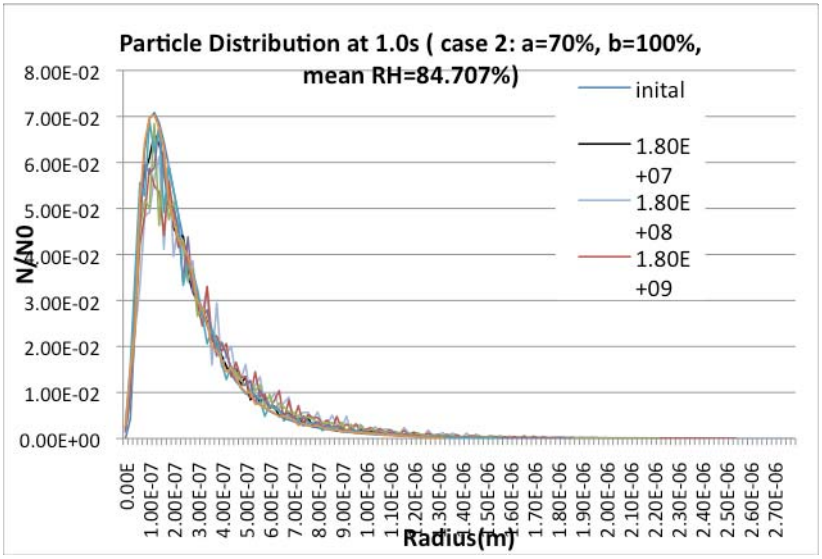

Figure 3.4(b) Calculation results at 1.0s of case 2 for NH_4SO_4

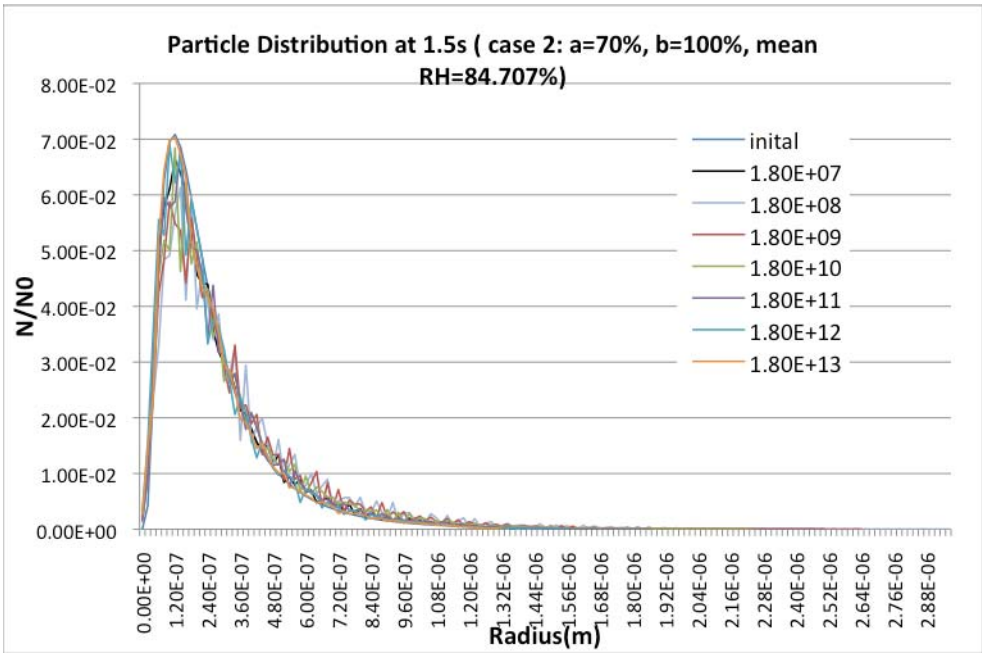

Figure 3.4(c) Calculation results at 1.5s of case 2 for NH_4SO_4

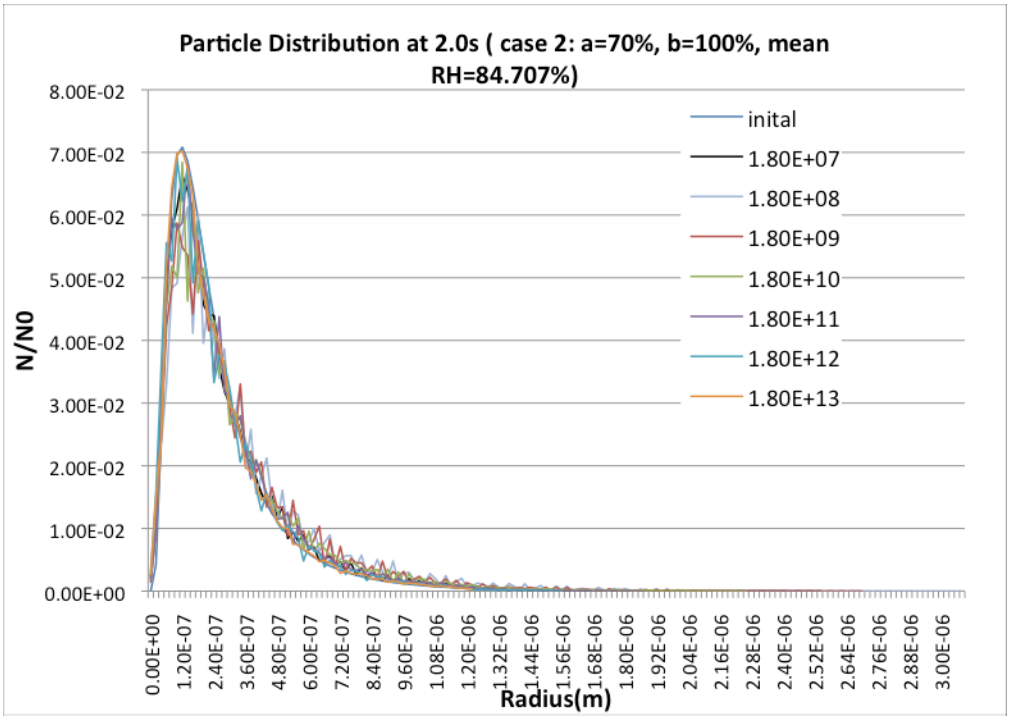

Figure 3.4(d) Calculation results at 2.0s of case 2 for NH_4SO_4

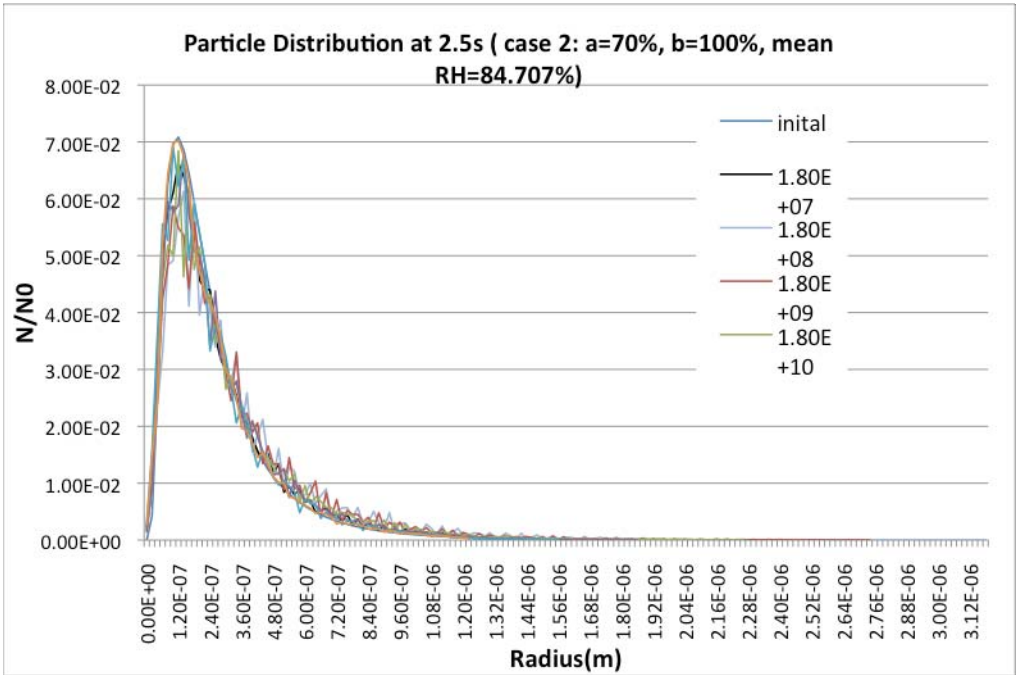

Figure 3.4(e) Calculation results at 2.5s of case 2 for NH_4SO_4

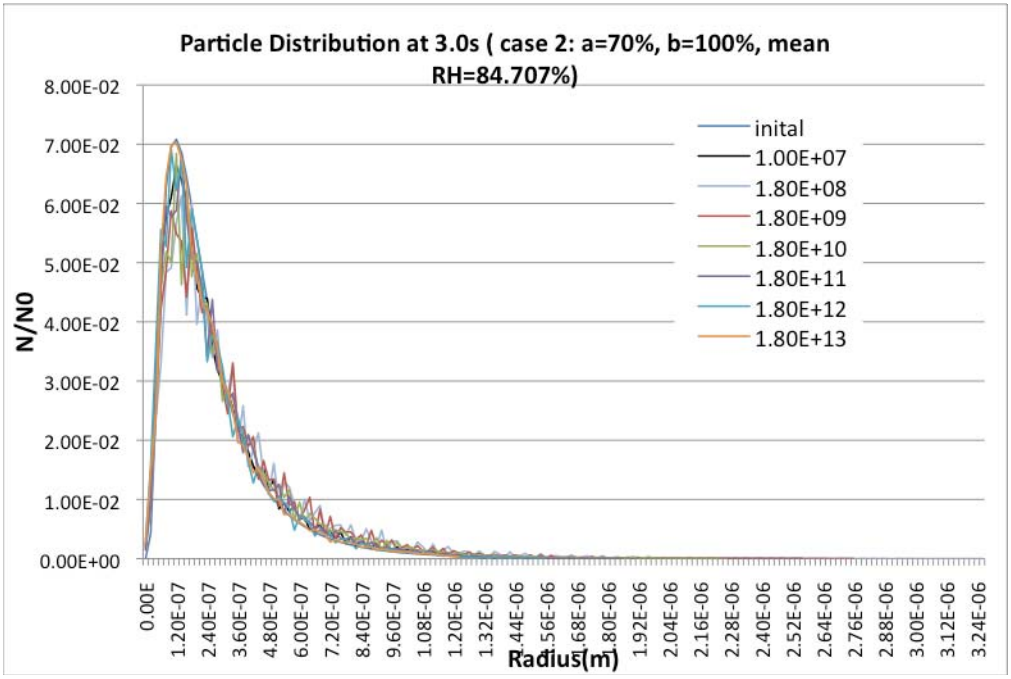

Figure 3.4(f) Calculation results at 3.0s of case 2 for NH_4SO_4

Unlike case1, in this case, we can see from Figures 3.4(a) - 3.4(f) that no matter what aerosol density is involved, the particles do not obviously grow. Even after 3.0 seconds' calculation, no particle grows beyond 3.3μm in radius even when the number density is as low as 1.8E7/m^3. Actually, when examining the particle distribution at 0.5s, 1.0s, 1.5s, 2.0s, 2.5s and 3.0s, we find that the only group of peaks remains at about 2.0μm for all densities. Also the largest particle's radius is about 2.40μm at 0.5s, 2.70μm at 1.0s, 2.88μm at 1.5s, 3.00μm at 2.0s, 3.12μm at 2.5s and 3.24at 3.0s, which means that all these particles grow at very low speeds. Even if these particles could keep growing at this kind of speed, which is actually not likely, it would still take 10.5s for the largest particle to grow to 5μm in radius. The real atmosphere is turbulent, and it is unlikely for particles to stay in the same environment for more than 13.5s. At this point, we can say that for this kind of relative humidity distribution, most of the particles cannot be activated.

What leads to so big different between case1 and case2? Compared the relative humidity distribution of this case with which in case1, the mean values are pretty close (84.707 here vs. 86.8536). This difference seems to be too small to account for the big difference between the calculation results of these two cases. The other possible reason is the upper limit of relative humidity distribution. In case1, the upper limit is above 100% and, in case 2, the upper limit is 100%, which means most particles are exposed to sub-saturation conditions. Under sub-saturation conditions, it is very difficult for particles as small as what we study here to grow beyond the limit of kohler curve and hence have the ability of continuous growth. To further study the effect of the upper limit of relative humidity distribution on particles' growth, we calculate cases 4-7 with upper limit of 101%, 102%, 104% and 106% while the lower limits are all 70%, which is the same as this case, and will present the results for these results later.

Case 3 for NH_4SO_4

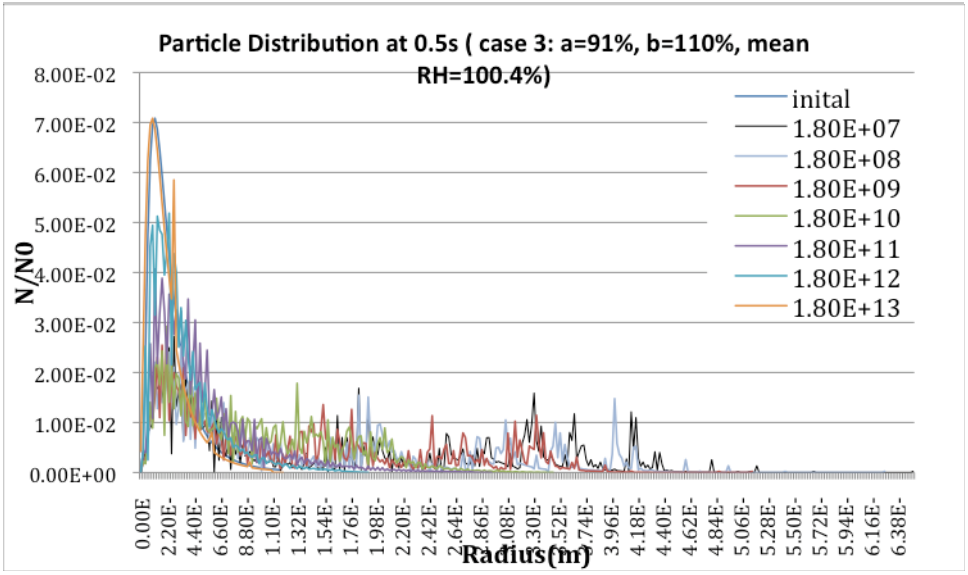

Figure 3.5(a) Calculation results at 0.5s of case 3 for NH_4SO_4

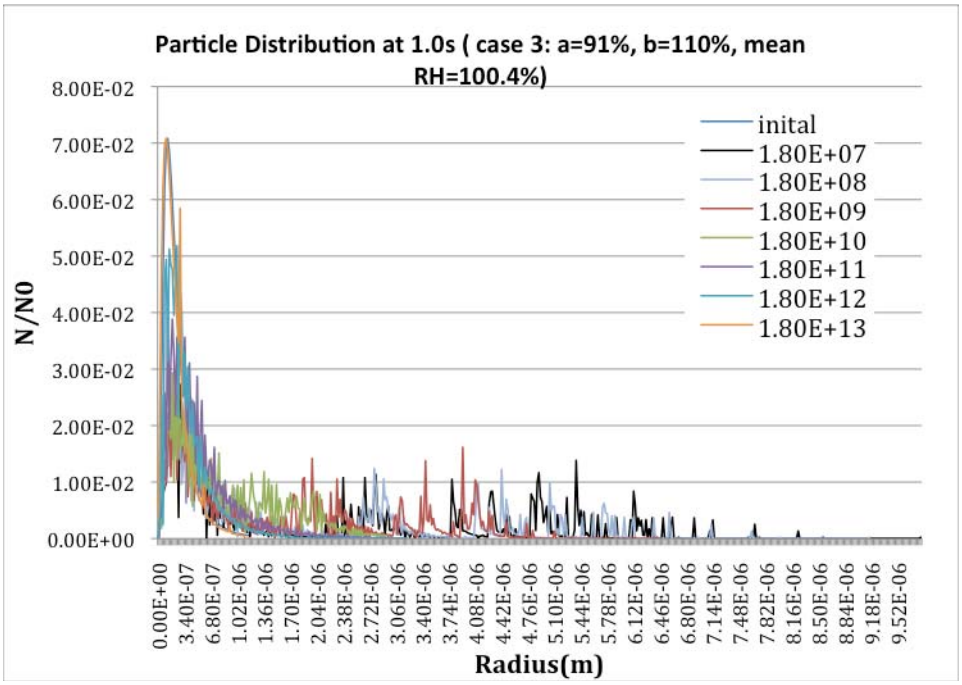

Figure 3.5(b) Calculation results at 1.0s of case 3 for NH_4SO_4

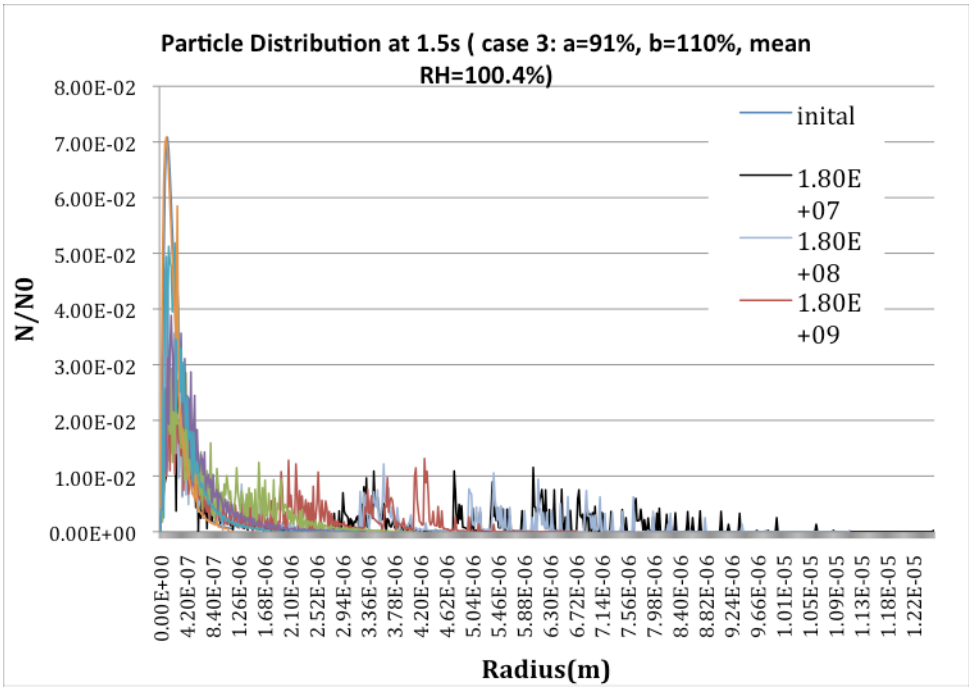

Figure 3.5(c) Calculation results at 1.5s of case 3 for NH_4SO_4

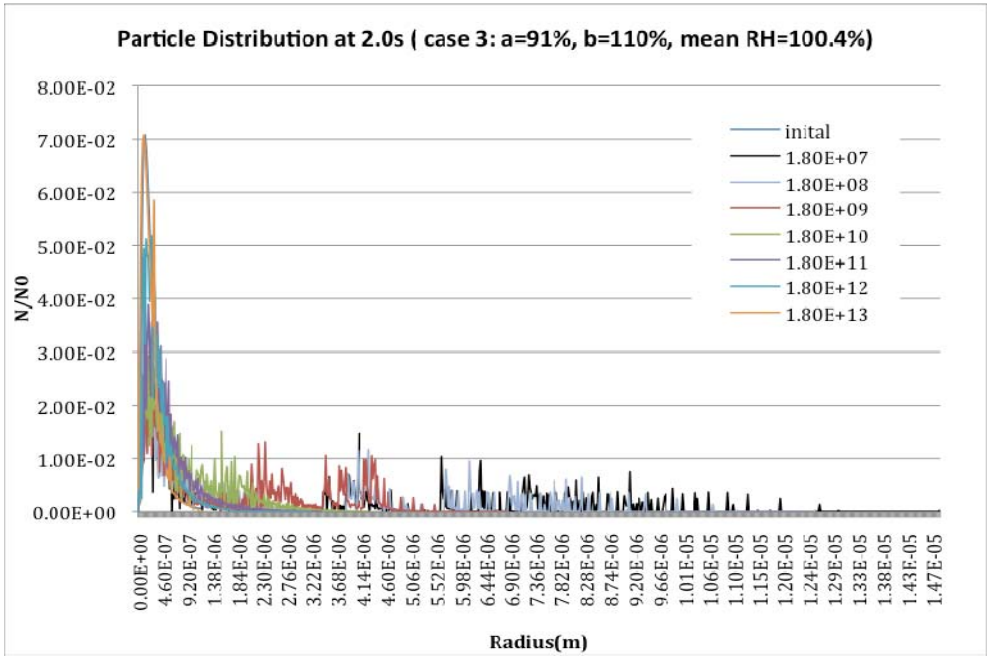

Figure 3.5(d) Calculation results at 2.0s of case 3 for NH_4SO_4

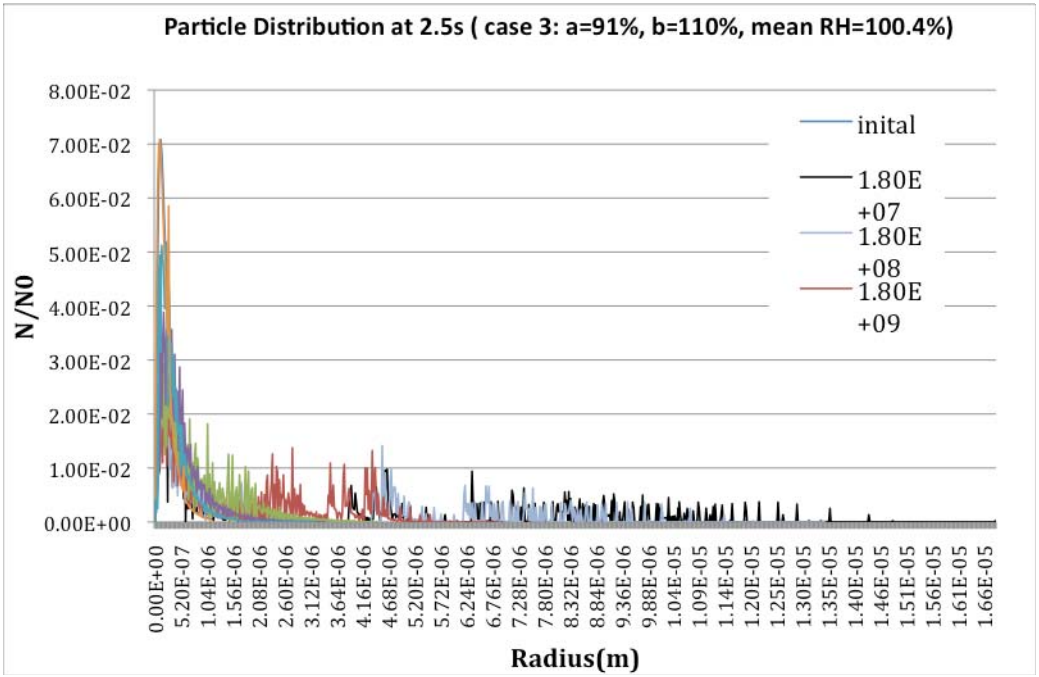

Figure 3.5(e) Calculation results at 2.5s of case 3 for NH_4SO_4

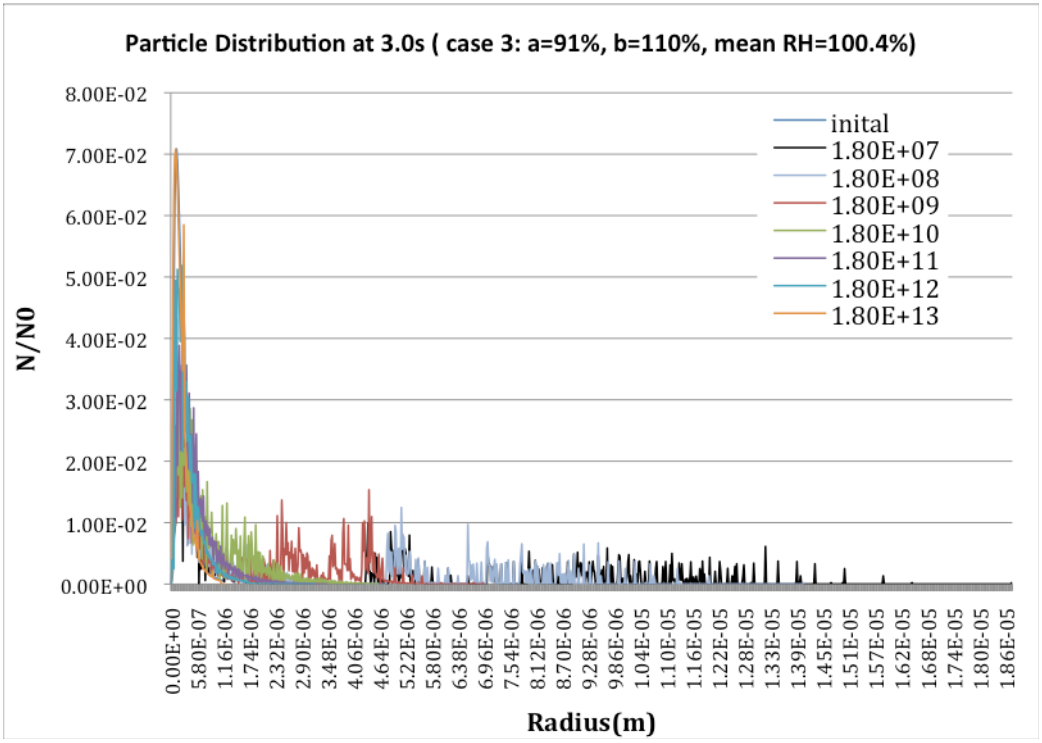

Figure 3.5(f) Calculation results at 3.0s of case 3 for NH_4SO_4

The upper and lower limits of the relative humidity distribution in this case are both high, which means most particles can be exposed to higher saturation ratioes than the particles in the previous two cases. Hence, we expected more growth. According to Figures 3.5(a) - 3.5(f), the same as in case1, when particle number densities are higher than 1.8E10/m^3 (1.8E11/m^3, 1.8E12/m^3, 1.8E13/m^3), the particles do not obviously grow. We may see a little growth with 1.8E11/m^3 in the 0.5s result, but this growth tendency did not persist. It is because the growth of large numbers of particles requires a large quantity of water vapor quickly and decreases the relative humidity drastically; also a large amount of heat was released and the temperature rises; both of these effects keep the particles from growing further. Still, when number density is equal to or lower than 1.8E10/m^3, the lower the particle density, the more the particles grow. At 0.5s, there is not much difference between the distribution of 1.8E7/m^3, 1.8E8/m^3 and 1.8E9/m^3. The distribution curve for 1.8E9/m^3 have peaks around 3.3μm while the distribution curve for 1.8E8/m^3 have peaks around 4.0μm and perks around 4.15μm for 1.8E7/m^3. The differences among these peaks are bigger than in case1. When number density is equal to 1.8E10/m^3, we can see peaks around 2.0μm at 0.5s, which is, similar to in case1. The discrepancy among different number densities increases along with time. After 3.0s, we can see peaks somewhat greater than 13μm and 10μm for number density of 1.8E7/m^3 and 1.8E8/m^3, respectively; and for number density of 1.8E9/m^3 it only goes to somewhere like 5μm. For density of 1.8E10/m^3, it seems the peaks still stay about 2.0 μm. So far, we can conclude that at this kind relative humidity condition, particles have chances to be activated only when the number density is lower than 1.8E10/m^3. Also, it is not surprising that particles in this case should be more easily activated and this process takes shorter time than that in case 1 because of the higher lower limit 65% for case1 and 91% here) and mean value (86.8536% for case1 and 100.4% here) for the relative humidity distribution. But when the number density is higher than 1.8E10/m^3, there is still no sign of activation of those particles, which strongly indicates that the high density could efficiently prevent particles to become CNN (cloud condensation nuclei) despite of the high saturation ratio.

Case 4 for NH_4SO_4

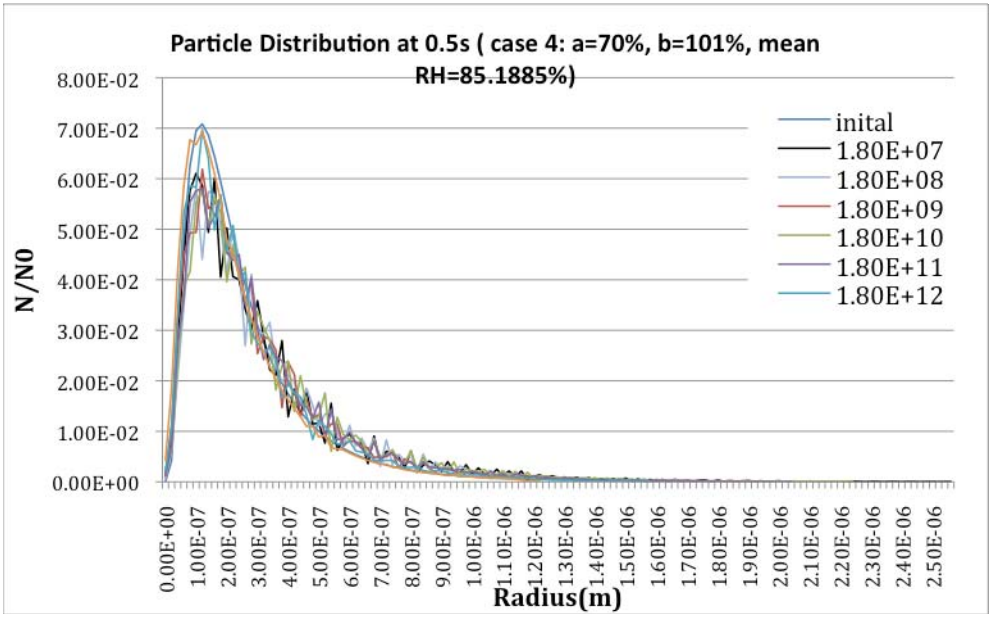

Figure 3.6(a) Calculation results at 0.5s of case 4 for NH_4SO_4

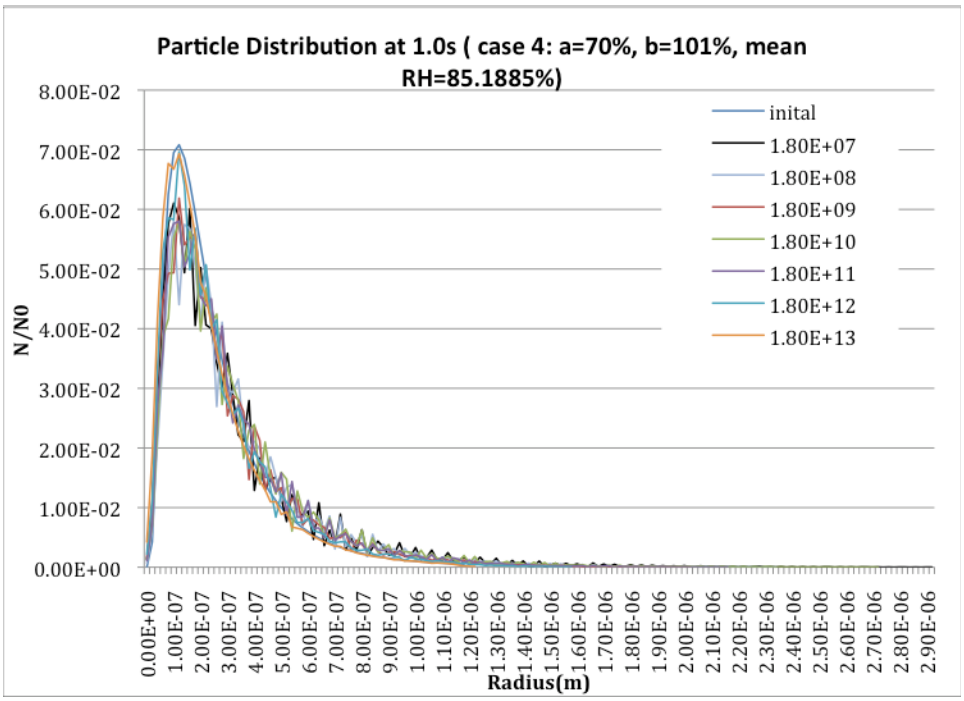

Figure 3.6(b) Calculation results at 1.0s of case 4 for NH_4SO_4

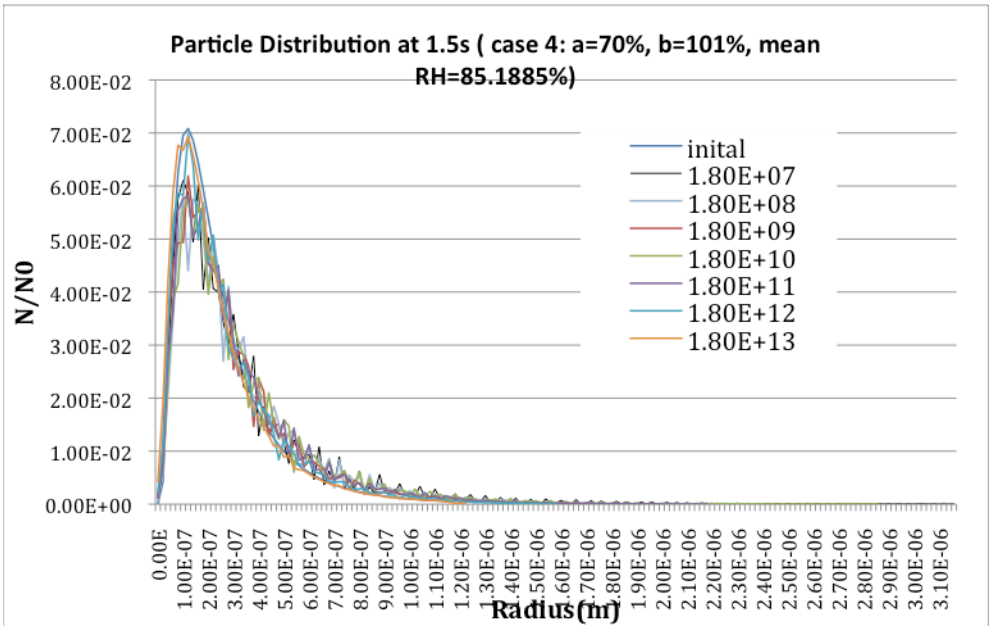

Figure 3.6(c) Calculation results at 1.5s of case 4 for NH_4SO_4

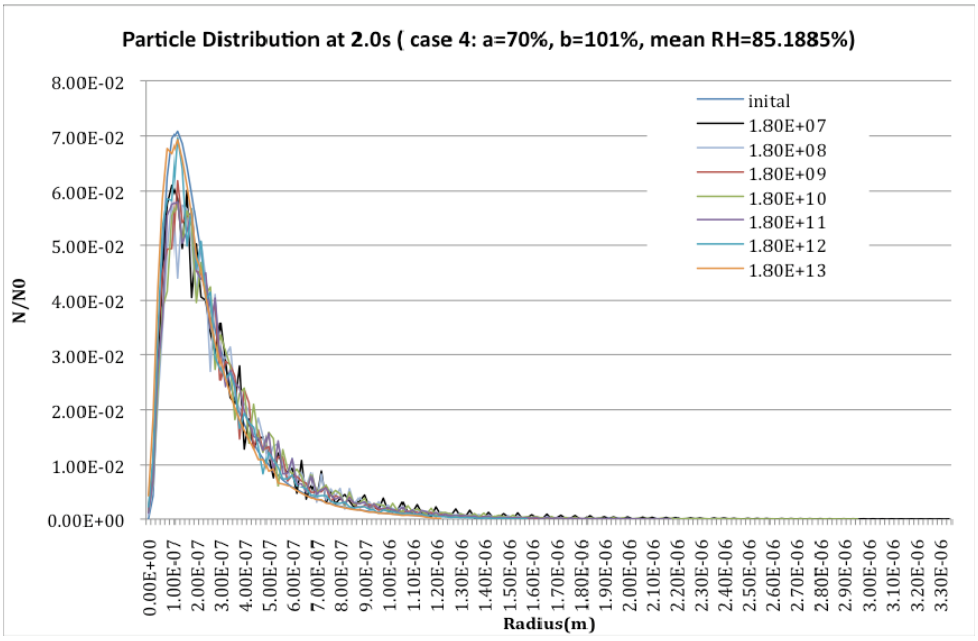

Figure 3.6(d) Calculation results at 2.0s of case 4 for NH_4SO_4

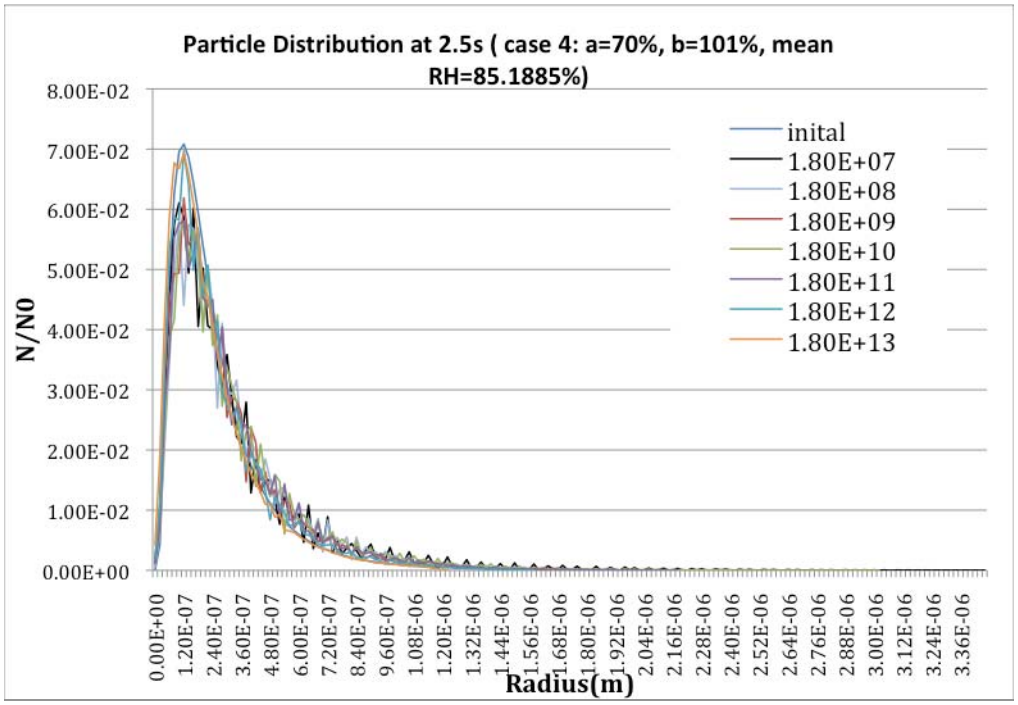

Figure 3.6(e) Calculation results at 2.5s of case 4 for NH_4SO_4

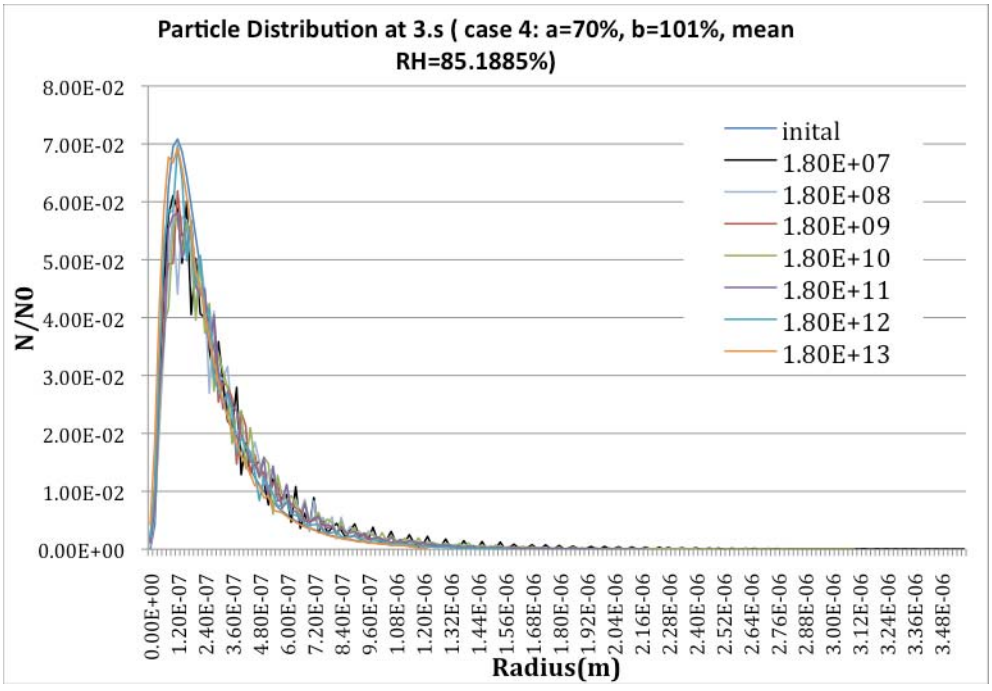

Figure 3.6(f) Calculation results at 3.0s of case 4 for NH_4SO_4

The difference between this case and case 2 is the upper limit of the relative humidity distribution, which is 101% here instead of 100% in case 2, and the mean value of relative humidity is 85.1885% instead of 84.707%. With such small difference, we don't expect to see much change in the results here from that in case2. Like case 2, here, we can see from Figures 3.6(a) - 3.6(f) that no matter what density it is, the particles do not get obvious growth. Even after 3.0s' calculation, no particle has grown beyond 3.0μm in radius even with number density as low as 1.8E7/m^3. Actually, until 3.0s, all the distributions remain unimodal. Also the largest particles' radius is about 2.50μm at 0.5s, 2.88μm at 1.0s, 3.12μm at 1.5s, 3.2μm at 2.0s, 3.3μm at 2.5s and 3.5μm at 3.0s, which means the particles have stopped growing or grow at a very low speed. At this point, it is not hard to tell that for this kind of relative humidity distribution, most of the particles cannot be activated. This agrees with what we expect based upon Köhler thoery.

Case 5 for NH_4SO_4

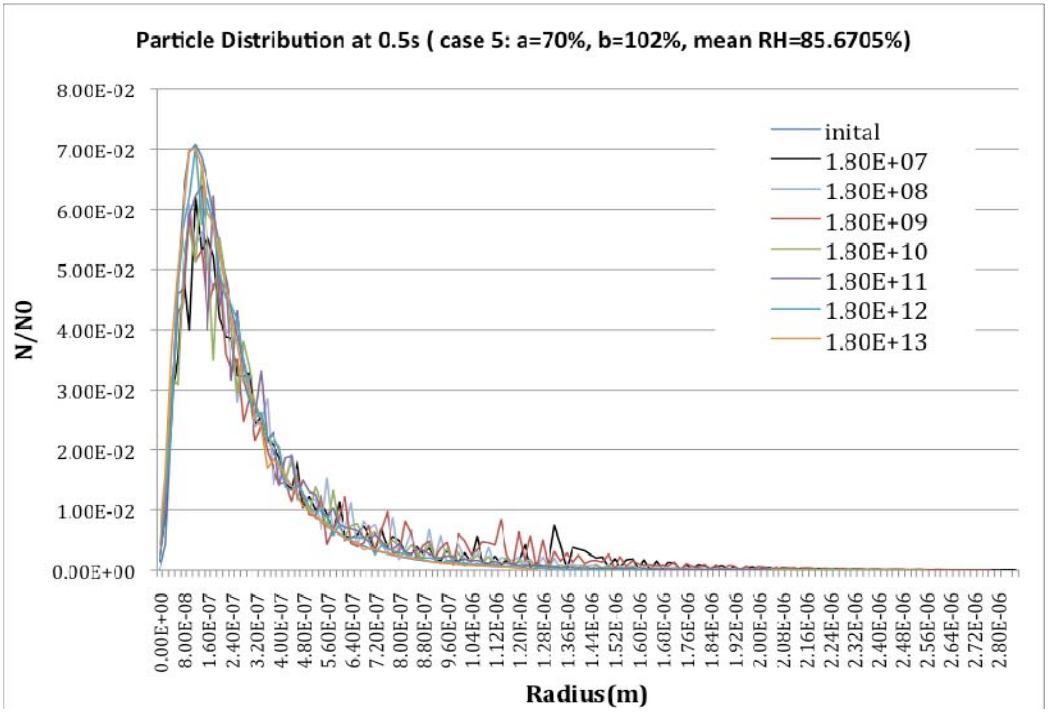

Figure 3.7(a) Calculation results at 0.5s of case 5 for NH_4SO_4

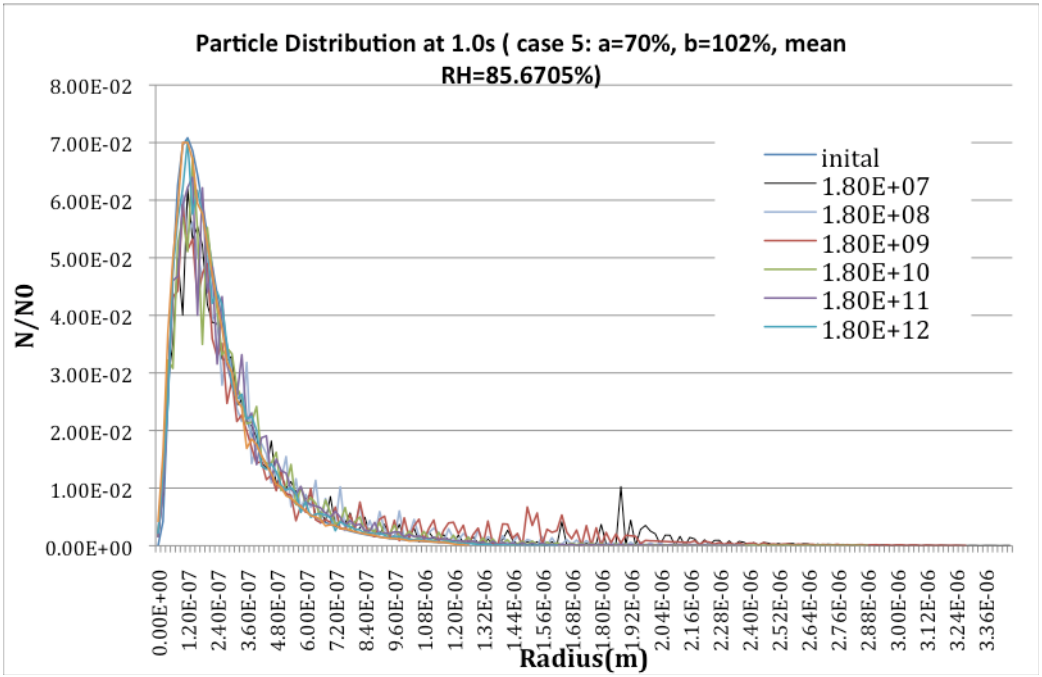

Figure 3.7(b) Calculation results at 1.0s of case 5 for NH_4SO_4

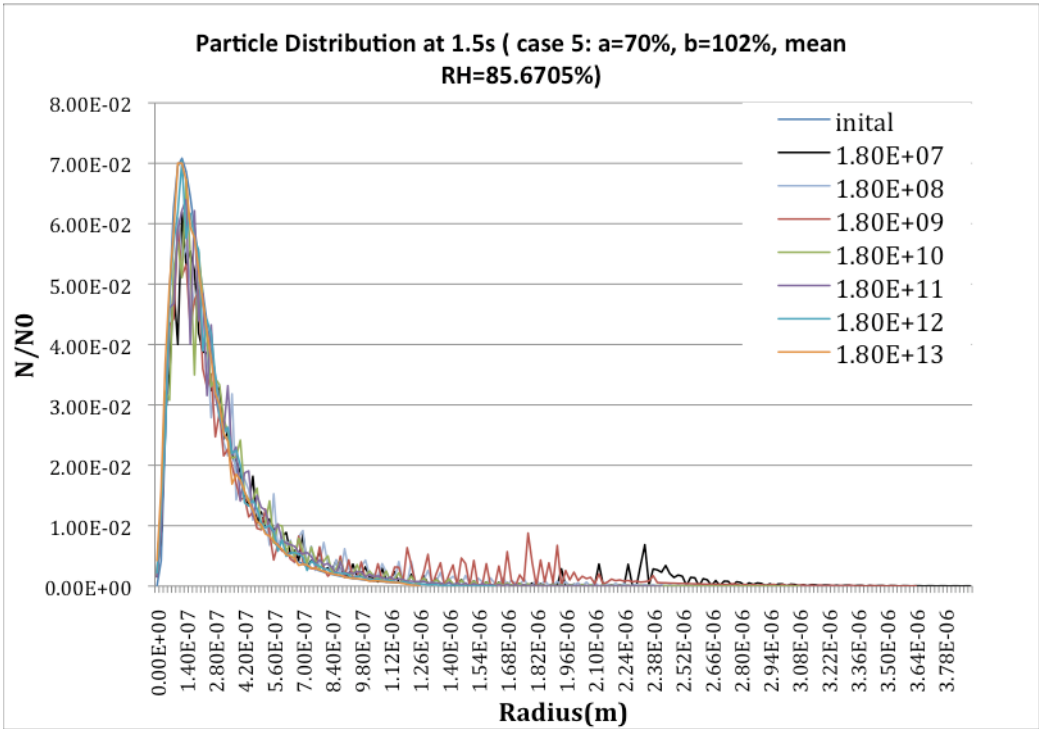

Figure 3.7(c) Calculation results at 1.5s of case 5 for NH_4SO_4

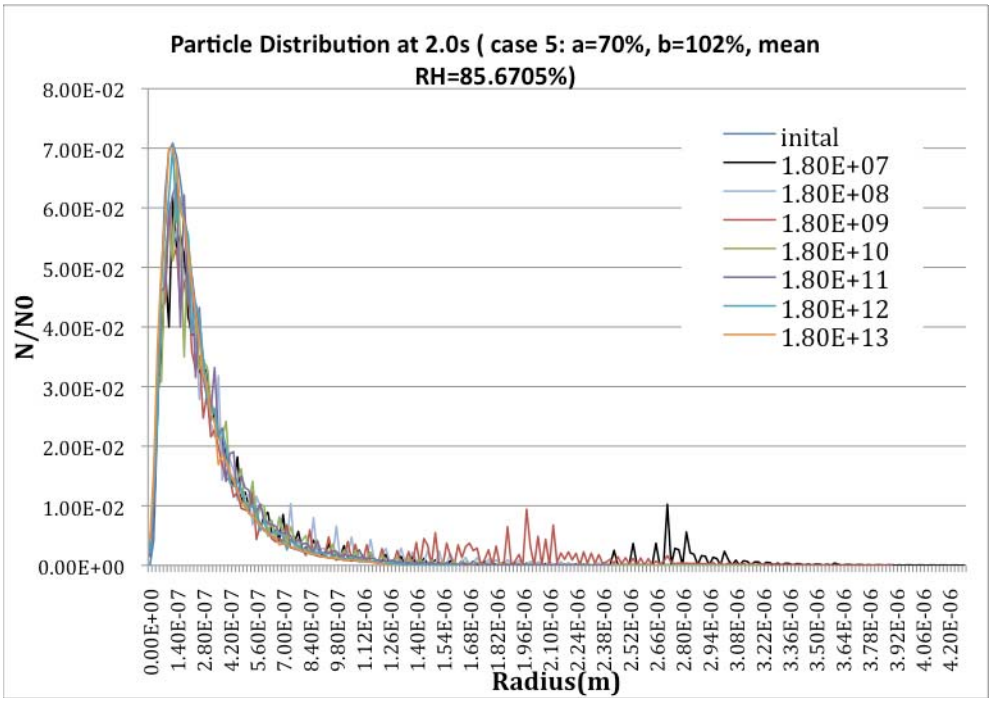

Figure 3.7(d) Calculation results at 2.0s of case 5 for NH_4SO_4

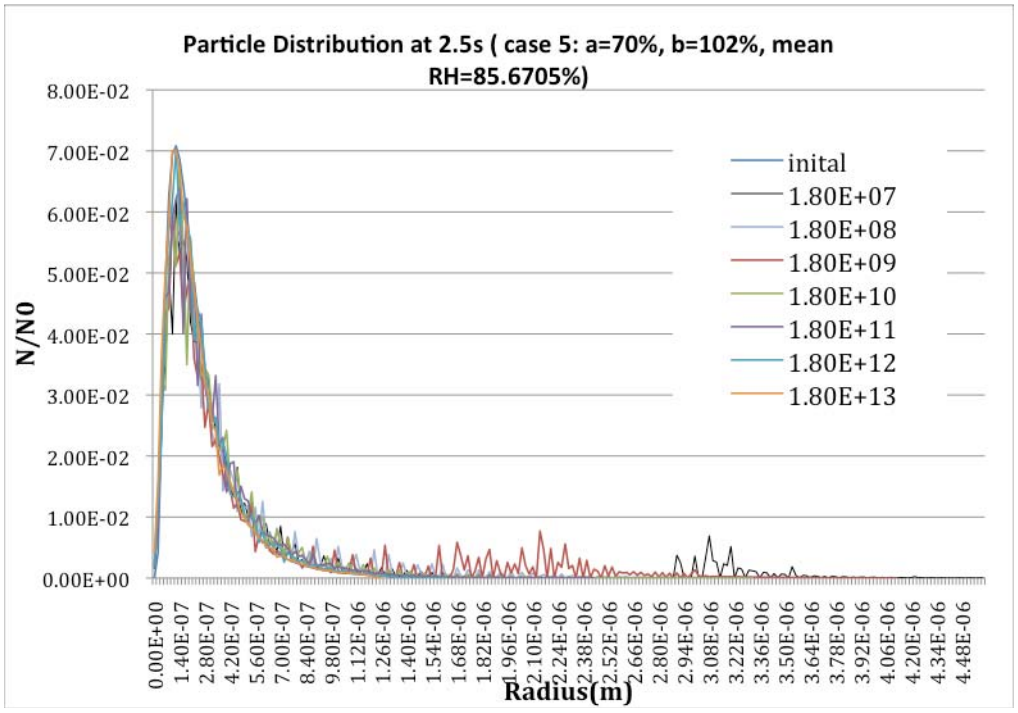

Figure 3.7(e) Calculation results at 2.5s of case 5 for NH_4SO_4

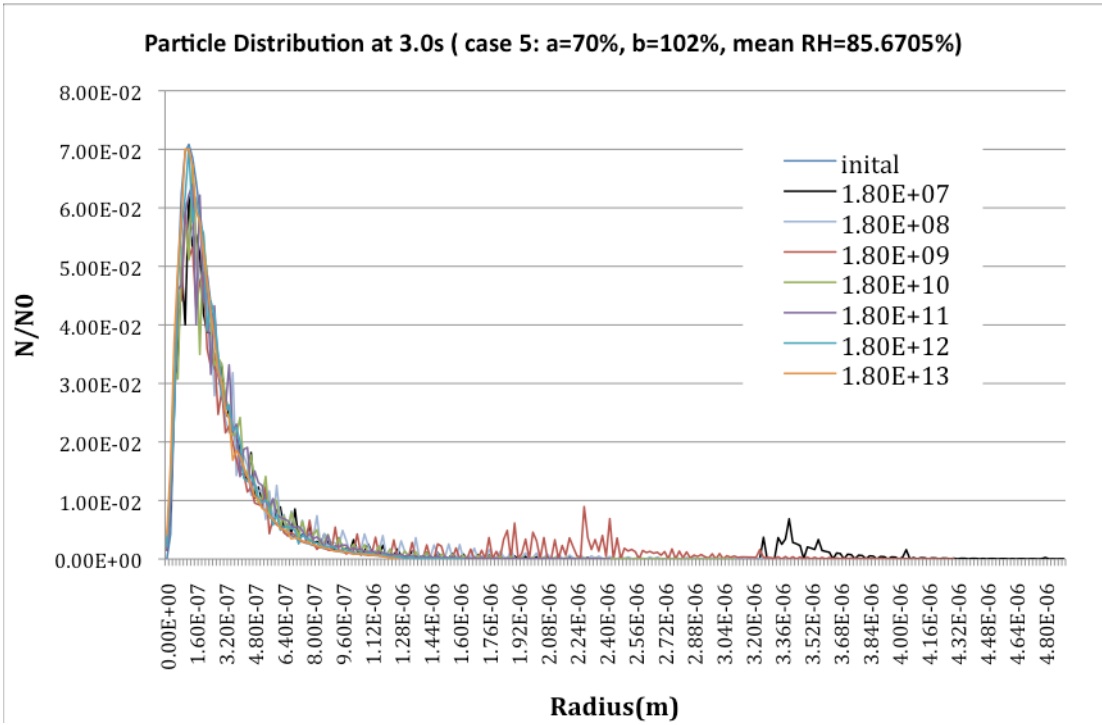

Figure 3.7(f) Calculation results at 3.0s of case 5 for NH_4SO_4

This time, we raise the upper limit of the relative humidity distribution to 102%. We hope to see more growth with the low-density particles in this case than in case 2 and 4; in any event, we do not expect this difference to be big. We do see from Figures 3.7(a) - 3.7(f) some new peaks in the calculated distributions with number density of 1.8E7/m^3, 1.8E8/m^3 and 1.8E9/m^3. However, none of these new peaks go further than 4.2μm after 3.0s and is still below the criterion (7μm) at which particles are generally considered activated. Also, the largest particle's radius is about 2.76μm at 0.5s, 3.76μm at 1.0s, 3.78μm at 1.5s, 4.16μm at 2.0s, 4.50μm at 2.5s and 4.86at 3.0s, which are all greater than that in case 2 and case 4. However, they are still below 5μm. Moreover, it shows that after 3s, when particle number density is greater than 1.8E7/m^3, the speed of particles' growing has slowed considerably or has even stopped growing. Even when the number density is 1.8E7/m^3, the growth rate has an obvious tendency of slowing

down. All this evidence tells us that for this kind of relative humidity distribution, most of the particles still cannot be activated.

One interesting observation is that in this case the particles with number density of 1.8E9/m^3 grows a little more than particles with number density of 1.8E8/m^3. This is not what to be expected but reasonable at some circumstances for a reason -- random selection of the relative humidity of the 19 small zones. The random character may make the relative humidity in the 19 small zones for the calculation of 1.8E9/m^3 so much higher than which in the calculation of 1.8E8/m^3 that overcome the advantage of the lower density. It is a reasonable statement for this case. Here, no matte what, with these two densities, particles are not activated. So, this random selection may be able to quantitatively change the results, like what we have seen here; but it cannot qualitatively change it, which means it will not have effects on whether or not the particles would be activated.

Case 6 for NH_4SO_4

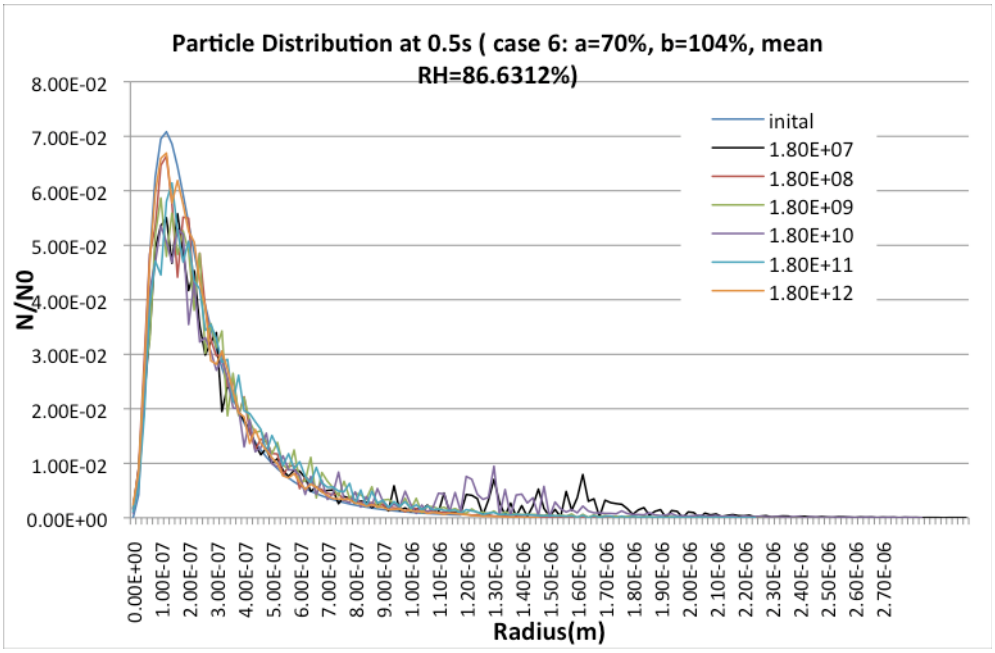

Figure 3.8(a) Calculation results at 0.5s of case 6 for NH_4SO_4

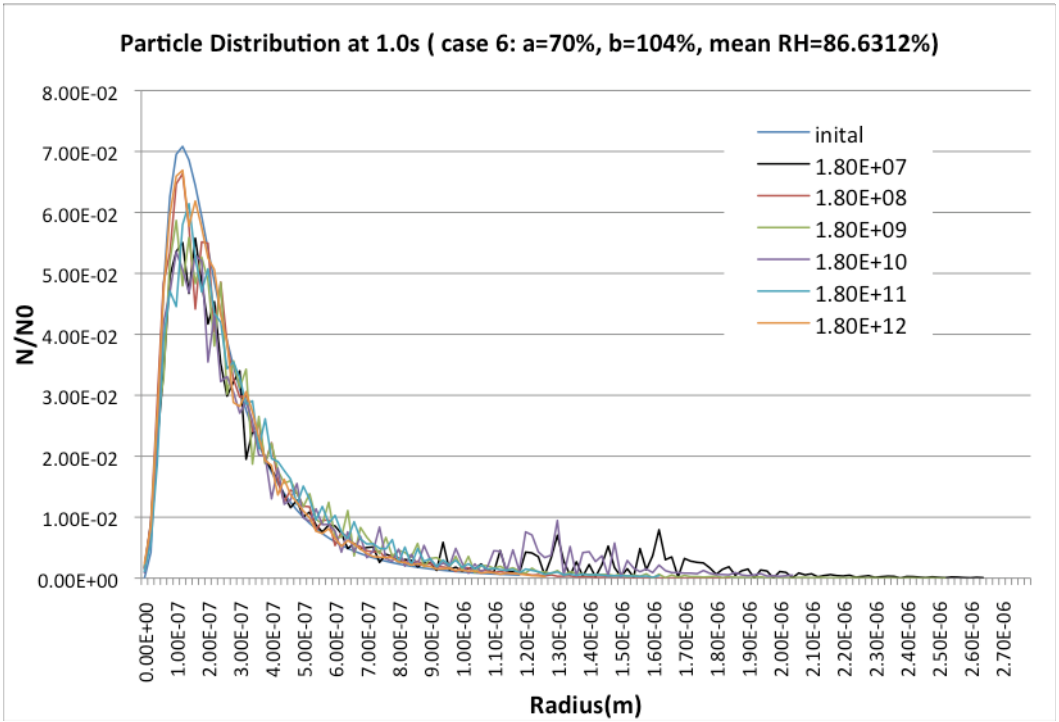

Figure 3.8(b) Calculation results at 1.0s of case 6 for NH_4SO_4

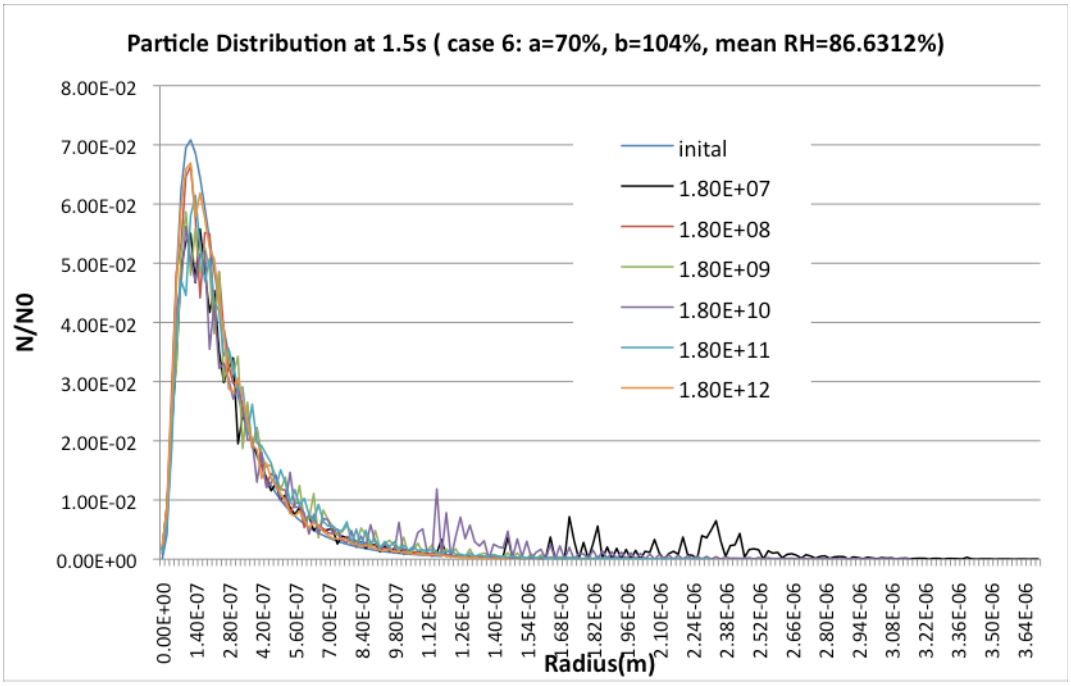

Figure 3.8(c) Calculation results at 1.5s of case 6 for NH_4SO_4

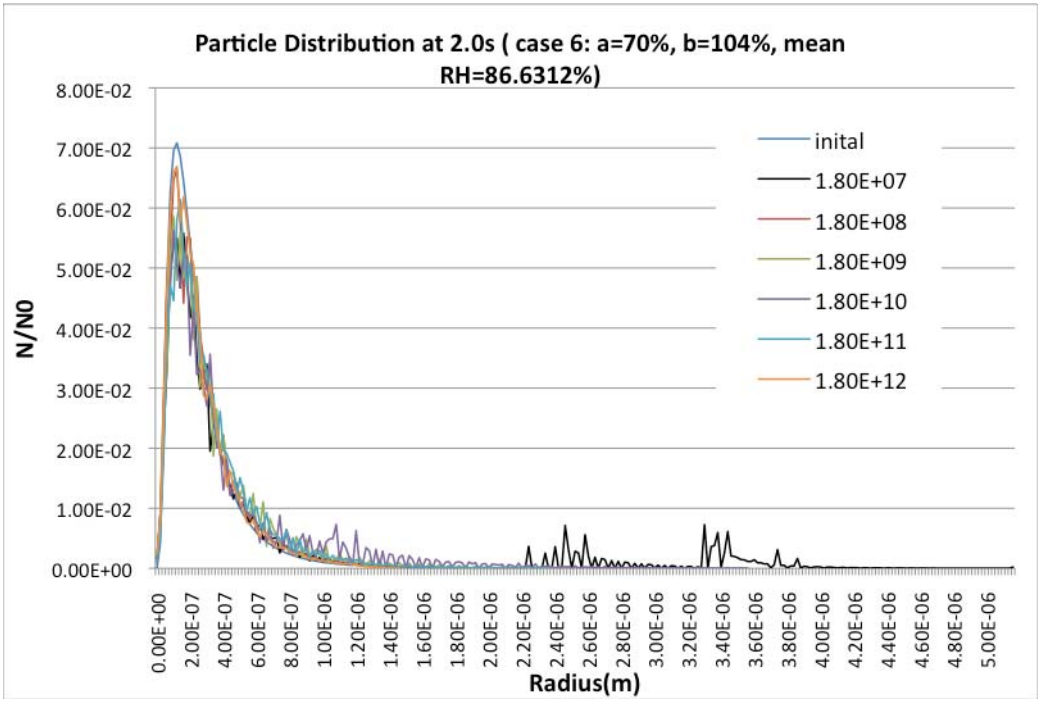

Figure 3.8(d) Calculation results at 2.0s of case 6 for NH_4SO_4

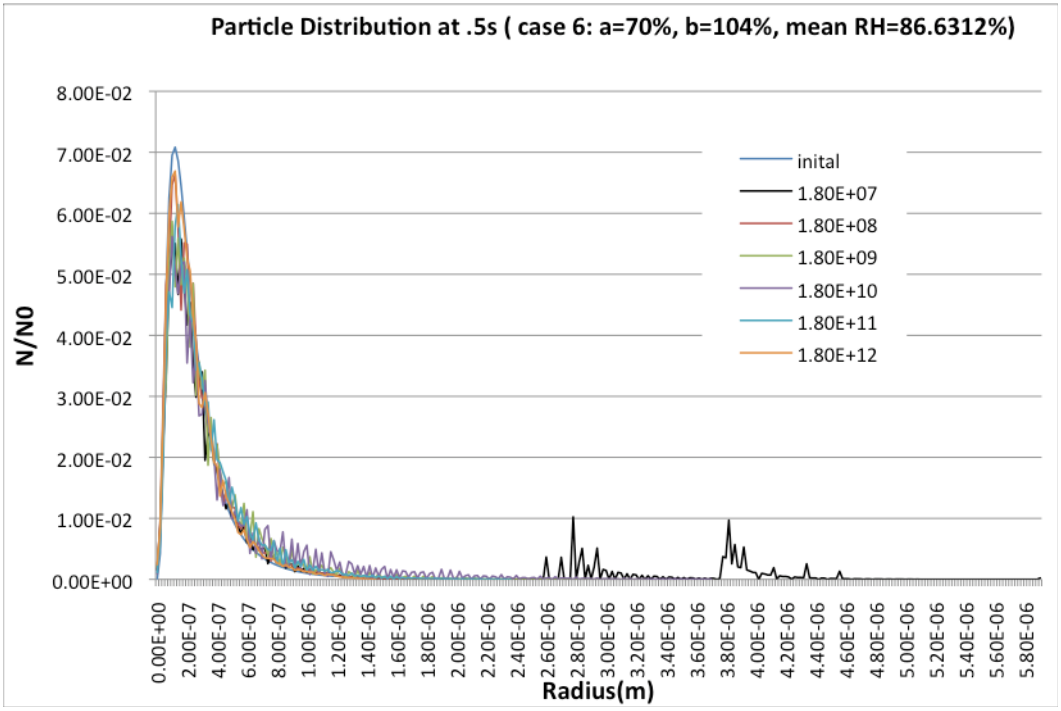

Figure 3.8(e) Calculation results at 2.5s of case 6 for NH_4SO_4

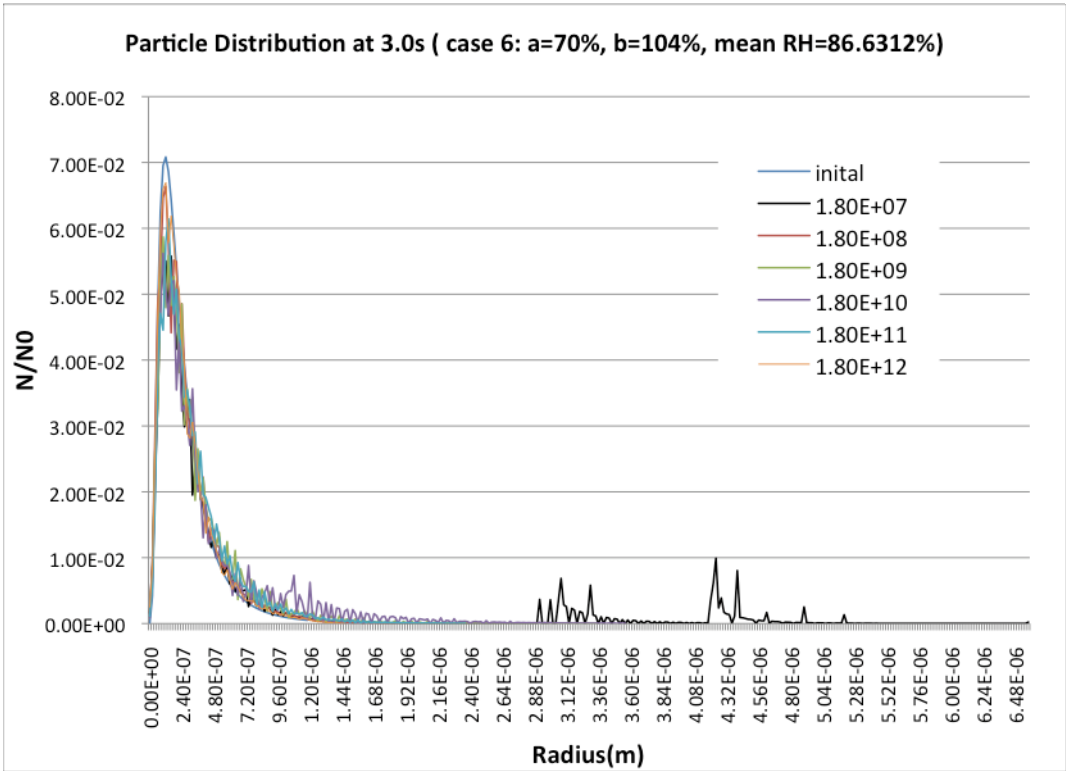

Figure 3.8(f) Calculation results at 3.0s of case 6 for NH_4SO_4

For this case and case 7, we did not do the calculations with number density of 1.8E13/m^3 since all the previous results have shown that with such high density, particles have no chance for significant growth. This time, the upper limit of the relative humidity distribution was raised to 104%. For this case, the largest particles' radius is about 2.40μm at 0.5s, 2.70μm at 1.0s, 3.64μm at 1.5s, 5.00μm at 2.0s, 5.80μm at 2.5s and 6.48at 3.0s, which are all greater than that in case 2, case 4 and case 5. Particles in this case still grow less than that in case 1 and case3, which both have the relative humidity distribution's upper limit of 110%. We can see some from Figures 3.8(a) – 3.8(f) that new peaks in the calculated distributions with number density of 1.8E7/m^3. New peaks have reached 5.0μm after 3.0s and particles still keep a considerable speed of growth. This tells us that for this kind of relative humidity distribution, some of the particles can be activated when the number density is equal to or lower than 1.8E7/m^3. Again, there is no sign of activation for particles with higher number densities.

We noticed that at 0.5s and 1.0s it looks like the particles with number density of 1.8E10/m^3 have a tendency to grow beyond that of 1.8E8/m^3, 1.8E9/m^3, even 1.8E7/m^3. However, this tendency has faded away at 1.0s. Moreover, at 1.5s, the new peaks of the calculated distribution for particles with number density of 1.8E10/m^3 have become insignificant and unnoticeable compared to that of 1.8E7/m^3. The same reason as we mentioned in the previous discussion of case 5 —the random selection of the relative humidity of the 19 small zones, caused the particles with number density of 1.8E10/m^3 to grow very fast in the first 1s. The random character may make the relative humidity in the 19 small zones for the calculation of 1.8E10/m^3 much higher than in all others. Anyway, the lower density finally compensated the advantage of randomly selected relative humidity. This is why after 1.5s; particles with density of 1.8E7/m^3 grow far more than all others. This also confirms our conclusion in the previous discussion, that this random selection may be able to quantitatively change the results; but it cannot qualitatively change it, which means It will not have effects on whether or not the particles can be activated.

Case 7 for NH_4SO_4

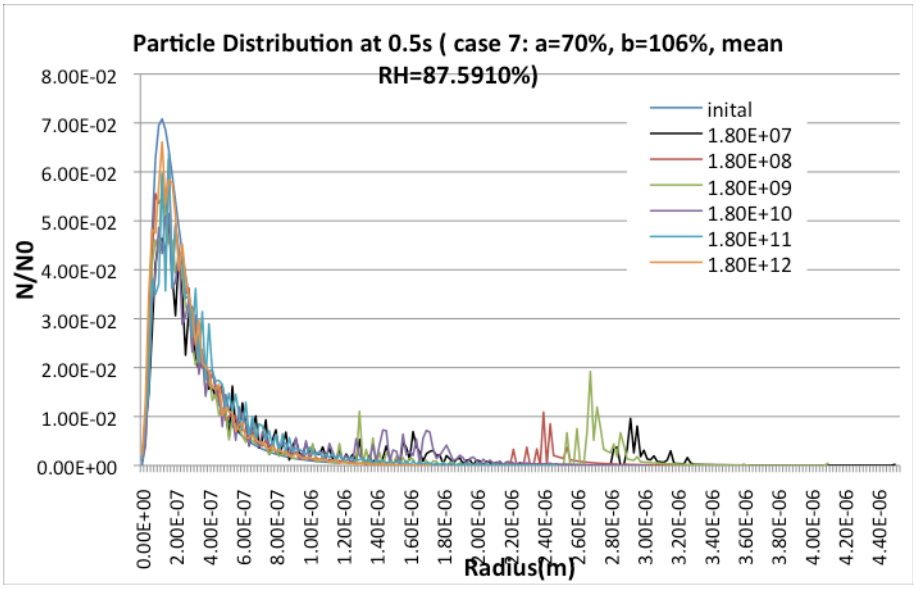

Figure 3.9(a) Calculation results at 0.5s of case 7 for NH_4SO_4

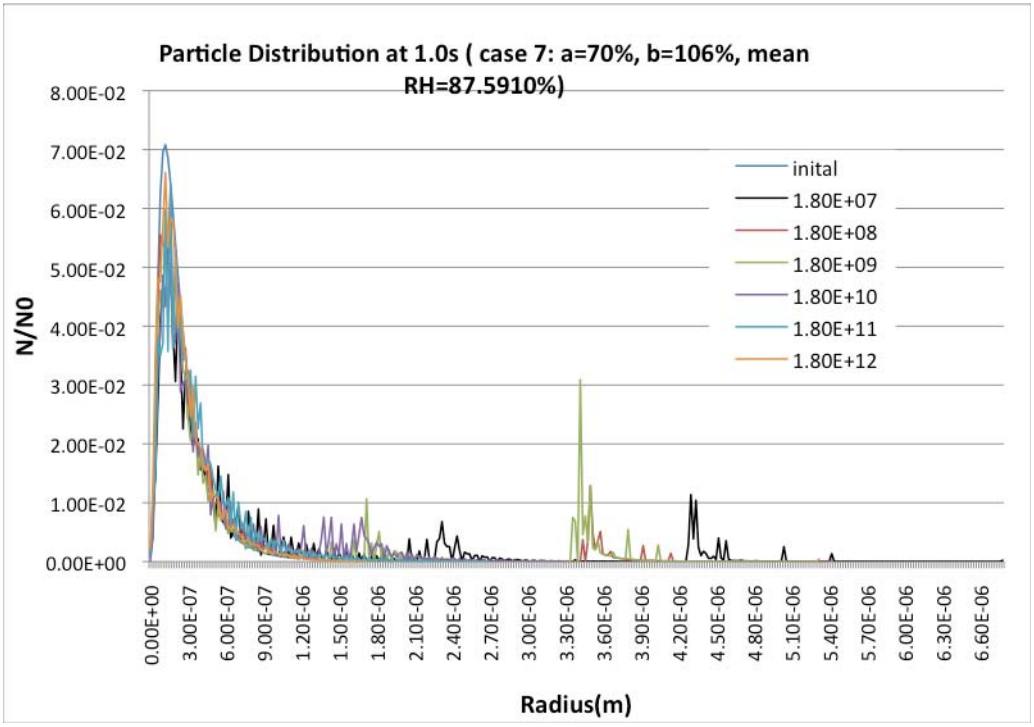

Figure 3.9(b) Calculation results at 1.0s of case 7 for NH_4SO_4

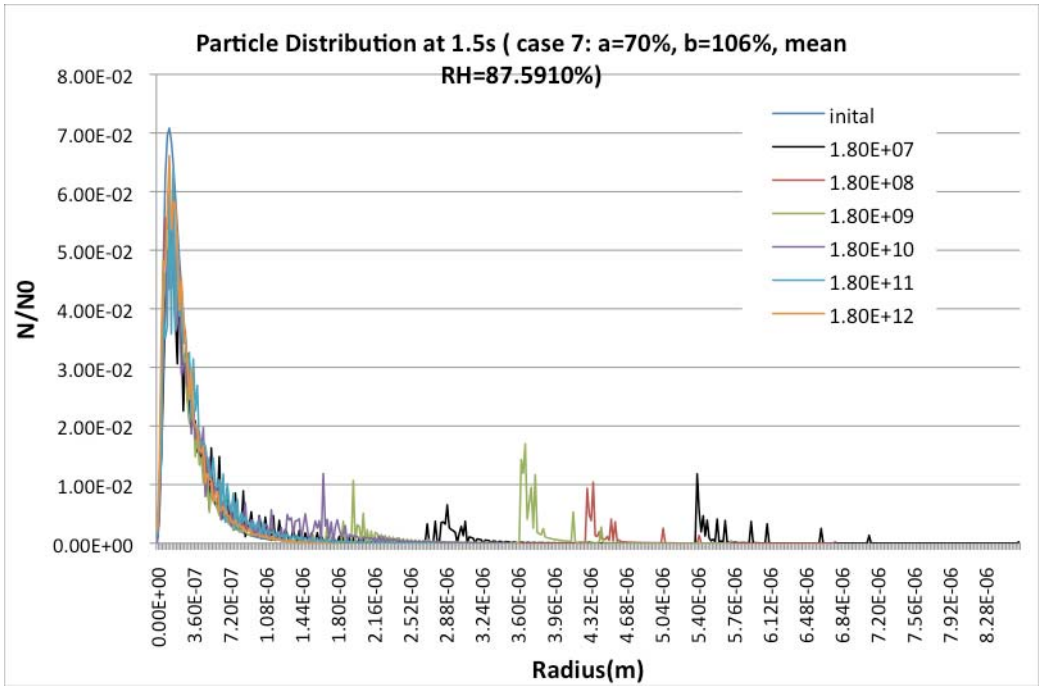

Figure 3.9(c) Calculation results at 1.5s of case 7 for NH_4SO_4

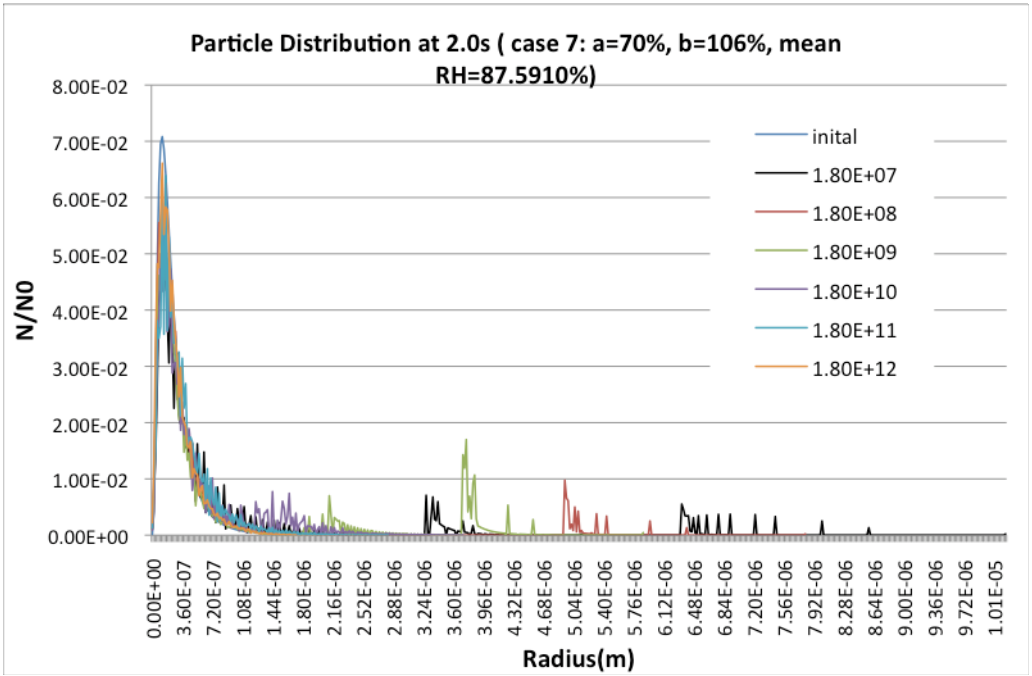

Figure 3.9(d) Calculation results at 2.0s of case 7 for NH_4SO_4

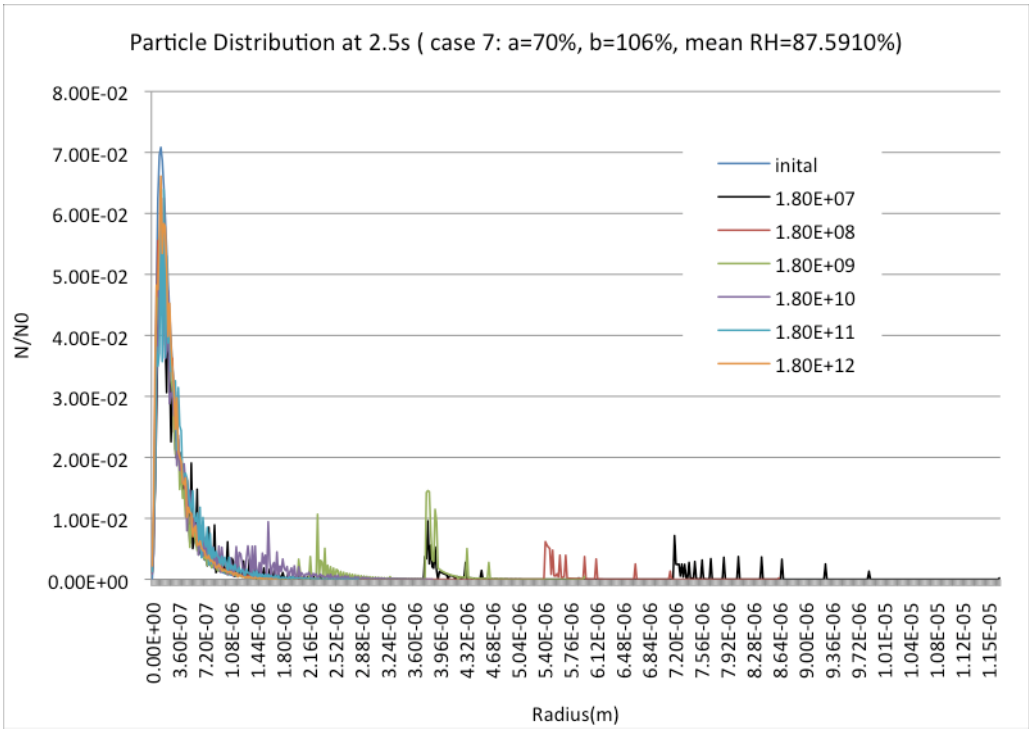

Figure 3.9(e) Calculation results at 2.5s of case 7 for NH_4SO_4

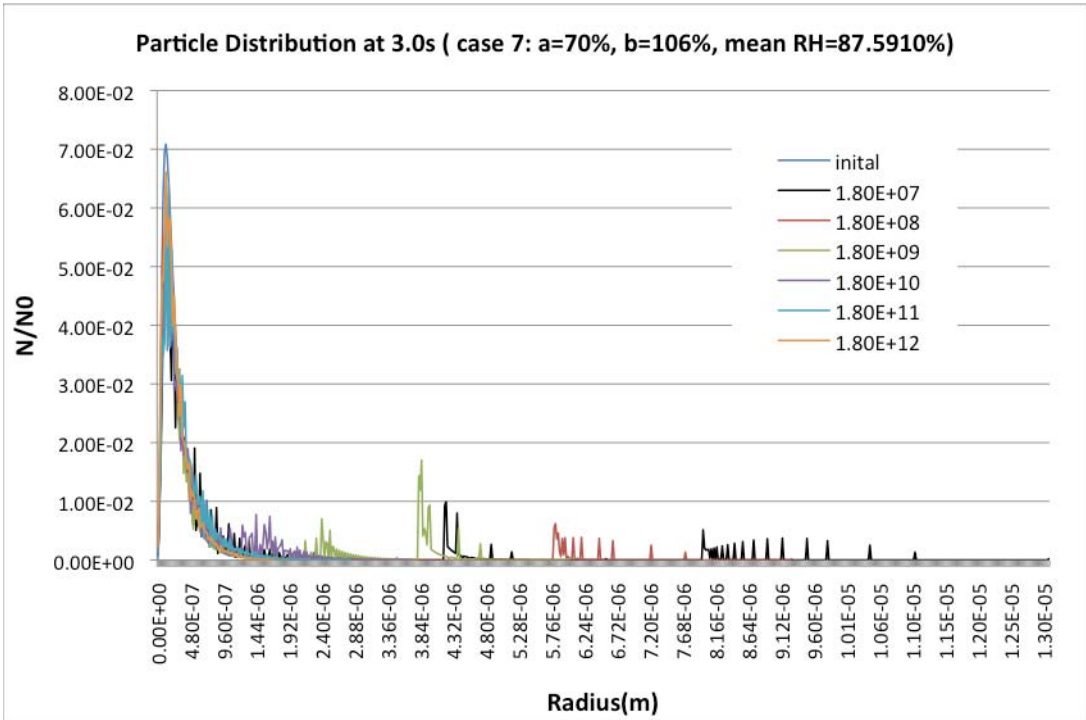

Figure 3.9(f) Calculation results at 3.0s of case 7 for NH_4SO_4

With the upper limit of relative humidity being raised to 107%, calculational results of Case 7 in Figures 3.9(a) – 3.9(f) shows significant differences compared to Cases 2, 4, 5 and 6. With number density of 1.8E7/m^3, some particles have grown larger than 5μm in radius after 1.5s and gone beyond 7 μm after 2.5μm. With number density of 1.8E8/m^3, after 2.0s, radius of some particles has reached 5 μm and after 3.0s, some of them have grown to 7μm. Even when the number density is equal to 1.8E9/m^3, some particles have grown as large as 5μm after 3.0s. So in this case, some particles with low number density can be activated. This indicates that, besides the particle number density, the upper limit of relative is another critical factor for the growth of particles.

Fraction of activated particles

As discussed previously, CCN with radius greater than 7μm are considered as activated. A less stringent criterion of ~5μm is also used sometimes (Hallett and Mossop, 1974). Here, we summarize the percentage of particles growing beyond 5μm and 7μm in radius after 3s in each case and list them in Tables 3.2 and 3.3.

Table 3.2 Percentage of particles having radii equal to or greater than 7μm

	Case1	**Case2**	**Case3**	**Case4**	**Case5**	**Case6**	**Case7**
1.8E7	15.7	0	31.4	0	0	0	5.22
1.8E8	5.22	0	17.7	0	0	0	0.407
1.8E9	0.223	0	0	0	0	0	0
1.8E10	0	0	0	0	0	0	0
1.8E11	0	0	0	0	0	0	0
1.8E12	0	0	0	0	0	0	0
1.8E13	0	0	0	0	0	N/A	N/A

For case 2, 4, 5 &6, no particle grows beyond 7μm for all number densities. Also, when particle number density is greater than 1.8E9/m^3, no particle grows beyond 7μm for all cases.

Table 3.3 Percentage of particles having radii equal to or greater than 5μm

	Case1	**Case2**	**Case3**	**Case4**	**Case5**	**Case6**	**Case7**
1.8E7	15.7	0	40.0	0	0	0.246	5.47
1.8E8	5.77	0	32.5	0	0	0	5.22
1.8E9	1.72	0	0.94	0	0	0	0.045
1.8E10	0	0	0	0	0	0	0
1.8E11	0	0	0	0	0	0	0
1.8E12	0	0	0	0	0	0	0
1.8E13	0	0	0	0	0	N/A	N/A

For Case1, 15.7%, 5.22% and 0.223% of all particles grow beyond 7μm when number densities are 1.8E7/m^3, 1.8E8/m^3 and 1.8E9/m^3 respectively. For Case 3, 31.4%

and 17.7% of all particles grow beyond 7μm when number density is 1.8E7/m^3 and 1.8E8/m^3 respectively. For Case 7, 5.22% and 0.407% of all particles grow beyond 7μm when number density is 1.8E7/m^3 and 1.8E8/m^3.

Then we lower the criterion to 5μm and look at how many particles can reach this criterion under different condition. Again, for case 2, 4 & 5, no particle grows beyond 5μm for all the number densities. Also, when particle number density is greater than 1.8E9/m^3, no particle grows beyond 5μm for all cases.

For Case 1, the fractions of particles, which have grown beyond 5μm, are 15.7%, 5.77% and 1.72% when the number densities are 1.8E7/m^3, 1.8E8/m^3 and 1.8E9/m^3 respectively. For Case 3, 40.9%, 32.5% and 0.94% of all particles grow beyond 5μm when number densities are 1.8E7/m^3, 1.8E8/m^3 and 1.8E9/m^3 respectively. For Case 7, 5.47%, 5.22% and 0.045% of all particles grow beyond 5μm when number densities are 1.8E7/m^3, 1.8E8/$m^3$and 1.8E9/m^3. For Case 6, 0.246% particles have radii greater than 5μm only when the number density is 1.8E7/m^3.

From these phenomena, one obvious point is that the high number density prevents particle from growing.

Another point is that when the upper limit of relative humidity is higher, particles can get more growth. We took Cases 2, 4, 5 and 6 as Group 1 with Cases 1, 3 and 7 as Group 2 and compared the upper limits, lower limits and mean value of relative humidity distributions in these two groups. The upper limits of the relative humidity of all cases in group1 are lower than that in group 2. Nothing was found for the lower limits. The mean values of group 1 are also all greater than in group 2; but the difference is very small. For example, the mean value in case 1 is 86.9% and in case 6 is 86.6%; the difference is smaller than 0.3%. As has been mentioned in the previous discussions, such small difference should not lead to so big divergence in the results. So we have reasons to believe that the upper limits of the relative humidity distribution is the major reason for the difference of the results for these two groups.

Then we look at only cases in group1 and found 1) particles grow least for the cases having the lowest upper limit (case 7) and this agrees with what we conclude in the

last paragraph; 2) when the upper limits are the same (case 1 and case 3), higher lower limit and mean value leads to more growth (case 3).

Absolute number of activated particles

Besides the percentage, a more practical and important factor for meteorological consideration is the absolute number of activated particles. Although the lower density cases have higher percentage of activated particles, they might not have the higher absolute number. Higher absolute number means more CCN and can result in more precipitation. Here, we summarize the absolute number of particles growing beyond 5μm and 7μm in radius after 3s in each case and list them in Tables 3.4 and 3.5.

Table 3.4 Absolute number of particles (/m^3) having radii equal to or greater than 7μm

	Case1	**Case2**	**Case3**	**Case4**	**Case5**	**Case6**	**Case7**
1.8E7	2.82E6	0	5.65E6	0	0	0	9.40E5
1.8E8	9.40E6	0	3.18E7	0	0	0	7.32E5
1.8E9	4.01E5	0	0	0	0	0	0
1.8E10	0	0	0	0	0	0	0
1.8E11	0	0	0	0	0	0	0
1.8E12	0	0	0	0	0	0	0
1.8E13	0	0	0	0	0	N/A	N/A

As can been seen in Tables 3.4 and 3.5, although the fraction of activations particles would be higher when the number density is lower, this is not always true for the absolute number of activated particles. The absolute numbers of particles greater than either 7μm or 5μm reach maximum when the number density is 1.8E8/m3. This number may be of great interest because it can predict how many CCN there would be, and hence be related to the amount of the local precipitation. The results here indicate that there exists an optimum number that allow greatest number of particles to be activated. This is consistent with what we have mentioned in the earlier part, that either

too little or too many particles will result in insufficient CCN, and hence suppress the urban rainfall.

Table 3.5 Absolute number of particles (/m^3) having radii equal to or greater than 5μm

	Case1	**Case2**	**Case3**	**Case4**	**Case5**	**Case6**	**Case7**
1.8E7	2.82E6	0	7.20E6	0	0	4.43E4	9.84E5
1.8E8	1.04E7	0	5.85E7	0	0	0	9.40E6
1.8E9	3.18E7	0	1.60E7	0	0	0	8.03E5
1.8E10	0	0	0	0	0	0	0
1.8E11	0	0	0	0	0	0	0
1.8E12	0	0	0	0	0	0	0
1.8E13	0	0	0	0	0	N/A	N/A

5. Conclusions

In this chapter, we use ammonium sulfate as representative and explore the possible effects of particle number concentration and distribution of the environmental relative humidity on the condensational growth of atmospheric aerosol particles. From the above discussions on the calculated results, we come to these conclusions:

a. High number concentration can definitely prevent condensational growth of atmospheric aerosol particles. According to our results, no matter what the relative humidity distribution might be, only when the particle number density is lower than 1.8E9/m^3, can the particles grow to 5μm after 3s; and the lower the density, the more the particle can grow.
b. The highest saturation ratio that atmospheric particles can be exposed to is the most important factor that determines how much of these particles can grow during the first several seconds, and hence can decide whether the particles can be activated.

c. The mean relative humidity of the environment also has effects on the particles' condensational growth. But this effect is not as crucial as the highest saturation ratios. When the distributions of two environments have the same upper limit, the higher the average relative humidity, the more the particle can grow.

CHAPTER IV

THE IMPACT OF ORGANIC SPECIES ON CLOUD AEROSOL CONDENSATIONAL GROWTH

1. Introduction

The chemical composition of fine particulate matter in urban and rural atmospheres is controlled to a significant extent by emissions from terrestrial, marine, and various anthropogenic sources. An important portion of atmospheric particles consists of organic anthropogenic and biogenic compounds related to several emissions sources (Spurny K. 2000). Studies (eg. Rosenfeld et al. 2008 and Twomey et al. 1984) have shown that anthropogenic contributions can change the local distribution of atmospheric aerosol particles. Over much of the land area, biogenitic aerosols have become dominant as more and more of them enter into the atmosphere (Andreae, M. O. 2008). Some studies conclude that organic aerosol makes up a large fraction (20 to 90%) of the submicron particulate mass (Zhang, Q. et al. 2007 and Murphy, D. M. et al., 2006).

How will the anthropogenic aerosols affect the clouds, precipitation and, hence climate? Our previous research work indicates that, with a large amount of man-made aerosols entering into the atmosphere, there can be too many competing for limited water vapor to permit significant vapor accretion by the aerosol particle, thereby suppressing growth to 10 μm -14μm, the requisite first step in the development of rain. This local (urban) suppression may well contribute to formation of regional rainfall when the heavily polluted air parcel moves beyond its principal, urban aerosol sources, becomes diluted, and rises in elevation (Rosenfeld et at. 2008).

Besides the increase of the total number of aerosol particles, organic species may externally and internally mix with inorganic species. Recent studies have shown that tropospheric aerosols composed of internal mixtures of organics with sulfates are quite

common with the organic composing up the 50% of the particle mass(Brooks, S. D. et al. 2002). A significant portion of the total organic content of the tropospheric aerosol has been identified as water- soluble organics, including dicarboxylic acids (Saxena and Hildemann, 1996). Dicarboxylic acids are found in aerosols, and their properties and behavior are likely to be typical of many polar atmospheric organic compounds that are soluble in water (Kawamura, K. et al. 2005 and Yu, L. E. 2003). Laboratory study (Brooks, S. D. et al. 2002) found that the solubilities of several dicarboxylic acids in ammonium sulfate, including maleic, glutaric, malonic, and L-malic acids, are quite high, and the presence of water-soluble dicarboxylic acids caused deliquescence to occur at a lower relative humidity than pure ammonium sulfate. Their study with dicarboxylic acids indicates that in the case of the soluble dicarboxylic acids, adding organic molar fractions up to and including eutonic proportions lowers the deliquescence relative humidity (DRH) below that found for pure ammonium sulfate, which suggests that atmospheric aerosols may become liquid at lower relative humidities than calculations based on pure ammonium sulfate would predict. These show that organics may have great influence on the chemical and physical properties, and hence on the growth of CCN.

The mixing, either internal (the mixture acts as a new single species) or external (two species act individually), of atmospheric organic and inorganic species has effects on CCN growth. Specifically, the internal mixing can change the thermodynamic character of the aerosol particles and hence is expected to have great impact. Here, by applying the thermodynamic data of recent research work, we will test with malic acid and maleic acid how internal and external mixing of organic and inorganic species (ammonium sulfate will be used as representative) could affect the growth of both species by using our CFD coupled aerosol competitive condensational growth model.

2. Results and discussion

To accomplish our projectile, we need water activity data for malic acid (Peng, C., 2001), maleic acid (Choi and Chan, 2002), and internal mixtures of them with ammonium sulfate (Wise et al. 2003).

The same as in the previous chapter, the change in water activity with temperature was ignored. The validation of this assumption will be discussed later.

a. Random relative humidity

This time, we did not repeat all cases 1- 7 (Table 3.1) in chapter III. We only choose cases 1, 3, and 7 (Table 4.1) for our study.

Table 4.1 Upper limit and lower limit of the relative humidity for cases 1, 3 and 7

Case No.	Lower Limit a	Upper Limit b	$\tilde{R}$
1	65%	110%	86.9%
3	91%	110%	100.4%
7	70%	106%	87.6%

We test pure malic acid (LMA), pure maleic acid (MA), external and internal mixture of malic acid with ammonium sulfate(LMA_ex & LMA_in), and external and internal mixture of maleic acid with ammonium sulfate (MA_ex & MA_in). We compare these results with the calculationed results we obtained with pure ammonium sulfate (AS). Since our previous results show that when the aerosol particle number density is greater than 1.8E11/m^3, nothing would be activated, we only do number concentration of 1.8E7/m^3, 1.8E8/m^3, 1.8E9/m^3, 1.8E10/m^3, and 1.8E11/m^3. We use the mole fractions of the acid in the eutonic solution, which are *n*H2Malic/(*n*H2Malic + *n* (NH4)2SO4) = 0.6579 and *n*H2Maleic/(*n*H2Maleic + *n*(NH4)2SO4) = 0.55.

Case 1

Figures 4.1(a) – 4.1(g) are the comparison of calculation results of case 1 after 3.0 s for (a) ammonium sulfate, (b) malic acid, (c) external mixing (d) and internal

mixing of malic acid and ammonium sulfate, (e) maleic acid, (f) external mixing and (g) internal mixing of malic acid and ammonium sulfate.

The x-axis of all graphs has been adjusted to have the same range for better comparison.

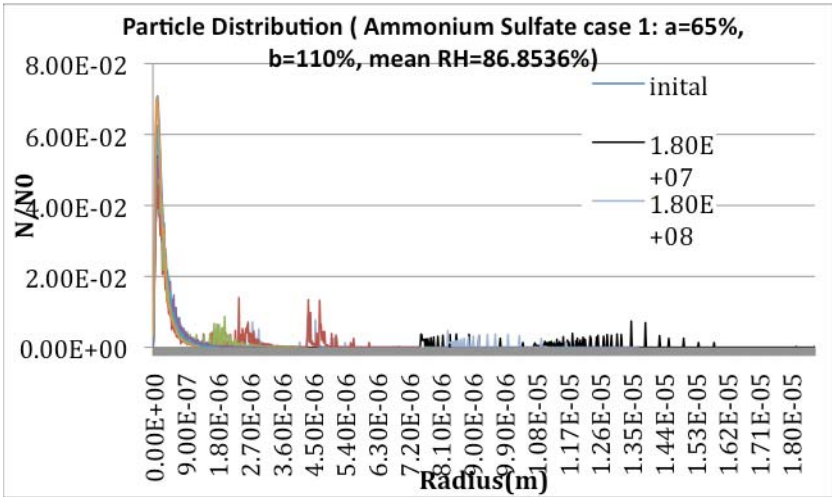

Figure 4.1(a) Calculation results at 3.0s of case 1 for NH_4SO_4

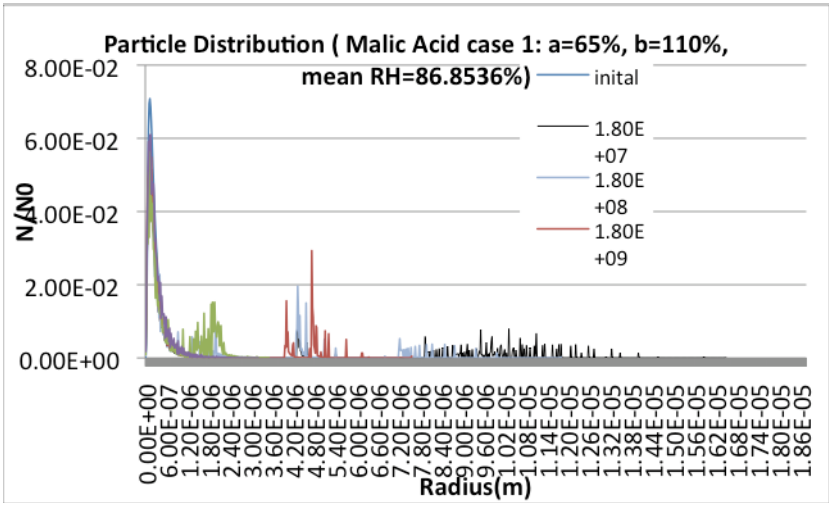

Figure 4.1(b) Calculation results at 3.0s of case 1 for malic acid

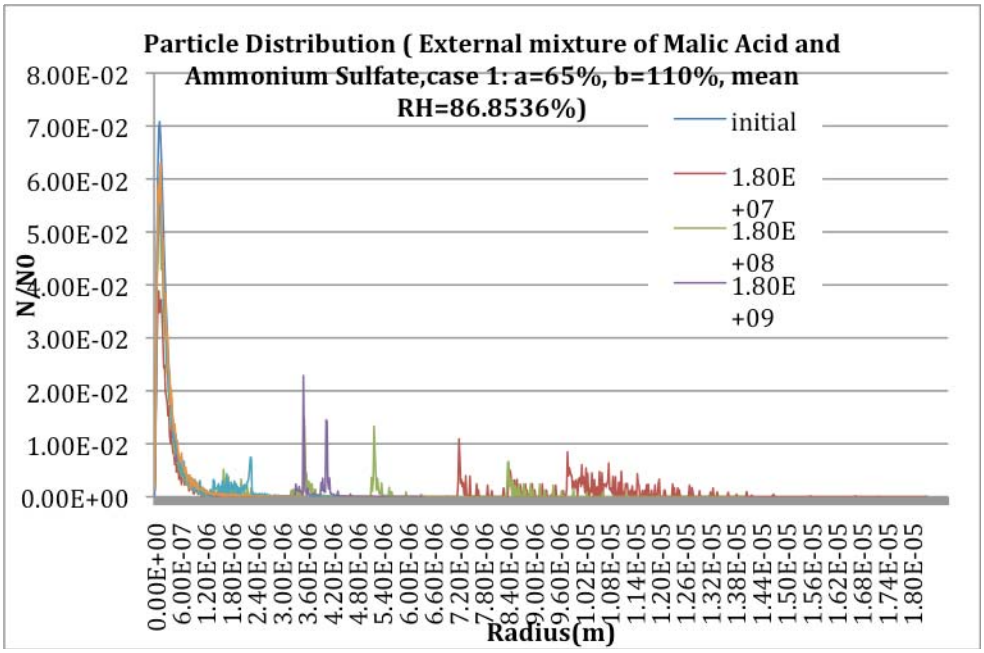

Figure 4.1(c) Calculation results at 3.0s of case 1 for external mixing of malic acid and NH_4SO_4

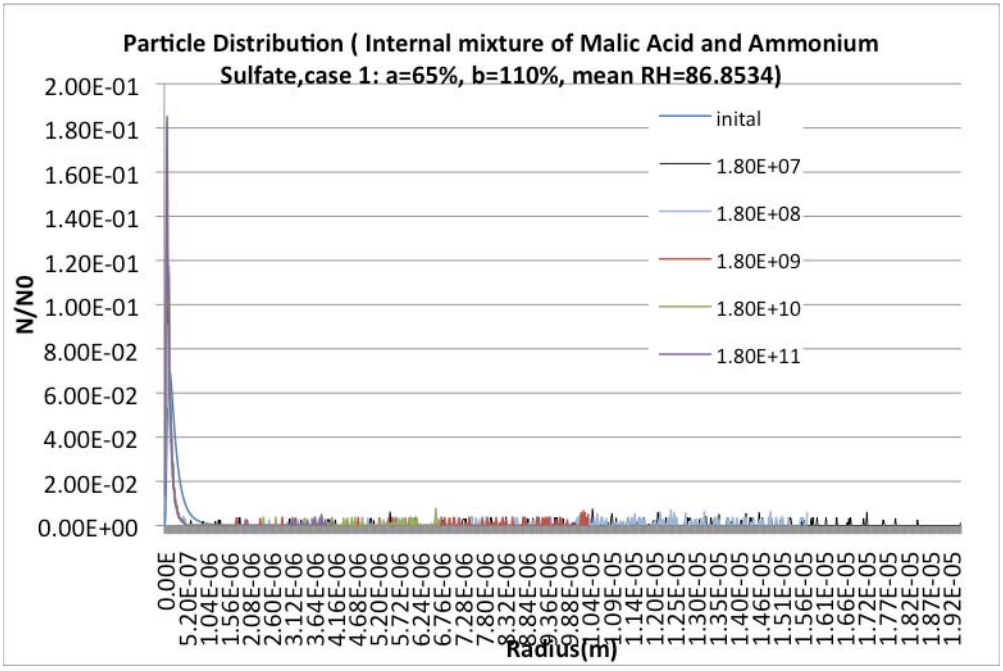

Figure 4.1(d) Calculation results at 3.0s of case 1 for internal mixing of malic acid and NH_4SO_4

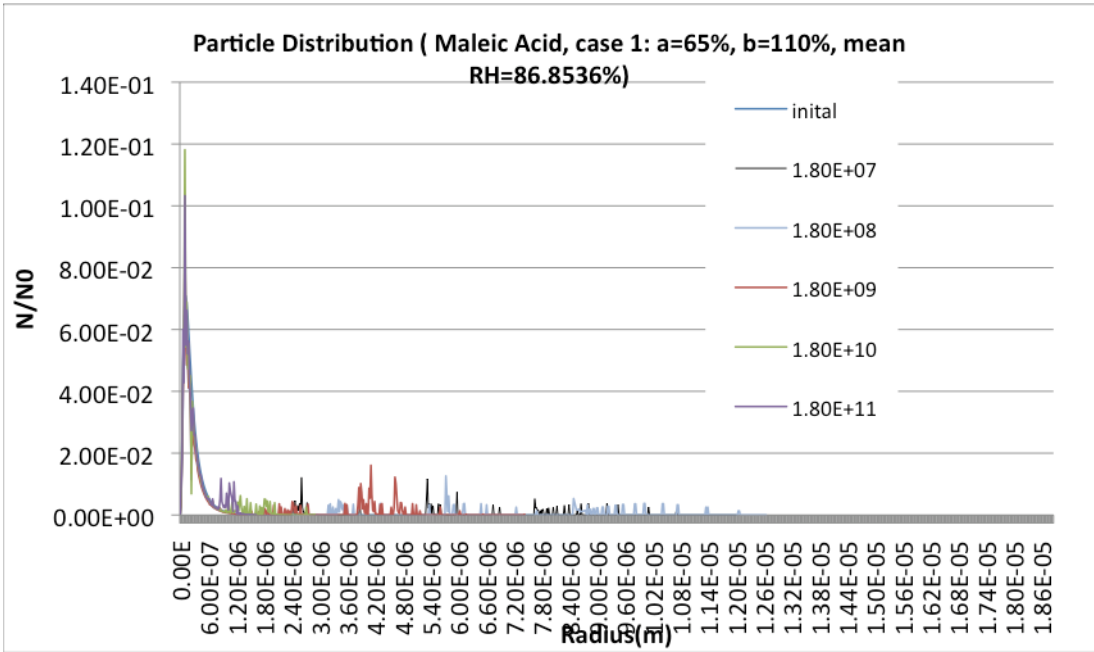

Figure 4.1(e) Calculation results at 3.0s of case 1 for maleic acid

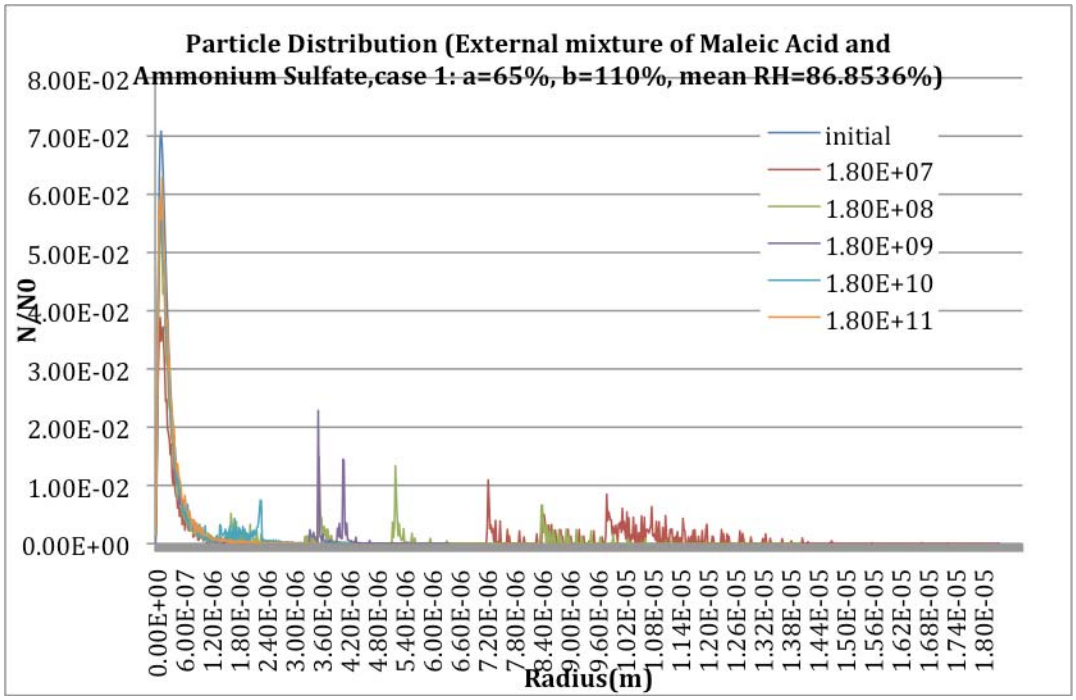

Figure 4.1(f) Calculation results at 3.0s of case 1 for external mixing of maleic acid and NH_4SO_4

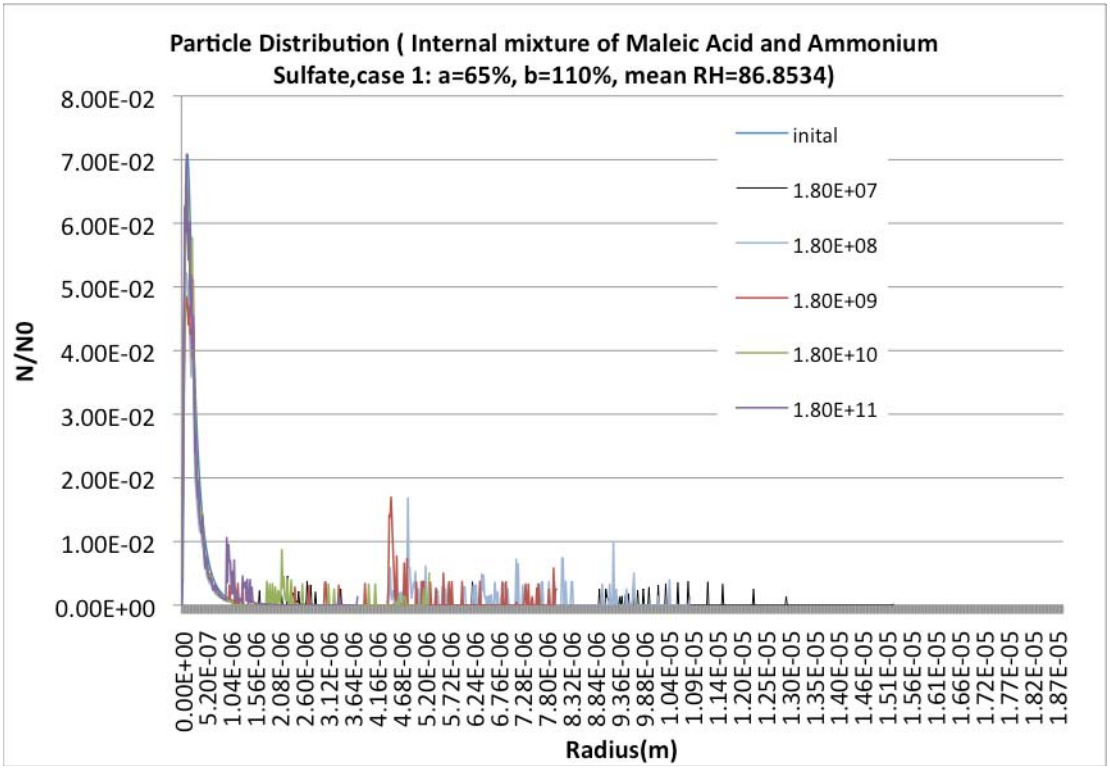

Figure 4.1(g) Calculation results at 3.0s of case 1 for internal mixing of maleic acid and NH_4SO_4

Lower number density leads to more growth, and this is what we have observed in the previous chapter. These results show that after 3.0 s, under the RH condition of case1, for the lowest density (1.8E7/m^3), the maximum radii are about 18.7 μm for pure ammonium sulfate, 16.5 μm for pure malic acid, 18.4 μm for external mixing of malic acid and ammonium sulfate, 19.5 μm for internal mixture of malic acid and ammonium sulfate, 12.7 μm for pure maleic acid, 18.4 μm for external mixing of maleic acid and ammonium sulfate, and 15.2 μm for internal mixture of maleic acid and ammonium sulfate. More details are provided in Table 4.2.

As discussed previously, CCN with radiuss greater than 7μm are considered as activated. A less stringent criterion of 5μm is also used sometimes. Here, we summarize the percentage of particles growing beyond 5μm and 7μm in radius after 3s in each case and list them in Tables 4.3 and 4.4.

There is something interesting for the calculated results of the mixtures. The internal mixture of malic acid and ammonium sulfate grow more than either of the pure materials. This internal mixture of can grow 4.3% more than pure ammonium sulfate, and 18.2% more than pure malic acid; this somehow indicates that the introduction of some water-soluble organic material might help activation of CCNs. But, we do not see the same thing for the external mixture of maleic acid and ammonium sulfate. It seems that the external mixture of maleic acid and ammonium sulfate actually grow less than either of the pure materials. The same thing happens when we look at the fraction of particles that is larger than 5μm or 7μm. The internal mixing of malic acid and ammonium sulfate leads more particles to grow beyond 5μm or 7μm after 3s; while the external mixing of malic acid and ammonium sulfate makes fewer particles to grow that much.

Table 4.2 Radius of the largest particles (μm) of 3s calculation results for case 1

	External mixing				**Pure material**			**Internal Mixing**	
	LMA+ AS		MA+ AS		AS	LMA	MA	LMA+ AS	MA+AS
	AS	LMA	AS	MA					
1.8E7	18.4	15.6	18.4	15.6	18.7	16.5	12.7	19.5	15.2
1.8E8	14.0	12.0	14.8	12.6	13.7	11.8	14.2	15.7	10.9
1.8E9	6.38	5.16	7.16	5.86	7.52	7.56	7.44	10.4	8.02
1.8E10	4.30	3.36	4.72	2.16	4.10	3.50	2.80	6.72	5.30
1.8E11	3.60	3.06	4.02	1.22	3.20	3.20	1.64	4.12	3.76

Why are there differences between the results of the two organic species? Is this because that the random character of relative humidity, which we discussed the chapter III, happened to suppress the growth of the external mixture of maleic acid and

ammonium sulfate? Or the increasing of growth is a specific character of only internal mixture malic acid and ammonium Sulfate? Or is it that the increasing is some artifact of random chosen RH? However, it is hard to conclude here, we will do more cases and see.

Secondly, for the results of external mixing, we can see separated peaks for each species from the figures, and the more soluble one always grow more than the less soluble one. Counting in the random effects we discussed in chapter III, at least according to these results, we think the external mixing does not have obvious effects on how much the aerosol particles can grow. We can see from these results, compared with pure material, either the size of the largest particle or the fraction of activated particles do not change much when they are externally mixed.

Table 4.3 Percentage of particles have radii equal to or greater than 7μm after 3s calculation for case 1

	External mixing						**Pure material**			**Internal Mixing**	
	LMA+ AS			MA+ AS			AS	LMA	MA	LMA+ AS	MA +AS
	AS	LMA	Total	AS	MA	Total					
1.8E7	31.6	31.6	31.6	18.1	16.9	17.3	15.7	20.9	5.32	29.9	6.3
1.8E8	5.29	5.26	5.27	11.0	10.9	11.0	5.22	5.22	10.8	30	9.64
1.8E9	0	0	0	0.02	0	0.01	0.02	0	0.02	11.2	2.90
1.8E10	0	0	0	0	0	0	0	0	0	0	0
1.8E11	0	0	0	0	0	0	0	0	0	0	0

Table 4.4 Percentage of particles have radii equal to or greater than 5μm after 3s calculation for case 1

	External mixing						**Pure material**			**Internal Mixing**	
	LMA+ AS			MA+ AS			AS	LMA	MA	LMA +AS	MA+ AS
	AS	LMA	Total	AS	MA	Total					
1.8E7	31.6	31.6	31.6	26.4	26.3	26.4	15.7	21.3	10.4	32.8	6.30
1.8E8	10.6	10.5	10.5	16.1	15.8	15.9	5.77	6.07	16.0	34.1	19.6
1.8E9	0.9	0.02	0.01	0.45	0.02	0.21	1.77	2.33	1.28	14.9	7.35
1.8E10	0	0	0	0	0	0	0	0	0	5.29	1.01
1.8E11	0	0	0	0	0	0	0	0	0	0	0

Case 3

We repeat the calculation for case 3 (Table 4.1). The relative humidity distribution has both higher lower and upper boundary, so we expect to see the particle grow more here. Figures 4.2(a) – 4.2(g) are the comparisons of calculated results of case 3 after 3.0 s for ammonium sulfate (a), malic acid (b), external mixing (c) and internal mixing (d) of malic acid and ammonium sulfate, maleic acid (e), their external mixing (f) and internal mixing (f) of malic acid and ammonium sulfate.

Again, the x-axis of all graphs has been adjusted to have the same range for better comparison.

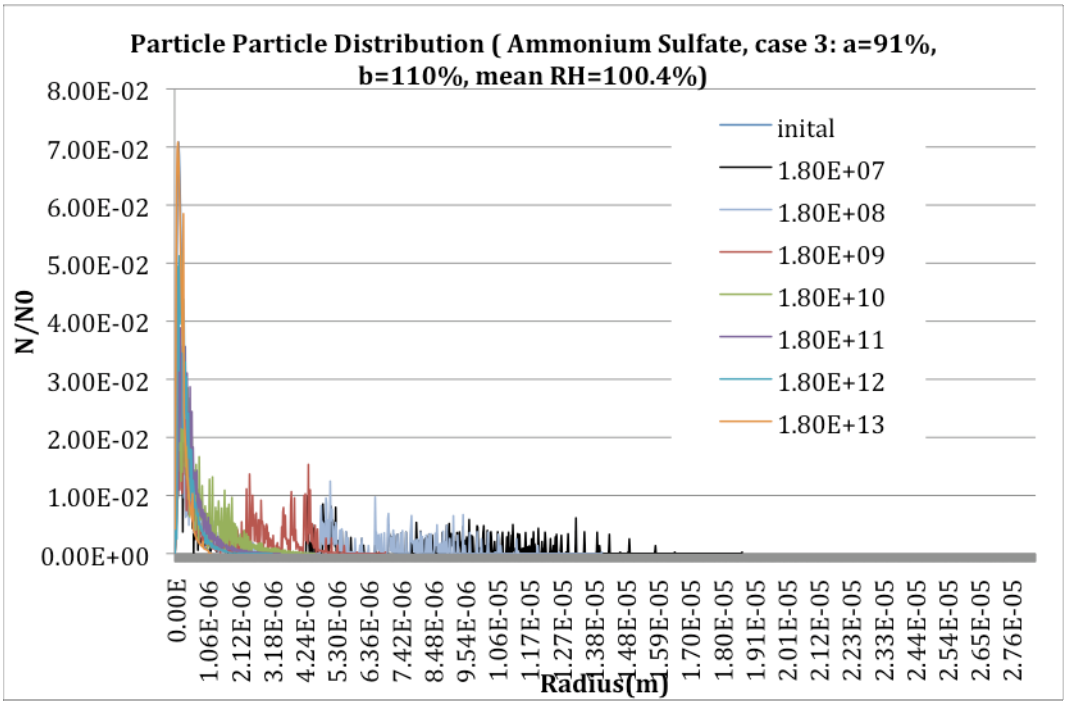

Figure 4.2(a) Calculation results at 3.0s of case 3 for NH_4SO_4

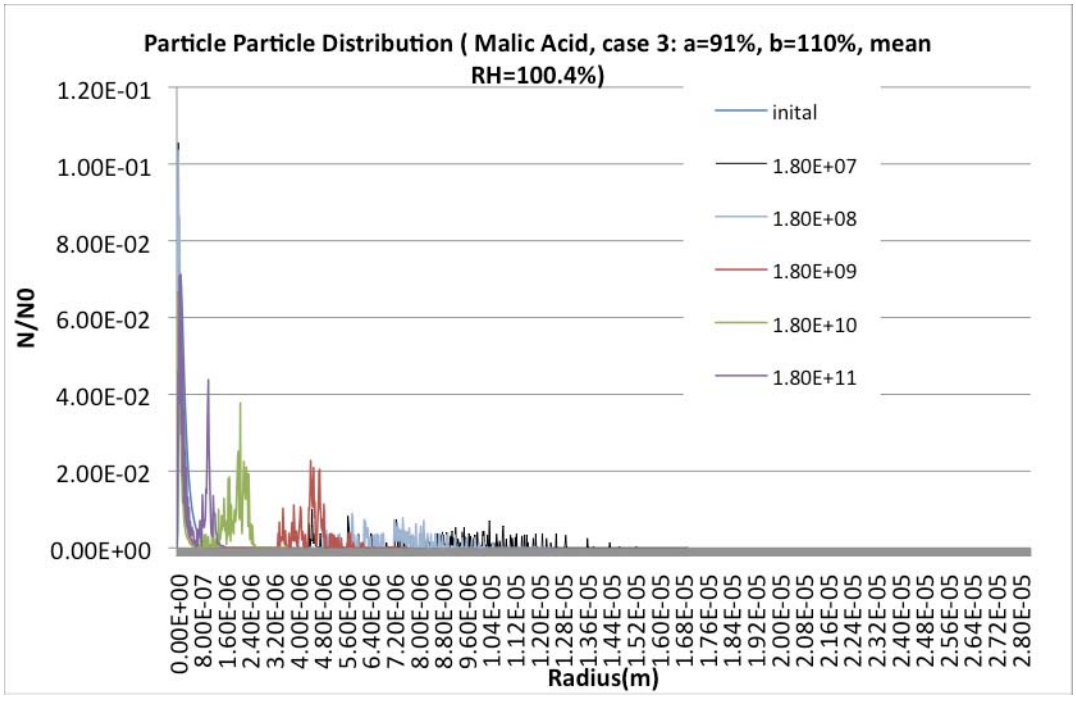

Figure 4.2(b) Calculation results at 3.0s of case 3 for malic acid

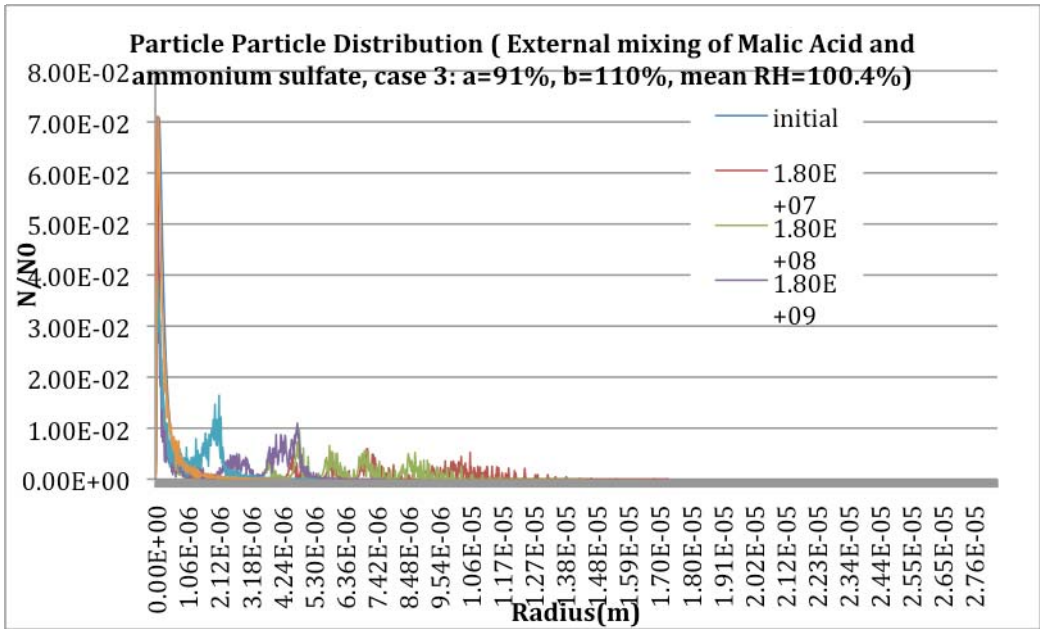

Figure 4.2(c) Calculation results at 3.0s of case 3 for external mixing of malic acid and NH_4SO_4

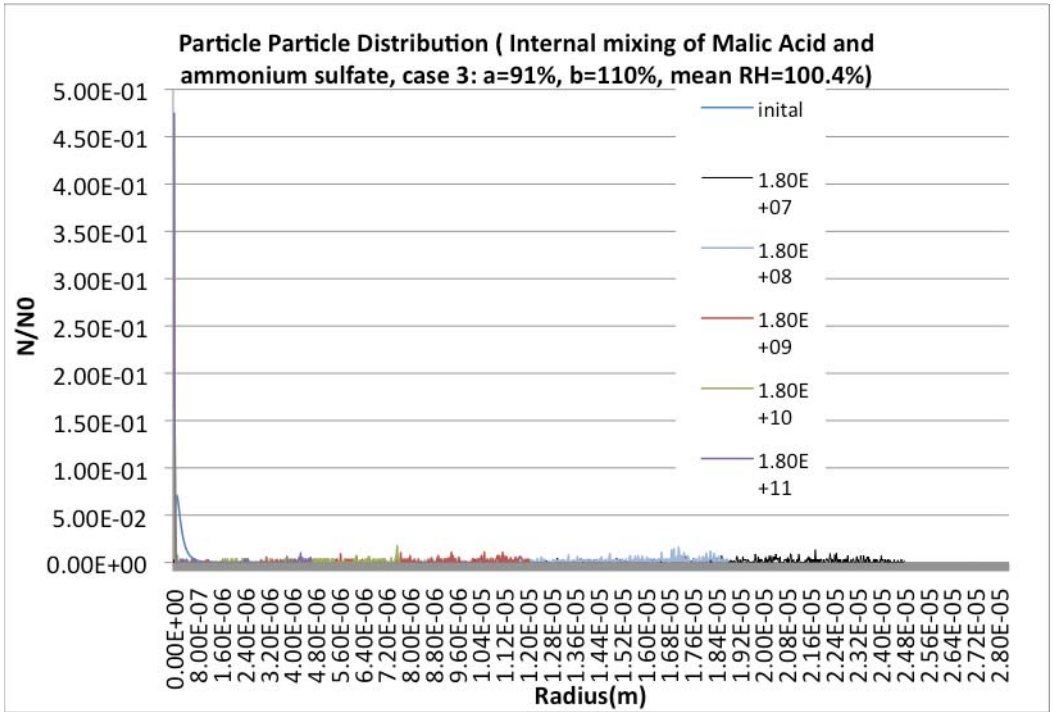

Figure 4.2(d) Calculation results at 3.0s of case 3 for internal mixing of malic acid and NH_4SO_4

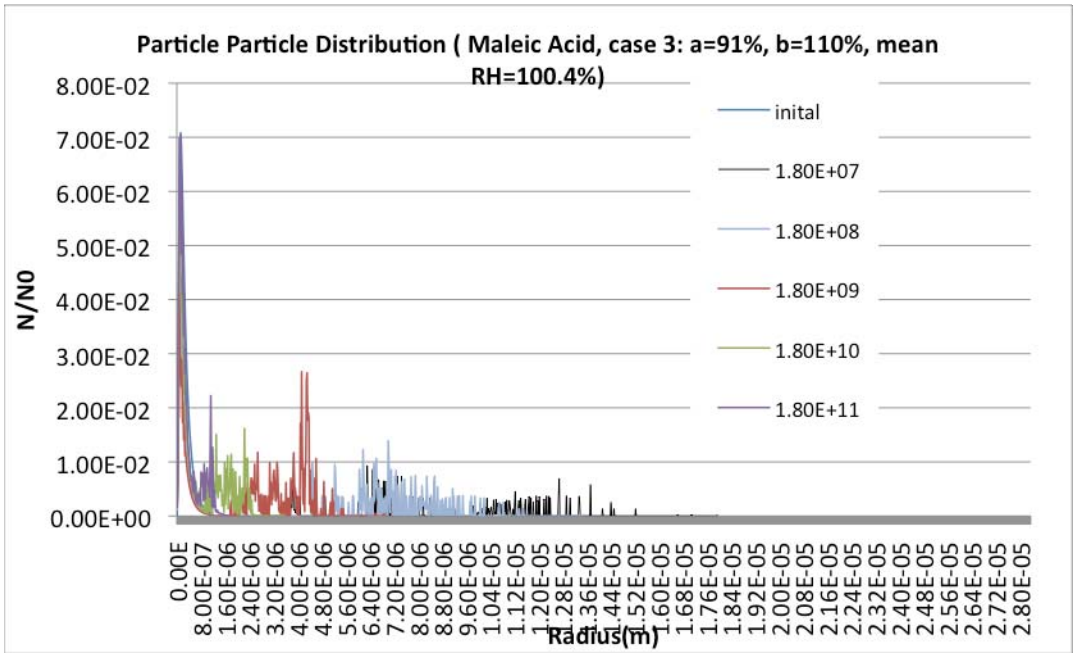

Figure 4.2(e) Calculation results at 3.0s of case 3 for maleic acid

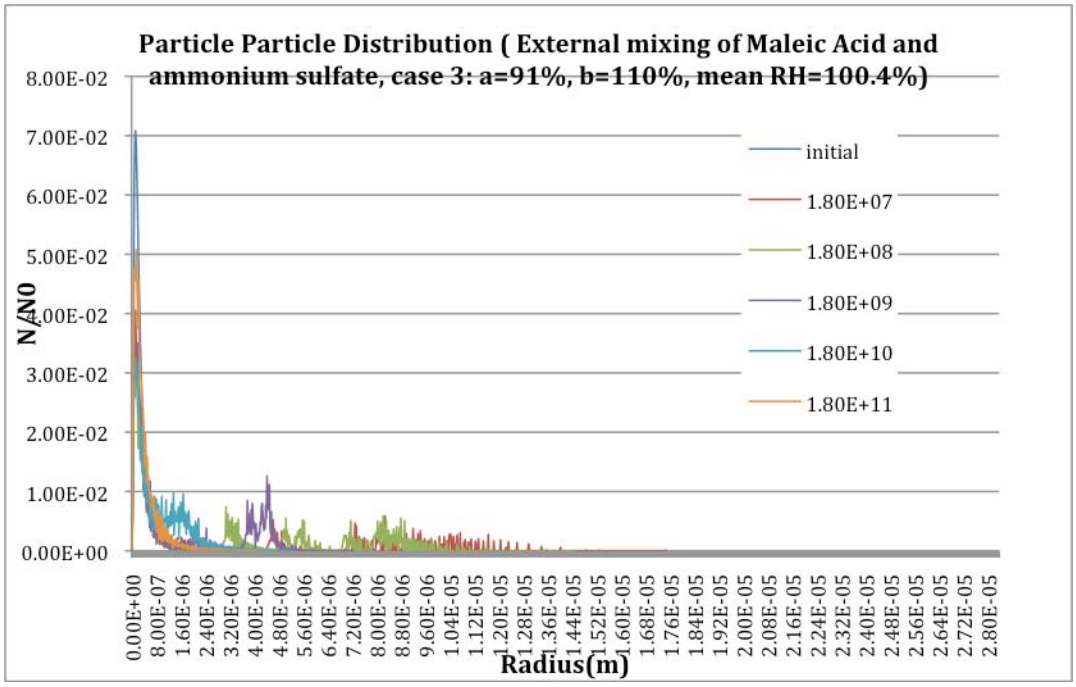

Figure 4.2(f) Calculation results at 3.0s of case 3 for external mixing of maleic acid and NH_4SO_4

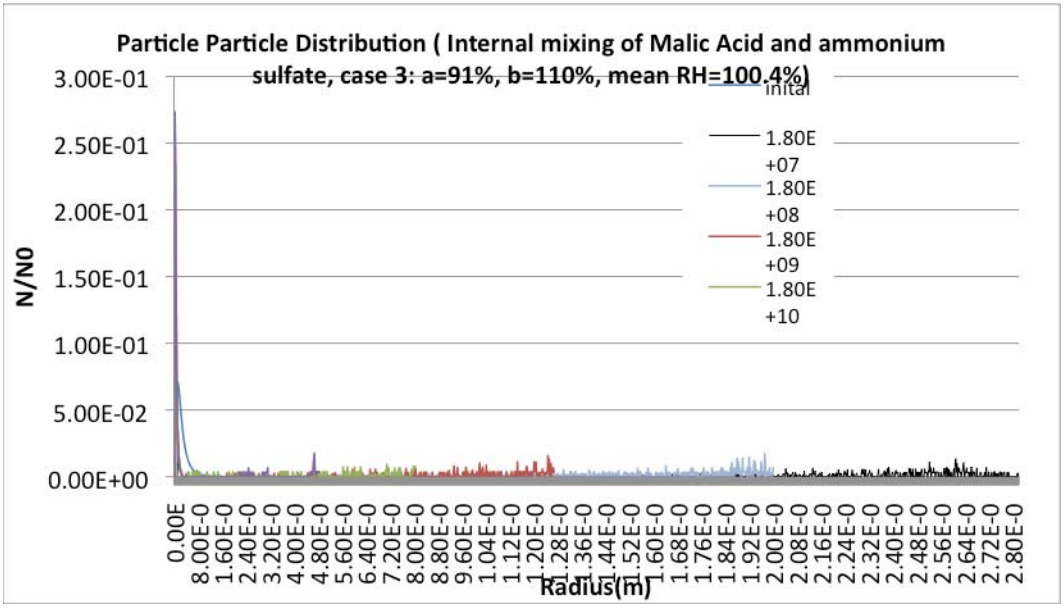

Figure 4.2(g) Calculation results at 3.0s of case 3 for internal mixing of maleic acid and NH_4SO_4

Table 4.5 Radius of the largest particles (μm) of 3s calculation results for case 3

	External mixing				**Pure material**			**Internal Mixing**	
	LMA+ AS		MA+ AS		AS	LMA	MA	LMA+AS	MA+AS
	AS	LMA	AS	MA					
1.8E7	17.3	14.7	17.5	14.9	18.7	17.0	18.0	19.5	28.2
1.8E8	14.5	12.4	14.5	12.4	14.1	12.4	13.5	15.7	20.0
1.8E9	7.74	6.38	7.20	5.88	6.94	7.62	6.90	10.4	12.7
1.8E10	5.44	2.34	5.38	2.18	4.60	3.64	3.58	6.72	8.06
1.8E11	4.52	1.06	4.22	1.20	3.46	1.64	1.66	4.12	4.82

Also, we summarize the details of the largest particles' size in Table 4.5.

We can see that after 3.0 s, under the RH condition of case3, for the lowest density (1.8E7/m^3) the maximum radii are about 18.7 μm for pure ammonium sulfate,

17.0 μm for pure malic acid, 17.3 μm for external mixing of malic acid and ammonium sulfate, 19.5 μm for internal mixture of malic acid and ammonium sulfate, 18.0 μm for pure maleic acid, 17.0 μm for external mixing of maleic acid and ammonium sulfate, and 28.2 μm for internal mixture of maleic acid and ammonium sulfate. More details are provided in Table 4.5.

The internal mixtures of both malic acid & ammonium sulfate and maleic acid & ammonium sulfate grow more than either of the pure material. This agrees with our speculation that the introduction of some water-soluble organic material might help activation of CCNs. The same thing happens when we look at the fraction of particles that is large than 5μm or 7μm. The internal mixing leads more particles to grow beyond 5μm or 7μm after 3s. Again, for the external mixing, we see 1) separated peaks for each species from the figures, and the more soluble one always grows more than the less soluble one; 2) when two materials that are externally mixed, the activated fractions of the two species are getting close to each other; but this time, we found this tendency is more obvious when the number concentration is low, which means there will be abundant water vapor for both to grow. We can see when the particle number density equals to 1.8E8/m3, there are 5% more particles >= 7μm or >=5μm of ammonium sulfate than of malic acid; however, for ammonium sulfate and maleic acid, we can still see that these fractions of the two species are getting closer at this density.

One question we want to examine further is whether either of the two species, which are externally mixed, affects the growth of each other. If the answer is yes, then, how do they interact with each other? From Tables 4.6 and 4.7, it looks like the activated fractions (if there is any) of the two external mixed species are close to each other. We can see for the external mixture of malic acid and ammonium sulfate, with number concentration of 1E7/m^3, the fraction of particles >= 7μm or >= 5μm are 31.6% of both species, while with number concentration of 1.8E8/m^3, the fraction of particles >= 7μm is 5.26% for malic acid and 5.29% for ammonium sulfate, and the fraction of particles >= 5 μm is 10.5 % for malic acid and 10.6% for ammonium sulfate. The numbers are very close for the two species. This is in agreement with Dusek et al

(2009)'s conclusion that particles' ability to act as CCN is largely controlled by aerosol size. Again, we will do more cases to see whether these phenomena repeat.

The percentage of particles growing beyond 5 μm and 7 μm in radius after 3s are summarized in Table 4.6 and 4.7.

Table 4.6 Percentage of particles having radii equal to or greater than 7μm after 3s calculation for case 3

	External mixing						**Pure material**			**Internal Mixing**	
	LMA+ AS			MA+ AS			AS	LMA	MA	LMA +AS	MA+ AS
	AS	LMA	Total	AS	MA	Total					
1.8E7	26.6	23.9	24.8	21.1	21.0	21.0	31.4	27.0	21.8	88.0	54.3
1.8E8	21.5	16.6	18.3	21.1	19.1	20.0	17.7	17.3	27.0	72.9	77.6
1.8E9	0.67	0	0.23	0.04	0.0	0.02	0	0.14	0.14	38.9	46.4
1.8E10	0	0	0	0	0	0	0	0	0	7.08	11.8
1.8E11	0	0	0	0	0	0	0	0	0	0	0

Table 4.7 Percentage of particles having radii equal to or greater than 5μm after 3s calculation for case 3

	External mixing						**Pure material**			**Internal Mixing**	
	LMA+ AS			MA+ AS			AS	LMA	MA	LMA +AS	MA+ AS
	AS	LMA	Total	AS	MA	Total					
1.8E7	33.0	31.7	32.2	22.5	21.2	21.8	40.0	32.4	31.5	89.6	55.3
1.8E8	37.1	32.4	34.0	31.9	28.2	29.8	32.5	28.0	47.7	75.9	79.9
1.8E9	5.28	0.79	2.33	1.98	0.09	0.9	0.9	4.03	1.69	45.1	52.3
1.8E10	0.16	0	0.06	0.07	0	0.03	0	0	0	18.0	21.3
1.8E11	0	0	0	0	0	0	0	0	0	0	3.76

Case 7

We again repeat the calculation for case 7 (Table 4.1). This relative humidity distribution is similar to that in case 1 but has a higher upper boundary of 70% instead of 65%, and a lower lower boundary of 107% instead of 110%. Figures 4.3(a) – (g) are the comparison of calculation results of case 7 after 3.0 for ammonium sulfate (a), malic acid (b), external mixing (c) and internal mixing (d) of malic acid and ammonium sulfate, maleic acid (e), their external mixing (f) and internal mixing (f) of malic acid and ammonium sulfate.

Again, the x-axis of all graphs has been adjusted to have the same range for better comparison.

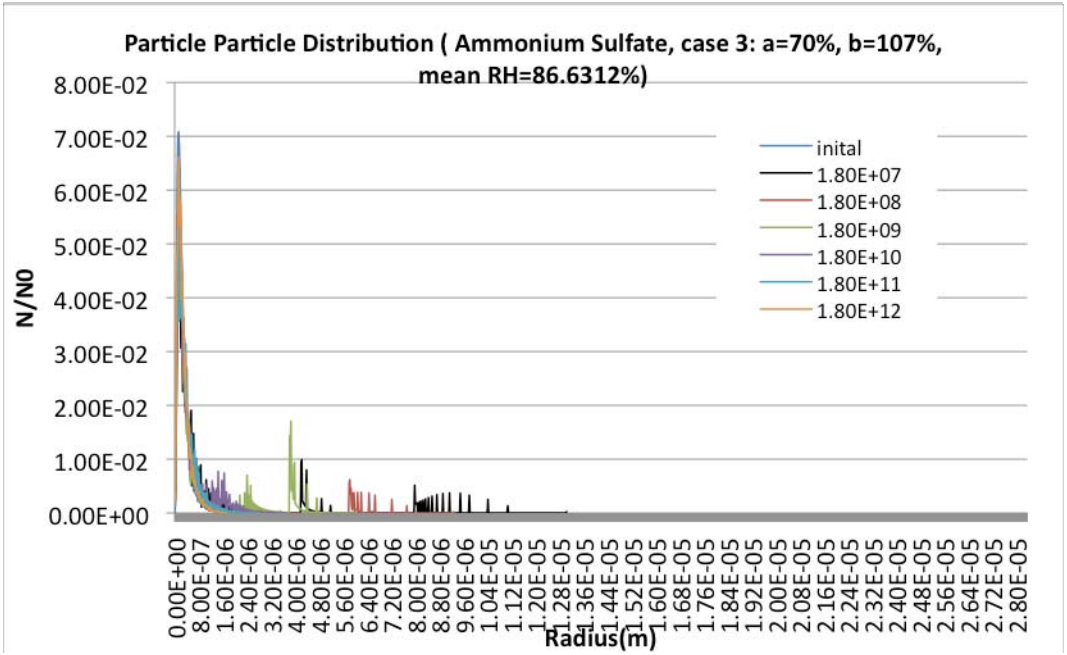

Figure 4.3(a) Calculation results at 3.0s of case 7 for NH_4SO_4

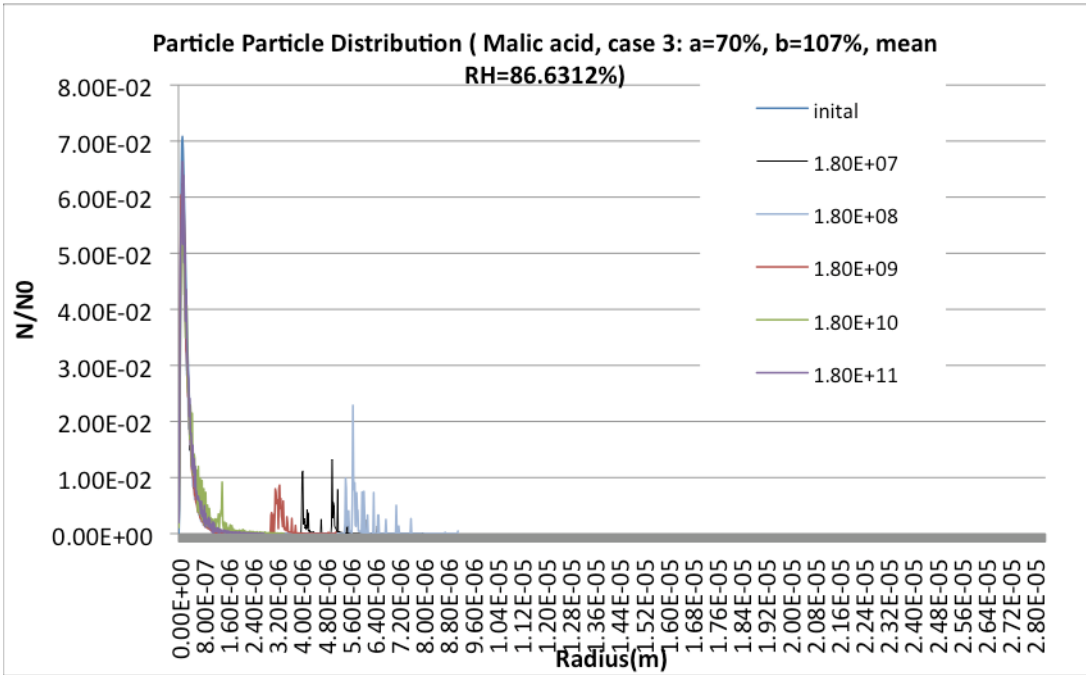

Figure 4.3(b) Calculation results at 3.0s of case 7 for malic acid

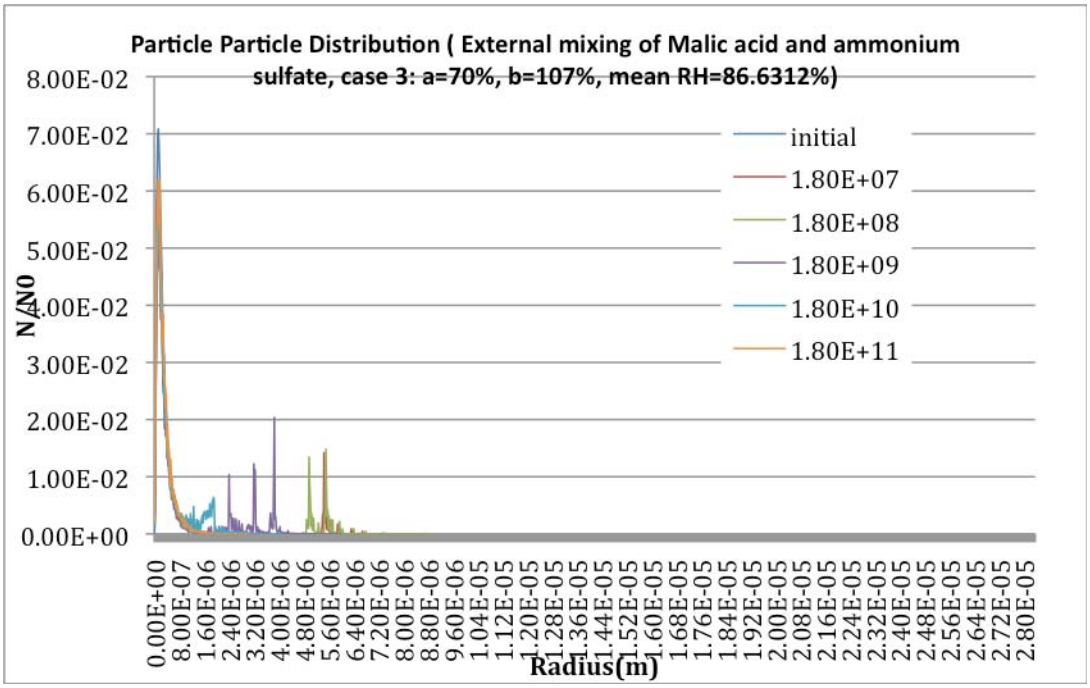

Figure 4.3(c) Calculation results at 3.0s of case 7 for external mixing of malic acid and NH4SO4

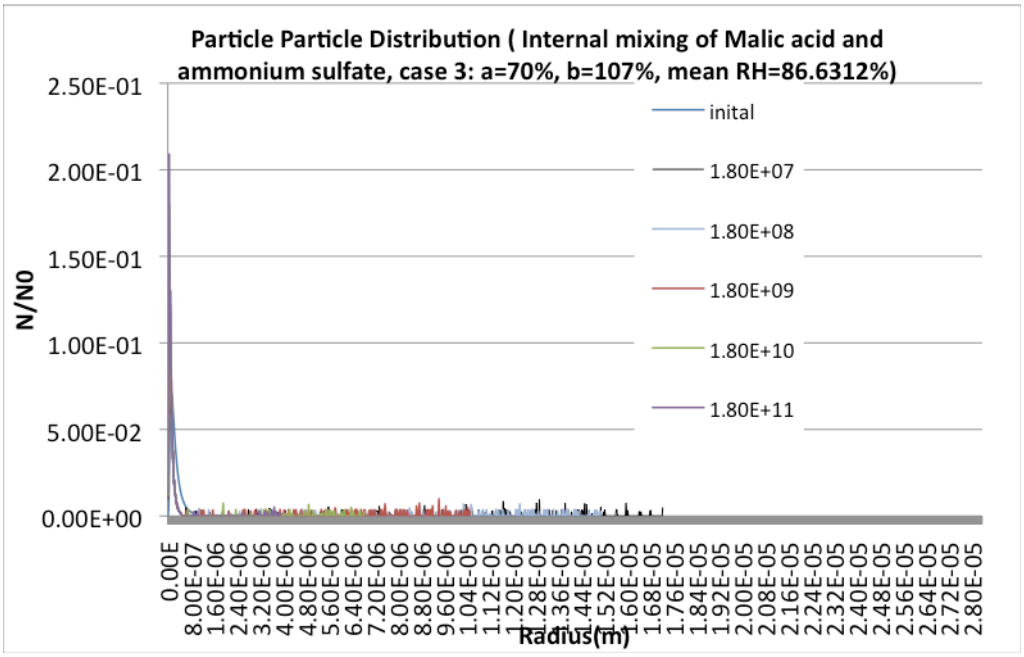

Figure 4.3(d) Calculation results at 3.0s of case 7 for internal mixing of malic acid and NH_4SO_4

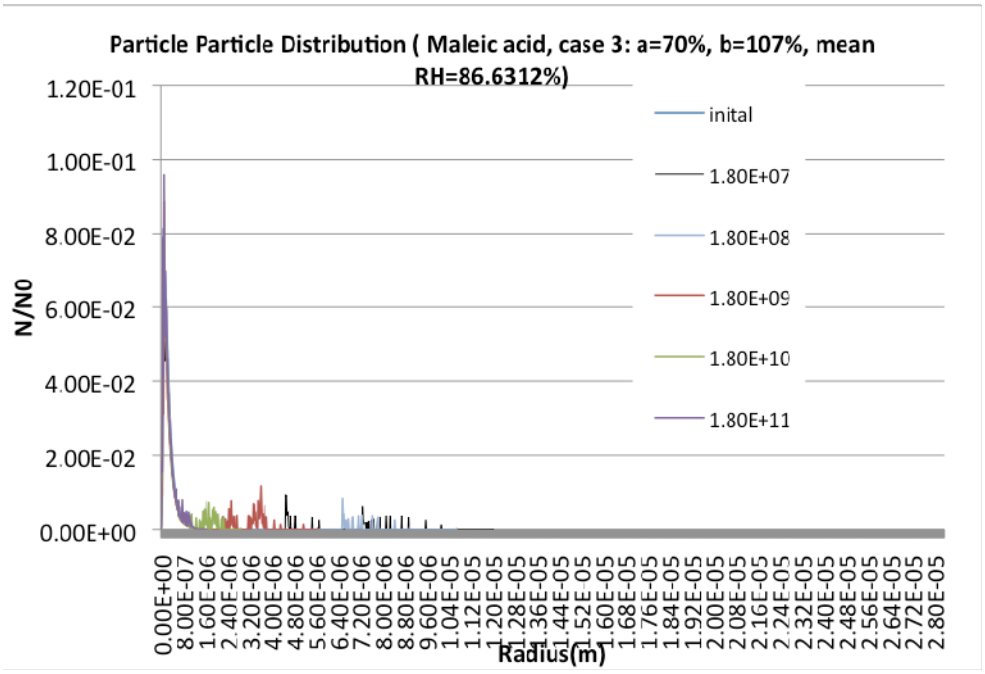

Figure 4.3(e) Calculation results at 3.0s of case 7 for maleic acid

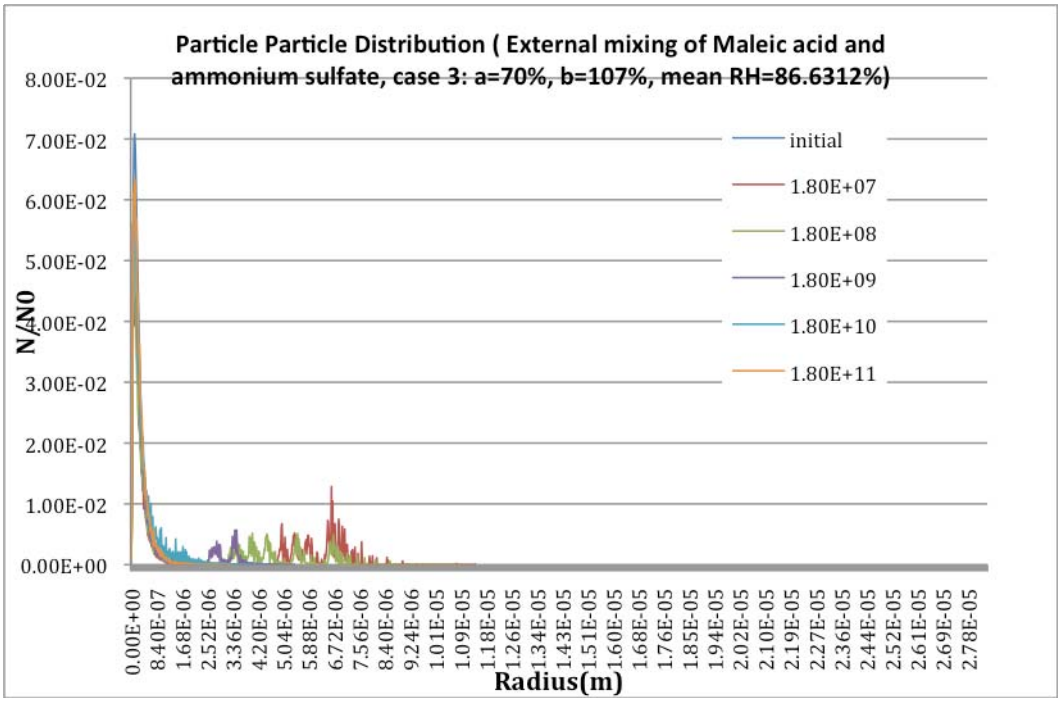

Figure 4.3(f) Calculation results at 3.0s of case 7 for external mixing of maleic acid and NH_4SO_4

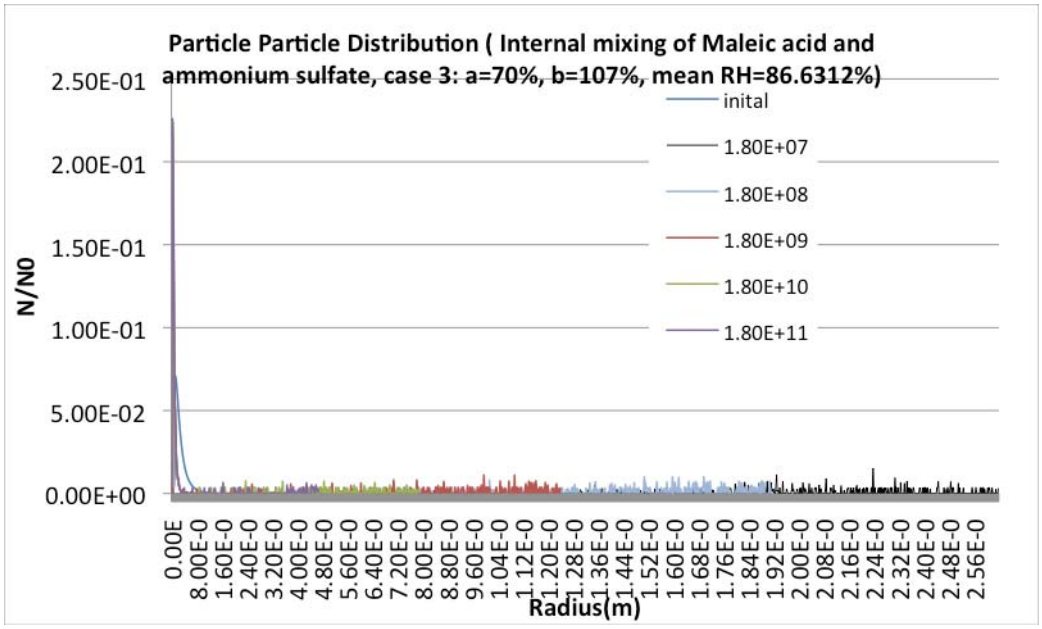

Figure 4.3 (g) Calculation results at 3.0s of case 7 for internal mixing of maleic acid and NH_4SO_4

Also, we summarized the details of the largest particles' size in Table 4.8, and percentage of particles growing beyond 5μm and 7μm in radius after 3s in Table 4.9 and Table 4.10.

Table 4.8 Radius of the largest particles (μm) of 3s calculation results for case 7

	External mixing				**Pure material**			**Internal Mixing**	
	LMA+ AS		MA+ AS		AS	LMA	MA	LMA+ AS	MA+AS
	AS	LMA	AS	MA					
1.8E7	8.74	7.34	11.4	9.68	13.0	8.00	12.1	17.2	26.4
1.8E8	8.86	7.42	10.9	9.24	9.28	9.14	10.7	15.1	19.2
1.8E9	5.98	4.78	5.40	4.24	6.04	5.14	5.64	10.5	12.4
1.8E10	4.16	3.30	4.50	1.84	4.00	3.44	2.90	6.84	7.90
1.8E11	3.06	2.76	3.28	1.22	3.40	2.78	1.60	3.94	4.68

Table 4.9 Percentage of particles have radii equal to or greater than 7μm after 3s calculation for case 7

	External mixing						**Pure material**			**Internal Mixing**	
	LMA+ AS			MA+ AS			AS	LMA	MA	LMA +AS	MA +AS
	AS	LMA	Total	AS	MA	Total					
1.8E7	0.02	0.02	0.02	6.97	3.72	5.08	5.22	0.02	5.35	31.2	81.7
1.8E8	0.05	0.02	0.03	1.46	0.77	1.08	0.41	0.9	1.84	22.8	68.4
1.8E9	0	0	0	0	0	0	0	0	0	15.4	37.9
1.8E10	0	0	0	0	0	0	0	0	0	7.08	4.68
1.8E11	0	0	0	0	0	0	0	0	0	0	0

Table 4.10 Percentage of particles have radii equal to or greater than 5μm after 3s calculation for case 7

	External mixing						**Pure material**			**Internal Mixing**	
	LMA+ AS			MA+ AS			AS	LMA	MA	LMA +AS	MA +AS
	AS	LMA	Total	AS	MA	Total					
1.8E7	5.26	5.26	5.26	30.8	28.8	29.7	5.47	5.38	5.94	36.3	83.7
1.8E8	8.22	8.60	8.47	11.6	10.7	11.1	5.22	15.7	5.22	25.7	71.5
1.8E9	0.05	0	0.02	0.06	0	0.03	0.05	2.23	0.15	21.3	44.5
1.8E10	0	0	0	0	0	0	0	0	0	4.69	15.7
1.8E11	0	0	0	0	0	0	0	0	0	0	3.76

These calculational results further confirm what we previously speculated. The enhancement of growth by internal mixing is easy to see. Here, the internal mixing can at most lead to 70% more particles being activated. Again, for the external mixing the activated fractions of the two species are getting close to each other.

So, we highly suspect that 1) internal mixing of malic acid or maleic acid with ammonium may greatly enhance the atmospheric aerosol's growth, and enable more of them to be activated. 2) External mixing of two species may make the specific materials not matter any more, which means, as long as they are water soluble, they eventually end up with the same (or very similar) number of activated fractions.

But, before we draw any conclusion, we have to make a way to eliminate the uncertainty that the random selection of relative humidity brings to our results. Although all the calculations in the same comparison group were done with the same relative humidity distribution, the RH of the 19 parcels, where the aerosol particles reside and grow, are still not exactly the same in every calculation. Before we finally conclude anything, we will do more calculations. So, we will next perform our final step to test the two speculations listed above. We abandon the technology of random selection of relative humidity, and make the relative humidities used in all the

calculations in the same comparison group exactly the same, including those assigned to the 19 individual air parcels and the larger environment.

b. Fixed relative humidity

Here, we select two groups of relative humidity (Table 4.11), and perform calculations for all the materials we used in section I with relative humidity in each group. The relative humidity in each group will be assigned to each of the 19 air parcels (AP) and also the large environment accordingly. Calculated results that use the same group of relative humidity will be compared.

Table 4.11 Relative humidity (%) information in Group 1 and 2

Relative humidity info in Group 2	**AP1**	**AP2**	**AP3**	**AP4**	**AP5**	**AP6**	**AP7**	**AP8**	**AP9**	**AP10**
	97.173	**99.052**	**104.95**	**96.985**	**102.27**	**94.19**	**96.424**	**91.056**	**106.11**	**109.4**
	AP11	**AP12**	**AP13**	**AP14**	**AP15**	**AP16**	**AP17**	**AP18**	**AP19**	**Large**
	107.46	**101.7**	**91.606**	**97.547**	**102.08**	**91.606**	**103.99**	**96.958**	**106.3**	**100.4**
Relative humidity info in Group 1	**AP1**	**AP2**	**AP3**	**AP4**	**AP5**	**AP6**	**AP7**	**AP8**	**AP9**	**AP10**
	73.82	**65.464**	**86.509**	**67.522**	**82.059**	**81.618**	**72.247**	**72.546**	**77.254**	**68.767**
	AP11	**AP12**	**AP13**	**AP14**	**AP15**	**AP16**	**AP17**	**AP18**	**AP19**	**Large**
	75.531	**75.96**	**94.713**	**83.83**	**108.92**	**95.176**	**94.713**	**109.4**	**104.59**	**86.854**

This enables us to absolutely eliminate the uncertainties that the randomness brings to the results. Based on the conclusion we have in chapter III, we expected to see the following results: 1) For the same material using the same group of relative humidity, with lower number concentration, there are always more activated particles than that with the higher number concentration, and the size of particles should also be larger after 3 s, as well; 2) For the same number concentration, using the same group of relative humidity, internal mixture should have a higher fraction of activated particles than all other material; 3) For external mixing, the activated fraction of the two material should be close to each other.

So, we will then see the following result and find out whether everything will be as what we expected. The largest particle radius and percentage larger than 7μm are summarized in Tables 4.12-4.15.

Table 4.12 Radius of the largest particles (μm) of 3s calculation results for group 1

	External mixing				**Pure material**			**Internal Mixing**	
	LMA+ AS		MA+ AS		AS	LMA	MA	LMA+ AS	MA+AS
	AS	LMA	AS	MA					
1.8E7	17.7	15.0	17.7	15.0	17.5	17.5	17.5	19.4	18.4
1.8E8	14.3	12.2	14.3	12.2	13.8	13.8	13.8		14.4
1.8E9	7.56	6.24	7.6	6.26	7.34	7.34	7.30	10.4	8.00
1.8E10	4.30	3.34	4.74	2.28	4.08	3.98	4.48	6.68	5.36

Table 4.13 Percentage of particles have radii equal to or greater than 7μm after 3s calculation for group 1

	External mixing						**Pure material**			**Internal Mixing**	
	LMA+ AS			MA+ AS			AS	LMA	MA	LMA+ AS	MA +AS
	AS	LMA	Total	AS	MA	Total					
1.8E7	11.9	11.6	11.8	12.1	11.6	11.8	13.4	13.1	13.6	23.6	15.6
1.8E8	10.7	10.7	10.7	10.7	10.7	10.7	10.8	10.8	10.8		13.2
1.8E9	0.04	0	0.02	0.04	0	0.02	0.05	1.35	0.05	9.21	0.07
1.8E10	0	0	0	0	0	0	0	0	0	0	0

Table 4.14 Radii of the largest particles (μm) of 3s calculation results for group 2

	External mixing				**Pure material**			**Internal Mixing**	
	LMA+ AS		MA+ AS		AS	LMA	MA	LMA+ AS	MA+AS
	AS	LMA	AS	MA					
1.8E7	17.6	15.0	17.7	15.0	17.5	17.5	17.5	24.8	28.2
1.8E8	14.4	12.2	14.3	12.2	13.8	13.8	13.8	18.8	20.1
1.8E9	7.62	6.28	7.56	6.22	7.28	7.42	7.30	12.0	12.7
1.8E10	5.42	2.24	5.38	2.16	4.50	3.52	4.40	7.62	8.06

Table 4.15 Percentage of particles have radii equal to or greater than 7μm after 3s calculation for group 2

	External mixing						**Pure material**			**Internal Mixing**	
	LMA+ AS			MA+ AS			AS	LMA	MA	LMA+ AS	MA +AS
	AS	LMA	Total	AS	MA	Total					
1.8E7	26.1	24.0	24.9	26.6	24.0	25.2	27.1	27.2	27.2	84.7	91.1
1.8E8	21.8	16.8	18.5	21.8	15.8	18.5	20.6	18.8	20.6	70.9	77.7
1.8E9	0.022	0	~0.01	0.02	0	0.01	0.02	0.02	0.05	38.2	45.2
1.8E10	0	0	0	0	0	0	0	0	0	6.72	10.7

The above results are exactly what we have expected: 1) When other conditions are identical, for most of our calculated resultslower particle concentration leads more growth; for pure materials and internal mixtures, no particle can grow beyond 7μm when the number density is greater than 1.8E9/m^3 and only a very small fraction can go beyond 7μm when the number density equals to 1.8E9/m^3; 2) Internally mixed particles are more able to grow. This phenomenon is mostly obvious with RH group 2, in which the average RH is higher (100.4%) than that for group 1(~86%). For group 2, the activated particle percentage can be as high as 90% for the internal mixtures while no more than 28% for the pure material and external mixtures. 3) For external mixing, the activated fractions of the two materials are close to each other.

c. Temperature effects

The water activity of particles will change with temperature. We stated in Chapter III that this change could be ignored since the change in temperature is very small (~+-3degree). But this statement is no longer valid here for the internal mixing

cases since in some calculations; the change in temperature can be higher than 40 degrees.

Specifically, in case 1 (group 1 in part II), for the LMA-AS internal mixture, when the number density is 1.8E7/m^3, the temperature changes remain as small as ~+-1 degree; when the number density is 1.8E8/m^3, the temperature changes increase to ~+-3 degree, which is still ignorable; when the number density is 1.8E9/m^3 and 1 .8E10/m^3, the biggest change in temperature can be as large as -30 and -40 degree respectively, which are definitely no longer ignorable. Also in case1, for the MA-AS internal mixture, when the number density is not higher than 1.8E8/m^3, the temperature changes remain as small as ~+-1 degree, which is still ignorable; when the number density is 1.8E9/$m^{3,}$, the change is no more than 7degree, which is , however, still not a big number; But when the number density is 1.8E10/m^3, the biggest change in temperature can be as large as -20 degree, which is no longer ignorable.

In case 3 (group 2 in part II), for the LMA-AS internal mixture, when the number density is 1.8E7/m^3, the temperature changes remain within ~+-3 degree; when the number density is 1.8E8/m^3, the temperature changes can decrease as much as 20 degree; when the number density is 1.8E9/m^3 and 1 .8E10/m^3, the biggest change in temperature can be as large as -40 and -50 degree respectively, which are definitely no longer ignorable. Also in case3, for the MA-AS internal mixture, when the number density is 1.8E7/m^3, the temperature changes remain within ~+-7 degree; when the number density is 1.8E8/m^3, the temperature changes can decrease as much as 17 degree; when the number density is 1.8E9/m^3 and 1 .8E10/m^3, the biggest change in temperature can be as large as -50 and -60 degree respectively, which are definitely no longer ignorable.

Since we did not do the identical study with case 7, we will not summarize the temperature change for the calculations in case 7. We expect it should also follow the rules we found in case 1 and 3.

From the above analysis, we can conclude two things: 1) with low density, temperature change is small, while the particles grow more 2) with high density, the temperature may decrease drastically, while the particles grow less. Why? Since as

what we know, the condensation process is a heat release process, while the evaporation is a heat absorbed one. So, the first guess we made is that the big decrease in temperature is caused by re-evaporation of the relative small particles. But, this explanation was based on the assumption that water vapor that re-evaporated largely exceeded that which condensed. However we checked all the results and found there is always more water vapor condensed than evaporated. This means, the whole particle condensation-evporation process is always one of heat release and should cause temperature rise. So the re-evaporation cannot be the reason. The other possible reason is that a lot of water vapor condensed while the total volume did not change; So the gas phase have expanded and done work. This will make the internal energy decrease and so does the temperature. To test this explanation, we choose a calculation (RH group II with MA+AMS internal mixture) in which the temperature had decreased much and did a rough calculation with it:

1) Total latent heat released is approx. Q =5.6E6J

2) Total volume loss of the gas: 2883 m^3. Assuming the pressure is constant 101325 pa, the PV work equals to 2883*101325 approx. =2.9E8 J

3) Since there is almost no change of volume-averaged temperature of the embedding volume, only the 19 air parcels were counted at this step. The total gas mass (use the data at the end of 3.0s calculation) in the 19 air parcels m = 1.6E4 kg. Assume cp=1kJ/Kg and cv=cp/1.4.

4) Use the equation pdV-Q=m* (cp-cv)dT, we got dT= 62k

The actual result shows an average 62.15k decrease of the 19 air parcels, which is very close to what we got from the calculation 62 k. The over-estimation of the cooling with our simple calculation is reasonable, because the actual changes will be incremental with a certain degree of heat loss to the surroundings and other mitigating factors.

So we can picture a staged process wherein the heat released due to the original condensation caused expansion and PV cooling; this would be followed by the decrease

in the humidity; finally, the decreased humidity causes evaporation of the smallest particles, which then causes additional cooling.

The above analysis for temperature change indicates that, for internal mixtures, for low number concentration, ignoring the change of water activity with temperature is still valid; with increasing number density, this assumption becomes less valid; and when the number density is higher than 1.8E8/m^3, the change of water activity with temperature should not be ignored any more.

But, due to the unavailability of experiment data, we are not able to perform calculation with temperature sensitive water activity. What we can do is to speculate what is the closest to the real situation from our results and analysis. The solubility of most material decreases when temperature decreases; so we expect to see less growth for the high number density calculations if this temperature effect is considered. But, the fact that the internal mixing will make particles grow more is not reversible. It is that the particles' growing more makes temperature to decrease, and the temperature decreasing makes the particles' growing slower. The two effects, more growth and temperature decreasing, interact with each other. The temperature effect can make the internal mixed particles not to grow that much; but it is for sure the particles will still grow more than that when they are not internally mixed.

Furthermore, some studies (Liljegren et al. 2001, Adler and Mack, 1986) show that there are temperature variations in clouds, particularly where tropical rainfall occurs. Liljegren et al.'s four days study shows that the difference between the cloud surface temperature and the water-weight cloud temperature can vary from 0 -10 k; the maximum and minimum have been observed in their four days measurement, are 297k-275k for the surface temperature and 297k to 267k for the water-weight cloud temperature. Adler and Mack (1986) pointed out that for overshooting convective clouds, adiabatic cooling dominates and the cloud temperature can be cooler than the environment by as much as 20 K. This inspired us to look at the temperature variation inside each of the 19 air parcels and also the big embedding volume.

Since we only have the information of the maximum and minimum temperatures for each of the air parcels and the embedding cube, we can only check the differences between these maxima and minima. We checked and found that the difference between the max and min temperature within the same air parcel varies from 13-19k and for the embedding cube there is always about 19k. It means that for the large embedding cube, the volume-averaged temperature has not changed after 3s calculation; but the temperature inside it becomes heterogeneous after 3s and the 19k is the difference between the highest and lowest. We picture it like this: during the calculation, the real border between the air parcels and embedding volume started to move. Temperature near the air parcels can increase or decrease because the gas in that area can either do work or be done work to, which is hard to tell. These results corresponded with the literature well.

But the non-uniformities in temperature that were found within individual parcels may very well be related to the drastically asymmetric shape of the hemisphere. So we repeated some calculations with a comparison model, which is almost the same as that used for the previous calculation except all the 19 air parcels are spheres with r=6.5m instead hemisphere. According to our results, the spherical shape does not have observational effects on the final temperature. Very similar temperature fluctuations to our previous calculation results were found for the air parcels and the embedding volume. So we can conclude this temperature fluctuation is a property that is not related to the shape of the individual air parcel.

3. Conclusions

In this chapter, we studied the effects of organic species on the condensational growth of CCN. From the above discussions on the calculation results, we have got these conclusions:

a. When other conditions are identical, lower particle concentration always leads to more growth; for pure materials and internal mixtures, no particle can grow beyond 7μm when the number density is greater than 1.8E9/m^3 and

only a very small fraction can go beyond 7μm when the number density equals to 1.8E9/m^3.

b. Internally mixed particles are more able to grow.
c. For external mixing, the activated fractions of the two materials are close to each other when the number density is lower than 1 .8E10/m^3.
d. When particles are internally mixed and the particles number concentration is relatively high, large amount water vapor loss due to particles' growth will lead to evaporation of a large fraction of particles, which lower the temperature later. Also, the heat released due the water condensation at the early period, temperature inside the air parcel increase rapidly, which leads the gas phase to expand and hence also lower the temperature. This may lower the air parcel's temperature drastically. At this point, temperature effect on the water activity cannot be ignored anymore.
e. 12-14 k and around 19k temperature fluctuation was found inside the air parcels and the embedding volume, respectively, after 3s calculation.

CHAPTER V

CONCLUSIONS

Atmospheric aerosols come from both natural and human sources. Cloud composition, precipitation, the hydrological cycle, and atmospheric circulation systems are all affected by both radiative and microphysical impacts of these aerosols (Rosenfeld et al. 2008).

My work focuses on condensational growth of atmospheric aerosols, especially, on how their composition, number concentration, and fluctuations in atmospheric relative humidity (RH) affect activation of CCN.

The basis of my work was the development of a code for the quasi-stationary solution of the coupled heat and mass transport equations for aerosols in a finite volume. Both mass and heat are conserved effectively in the volume, which results in a competitive aerosol condensation growth computational model. Using this model, we found that under normal atmospheric relative humidity conditions, the high number density can suppress the particle condensational growth.

Further model development has coupled this competitive aerosol condensation growth computational model with CFD software (by ANSYS FLUENT), enabling the simulation of the realistic atmospheric environment. With the contribution of CFD simulation, the aerosols grow more and the average temperature within the air parcel is more stable than without its implementation.

Our model study quantifies the suppression of aerosol condensational growth by high number densities. Sensitivity study with ammonium sulfate has shown that in most cases, when the aerosol number concentration is equal to or higher than $1.8E11/m^3$, no particle will be able to grow more than 5μm. When number density is lower than $1.8E11/m^3$, lower density leads to more fraction of particles to grow beyond 7μm or 5μm. However, the absolute numbers of particles greater than either 7μm or 5μm reach maximum when the number density is $1.8E8/m^3$.

Moreover, by using more than one air parcel (19 was actually used), which are randomly assigned with different initial RH values according to a power law distribution, we use this model to study the effects of atmospheric stochastic RH distribution on the growth of CCN. Our results indicate that 1) the highest saturation ratio that atmospheric particles can be exposed to is the most important factor that determines how much of these particles can grow during the first several seconds, and hence can decide whether the particles can get activated; 2) The mean relative humidity of the environment also has effects on the particles' condensational growth. But this effect is not as crucial as the highest saturation ratios. When the distributions of two environments have the same upper limit, the higher the average relative humidity, the more the particle can grow.

Model study of organic particles (L-malic acid and maleic acid) indicates that 1) when organic and inorganic species ($(NH_4)_2SO_4$ was used as a representative) are externally mixed, if the density is high, the growth of the species with higher water activity can suppress the growth of the species with lower water activity, while the growths of these two species have a tendency to get close if the density is relatively low; and 2) when organic and inorganic species are internally mixed, the particles can grow much more. These results can help us to further understand how the anthropogenic aerosols affect the clouds and precipitation.

In summary, we built a CFD-coupled competitive aerosol condensational growth computational model and used it to exam the effects of aerosol density, organics mixing, and atmospheric RH fluctuations. These studies will greatly contribute to the understanding and quantification of aerosol-cloud interactions.

REFERENCES

Adler, R. F., and Mack, R. A., 1986, Thunderstorm cloud top dynamics as inferred from satellite observations and a cloud top parcel model. *Journal of the Atmospheric Science,* **43**, pp. 1945-1960.

Andreae, M. O., 2008, Correlation between cloud condensation nuclei concentration and aerosol optical thickness in remote and polluted regions. *Atmospheric Chemistry and Physics Discussion.* , **8**, 11293, doi: 10.5194/acp-9-543-2009.

FLUENT INC., 2006, ANASYS FLUENT UDF manual (Centerra Resource Park: FLUENT INC).

Barrett, J. C. and Clement, C. F., 1988, Growth rates for liquid drops. *Journal Aerosol Science*, **19**, pp. 223-242.

Bott, A., Sievers, U. and Zdunkowski, W., 1990, A radiation fog model with a detailed treatment of the interaction between radiative transfer and fog microphysics. *Journal of the Atmospheric Sci*ence, **47**, pp. 2153–2166.

Brooks, S. D., Wise, M. E., Cushing, M. and Tolbert, M. A., 2003, Deliquescence behavior of organic/ammonium sulfate aerosol. *Geophysical Research Lett*ers, **29**, 1917, doi: 10.1029/2002GL014733.

Chen, J. P. and Lamb, D., 1994, Simulation of cloud microphysical and chemical processes using a multicomponent framework. Part I: Description of the microphysical model. *Journal of the Atmospheric Sc*ience, **51**, pp. 2613–2630.

Choi, M. Y. and Chan, C. K., 2002, Effect of organic species on the hygroscopic behaviors of inorganic aerosols. *Environmental Science & Technology*, **36**, pp. 2422-2428.

Clark, T. L., 1976, Use of log-normal distributions for numerical calculations of condensation and collection. *Journal of the Atmospheric Sc*ience, **33**, pp. 810-821.

Clegg, S. L. and Brimblecombe, P., 1994, A generalized muliticomponent thermodynamic model applied to the $(NH_4)_2SO_4$-H_2SO_4-H_2O system to high supersaturation and low relative humidity at 298.15k. *Journal of Aerosol Sc*ience, **26**, pp. 19-38.

Cruz, C. N. and Pandis, S. N., 2000, Deliquescence and hygroscopic growth of mixed inorganic-organic atmospheric aerosol. *Environment Science and Technology*, **34**, pp. 4313-4319.

Dick, W. D., Eaxena, P. and McMurry, P. H., 2000, Estimation of water uptake by organic compounds in submicron aerosols measured during the Southeastern Aerosol and Visibility Study. *Journal of Geophysical Research*, **105**, pp.1471-1479.

Dusek, D., Frank, G. P. and Hildebrandt, L. A. et al., 2006, Size matters more than chemistry for cloud-nucleating ability of aerosol particles. *Science*, **312**, pp. 1375-1378.

Facchini, M.C., Mircea, M., S. Fuzzi, S. and R.J. Charlson, 1999, Cloud albedo enhancement by surface-active organic solutes in growing droplets. *Nature*, **401**, pp. 257–259.

Feingold, G., Boers, R., Stevens, B. and Cotton, W. R., 1998, Simulations of marine stratocumulus using a new microphysical parameterization scheme. *Atmospheric Res*earch, **47-48**, pp. 505-528.

Feingold, G. and Chuang, 2002, Analysis of the influence of film-forming compounds on droplet growth: implications for cloud microphysical processes and climate. *Journal of the Atmospheric Sciences*, **59**, pp. 2006-2018.

Fitzgerald, J. W., 1972, Dependence of the supersaturation spectrum of CCN on aerosol size distribution and composition. *Journal of the atmospheric sciences,* **30**, pp. 628-634.

Fuchs, N. A., 1959, *Evaporation and Droplet Growth in Gaseous Media* (New York: Pergamon Press).

Fuchs, N. A. and Sutugin, A. G., 1971, *International Reviews in Aerosol Physics and Chemistry.* G. M. Hidy and J. R. Brock (Eds.) (New York: Pergamon Press).

Givati, A. and Rosenfeld, D., 2004, Quantifying precipitation suppression due to air pollution. *Journal of Applied Meteorology*, **43**, pp. 1038-1056.

Gong, S. L., Barrie, L. A. and Lazare, M., 2002, Canadian Aerosol Module (CAM): A size-segregated simulation of atmospheric aerosol processes for climate and air quality models. 2. Global sea-salt aerosol and its budgets. *Journal of Geophysical Research*, **107**, 4779, doi: 10.1029/2001JD002004.

Hallett J. and Mossop, S.C., 1974, Production of secondary ice particles during the riming process. *Nature,* **249**, pp. 26-28.

Heidenreich. S., 1994, Condensational droplet growth in the continuum regime-A critical review for the system air-water. *Journal of Aerosol Sci*ence, **25**, pp. 49-59.

Hidy, G. M. and Brock, J. R., 1970, *The Dynamics of Aerocolloidal Systems* (New York, Pergamon Press).

Hirschfelder, J. O., Curtis, C. F. and Bird, R. B., 1954, *Molecular Theory of Gases and Liquids*. pp. 1210-1226 (New York: John Wiley and Sons).

Hounslow, M.J., Ryall, R. L. and Marshall, V. R., 1988, A discretized population balance for nucleation, growth and aggregation. *AIChE Journal*, **34**, pp. 1821–1832.

Howell, W. E., 1949, The growth of cloud drops in uniformly cooled air. *Journal of Meteorology*, **6**, pp. 134-149.

Jaffrezo J. L., Aymoz , G., Delaval, C. and Cozic, J., 2005, Seasonal variations of the water soluble organic carbon mass fraction of aerosol in two valleys of the French alps. *Atmospheric Chemistry and. Physics*, **5**, pp. 2809-2821.

Ji, Q. and Shaw, G. E., 1998, On supersaturation spectrums and size distributions of cloud condensation nuclei. *Geophysical Research Letters*, **25**, pp.1903-1906.

Jirak, I. L. and Cotton, W. R., 2005, Effect of air pollution on precipitation along the front range of the Rocky Mountains. *Journal of Applied Meteorology and Climatology*, **45**, pp. 236-245.

Kalyanasundaram, M., 1999, Computation and applications of time dependent condensational aerosol growth. PhD Dissertation, Texas A&M University, College Station, TX.

Kawamura, K., Umemoto, N., Mochida, M., Bertram, T., Howell, S. and Huebert, B. J., 2003, Water-soluble dicarboxylic acids in the tropospheric aerosols collected over east Asia and western North Pacific by ACE-Asia C-130 aircraft. *Journal of Geophysical Research,* **108**, pp. 101029-101043.

Kerkweg, A., S. Wurzler, T. R. and Bott, A., 2003, On the cloud processing of aerosol particles: An entraining air-parcel model with two dimensional spectral cloud microphysics and a new formulation of the collection kernel. *The Quarterly Journal of the Royal Meteorological,* **129**, pp. 1–18.

Kulmala, M., 1993, Condensation growth and evaporation in the transition regime: An analytical expression. *Aerosol Science and Technol*ogy, **19**, pp. 381–388.

Kulmala, M. and Vesala, T., 1991, Condensation in the continuum regime**.** *Journal of Aerosol Sci*ence, **22**, pp. 337-336.

Kulmala, M., Majerowicz, A. and Wanger, P. E., 1989, Condensational growth at large vapors concentration: Limits of applicability of the mason equation. *Journal of Aerosol Science*, **20**, pp. 1023-1026.

Kulmala, M., Rannik, U., Zapadinsky, E. L. and Clement, C. F., 1997, The effect of saturation fluctuations on droplet growth. *Journal of Aerosol Science,* **28**, pp. 1395-1409.

Langmuir, I., 1915, The disassociation of hydrogen into atoms. Part II: Calculation of the degree of disassociation and the heat of formation. *Journal of the American Chemical Society,* 27, pp. 417-458.

Lave, L. B. and Seskin, E. P., 1973, An analysis of the association between U.S. mortality and air pollution. *Journal of the American Statistical Association*, **68**, pp. 284-290.

Leroy, D., Monier, M., Wobrock, W. and Flossmann, A. I., 2006, A numerical study of the effects of the aerosol particle spectrum on the development of the ice phase and precipitation formation. *Atmospheric Res*earch, **80**, pp. 15–45.

Levin, Z. and Cotton (edis.), W. R., 2009: *Aerosol Pollution Impact on Precipitation* (Springer Science and Business Media B. V).

Liljegren, J. C, Clothiaux, E. E., Mace, G. G., Kato, S. and Dong, X., 2001, A new retrieval for cloud liquid water path using a ground-based microwave radiometer and measurements of cloud temperature. *Journal of Geophysical Research*, **106**, pp. 14485-14500.

Mason, B. J., 1971: *The Physics of Clouds* (Oxford: Cameron Press).

Maxwell, J. C., 1877, *The Scientific Papers of James Clerk Maxwell* (New York: Dover Press).

McGraw, R., 1997, Description of aerosol dynamics by the quadrature method of moments. *Aerosol Science and Tech*nology, **27**, pp. 225-265.

Ming, Y. and Russell, L. M., 2002, Thermodynamic equilibrium of organic-electrolyte mixtures in aerosol particles. *AIChE J*ournal, **48**, pp. 1331-1348.

Mokdad, Ali H., Marks, J. S., Stroup. D. F. and Gerberding, J. L., 2004, Actual causes of death in the United States, 2000. *Journal of the American Medical Association*, **291**, pp. 1238-1235.

Mordy, W. A., 1959, Computations of the growth by condensation of a population of cloud droplets. *Tellus*, **11**, pp. 16-44.

Murphy, D. M., Cziczo, D. J., Froyd, K. D., Hudson, P. K. and Matthew, B. M. et al., 2006, Single-particle mass spectrometry of tropospheric aerosol particles. *Journal of Geophysical Research*, **111**, doi: 10.1029/2006JD007340.

Murphy, D. M., Anderson, J. R., Quinn, P. K., McInnes, L. M. and Brechtel, F. J. et al., 1998, Influence of sea-salt on aerosol radiative properties in the Southern Ocean marine boundary layer. *Nature*, **392**, pp. 62-65.

O'Dowd, C.C. and Smith, M. H., 1993, Physicochemical properties of aerosols over the Northeast Atlantic: Evidence for wind-speed-related submicron sea-salt aerosol production. *Journal of Geophysical Research,* **98**, pp. 1137-1149.

Paredes-Miranda. G., Arnott, W. P., Jimenez, J. L., Aiken, A. C., Gaffney, J. S. and Marley, N. A., 2009, Primary and secondary contributions to aerosol light scattering and absorption in Mexico City during the MILAGRO 2006 campaign. *Atmospheric Chemistry and Physics*, **9**, pp. 3721–3730.

Park S. S., Harrison D., Pancras, J. P. and Ondov, J. M., 2005, Highly time-resolved organic and elemental carbon measurements at Baltimore supersite in 2002. *Journal of Geophysical Res*earch, **110**, D07S06, doi: 10.1029/2004JD004610.

Patankar, S., 1980, *Numerical heat transfer and fluid flow* (New York: Hemisphere Publishing Corp.).

Peng C., Chan, M. N. and Chan, C. K. 2001, The Hygroscopic properties of dicarboxylic and multifunctional acids: Measurements and UNIFAC predictions. *Environmental Science and Technology*, **35**, pp. 4495-4501.

Pruppacher, H. R. and Klett, J. D., 1997, *Microphysics of Clouds and Precipitation*. (Kluwer Academic Publishers).

Quinn, P. K., Coffman, D. J., Kapustin, V. N., Bates, T. S. and Cover, D. S.,1998, Aerosol optical properties in the marine boundary layer during the First Aerosol Characterization Experiment (ACE 1) and the underlying chemical and physical aerosol properties. *Journal of Geophysical Research.,* **103**, pp. 547-563.

Rosenfeld, D., 1999, TRMM observed first direct evidence of smoke from forest fires inhibiting rainfall. *Geophysical Research Letters.*, **26**, pp. 3105-3108.

Rosenfeld, D., Rudich, Y. and Lahav, R., 2001, Desert dust suppressing precipitation: A possible desertification feedback loop. *Proceedings of the National Academy of Sciences USA*, **98**, pp. 5975-5980.

Rosenfeld, D., Lohmann, U., Raga, G. B., O'Dowd, C. D. and Kulmala, M. et al, 2008, Flood or drought: How do aerosols affect precipitation? *Science*, **321**, pp. 1309-1313.

Sageev, G., Flagan, G. C., Seinfeld, J. H. and Arnold, S., 1986, Condensation rate of water on aqueous droplets in the transition regime. *Journal of Colloid Interface Sci*ence, **113**, pp. 421-429.

Saxena, P. and Hildemann, L. M., 1996, Water –soluble organics in atmospheric particles: A critical review of the literature and application of thermodynamics to identify candidate compounds. *Journal of Atmospheric Chem*istry, **24**, pp. 57-109.

Seifert, A. and Beheng, K. D., 2006a, A two-moment cloud microphysics parameterization for mixedphase clouds. Part I: Model description. *Meteorology and Atmospheric Physics*, **92**, pp. 45–66.

Seifert, A. and Beheng, K. D., 2006b, A two-moment cloud microphysics parameterization for mixed phase clouds. Part II: Maritime vs. continental deep convective storms. Meteorology and *Atmospheric Physics*, **92**, pp. 67–82.

Seinfeld, J. H. and Pandis, S. N., 2006*, Atmospheric Chemistry and Physics*. Second Edition (John Wiley & Sons, Inc.).

Sherwood, S. C., Kursinski, E. R. and Read, W. G., 2006, A distribution law for free-tropospheric relative humidity. *Journal of Climate,* **19**, pp. 6267-6277.

Shinozuka, Y., Clarke, A. D., Howell, S. G., Kapustin, V. N. and Huebert, B. J., 2004, Sea-salt vertical profiles over the Southern and tropical Pacific oceans: Microphysics, optical properties, spatial variability, and variations with wind speed. *Journal of Geophysical Res*earch, **109**, D24201, doi: 10.1029/2004JD004975.

Spurny, K. R., 2000, *Aerosols Chemical Processes in the Environment* (CRC Press LLC).

Tang, I. N., 1997, Thermodynamic and optical properties of mixed-salt aerosols of atmospheric importance. *Journal of Geophysical Research,* **103**, pp. 1883-1893.

Twomey, S., 1959, The nuclei of natural cloud formation. Part II: The supersatruation in natural clouds and the variation of cloud droplet concentration. *Geofisica pura e applicata,* **43**, pp. 243-249.

Twomey, S., 1974, Pollution and planetary albedo. *Atmospheric Environment*, **8**, pp. 1251-1256.

Twomey, S. and Piepgrass, M. and Wolf, T. L., 1984, An assessment of the impact of pollution on global cloud albedo. *Tellus*, **36B**, pp. 356-366.

Tzivion, S., Feingold, G. and Levin, Z., 1987, An efficient numerical solution to the stochastic collection equation. *Journal of the Atmospheric Science*, **44**, pp. 3139–3149.

Wagner, P. E., 1982, *Aerosol Growth by Condensation Aerosol Microphysics II*, W. H. Marlow (Ed.) (Berlin: Springer-Verlag).

Wise M. E, Surratt, J. D., Curtis, D. B., Curtis, Shilling, J. E. and Tolbert, M. A., 2003, Hygroscopic growth of ammonium sulfatet/dicarboxylic acids. *Journal of Geophysical Research,* **108**, 4638, doi: 10.1029/2003JD003775.

Yu, L. E., Shulman, M. L., Kopperud, R. and Hildemann, L. M., 2005, Fine organic aerosols collected in a humid, rural location (Great Smoky Mountains, Tennessee,

USA): Chemical and temporal characteristics. *Environmental Science and Technology* ***39***, pp. 707-715.

Zhang, Q., Jimenez, J. L., Canagaratna, M. R., Allan, J. D., Coe, H. and Ulbrich, I. et al., 2007, Ubiquity and dominance of oxygenated species in organic aerosols in anthropogenically-influenced Northern Hemisphere midlatitudes. *Geophysical Research Lett*ers, **34**, L13801, doi: 10.1029/2007GL029979.

APPENDIX A

NUMERICAL METHOD FOR CALCULATION OF DROPLET GROWTH

initr.c

```
#include <stdio.h>
#include "udf.h"
#include <time.h>
#include <math.h>
#include <stdlib.h>


#define NR_END 1
#define M_PI    3.14159265358979323846
#define RHOW    1.0495E3
#define UGC     8.3143
#define MV      0.018016
#define ST      0.072
#define MNANO3  0.085
#define MNH4SO4 0.13215
#define ZONE_N 19
#define PHO_NANO3 2261
#define PHO_NH4SO4 1769

double *dvector(int nl,int nh);
double fx(double x, double r);
double f1x(double x);
double newton(double a,double xtol, double aw);
double mfalsi (double a, double b, double xtol, double aw);
double **dmatrix(int nrl, int nrh, int ncl, int nch);

double *co, *rsurf;
double DR;
double *Imini;
double *mass, *mini, *mcond;
int nz;
double RSigma;
double RMean;
int ti;
double **zrsurf, **zmcond, **zmass;

DEFINE_INIT(init_r, d)
{


#if !RP_HOST
      Thread *thrd;
    cell_t ct;
```

```
#endif
#if !RP_NODE
      FILE *fp,*fp0, *fp1,*fp2,*fp3;
#endif
      int zi;
      double NTotal;
      int ZiFlag;
      double GRSigma;
      int q, w;
      double RI;
      double RH;
      double RH_E;
      int i;
    double rhinfo[ZONE_N+1];
      DR=2.0E-8;
      NTotal=1.8E9;
      RMean=2.0E-7;
      RSigma=1.5E-7;
      RI=RMean-3*RSigma;
      GRSigma=(1.46*RSigma+RMean)/RMean;
      nz=1;
      zi=1;
      ZiFlag=(int)((RMean+5*RSigma-RI)/DR);
      rsurf=dvector(1,ZiFlag);

      ti=0;
      RH_E=0.868536;
    co= dvector(0,70);
    mass=dvector(0,70);
    mini=dvector(0,70);
    mcond=dvector(0,70);
    Imini = dvector(0,70);
    rhinfo[1]=0.7382;
    rhinfo[2]=0.65464;
    rhinfo[3]=0.86509;
    rhinfo[4]=0.67522;
    rhinfo[5]=0.82059;
    rhinfo[6]=0.81618;
    rhinfo[7]=0.74247;
    rhinfo[8]=0.72546;
    rhinfo[9]=0.77254;
    rhinfo[10]=0.68767;
    rhinfo[11]=0.75531;
    rhinfo[12]=0.7596;
    rhinfo[13]=0.94713;
    rhinfo[14]=0.8383;
    rhinfo[15]=1.0892;
    rhinfo[16]=0.95176;
    rhinfo[17]=0.94713;
    rhinfo[18]=1.094;
    rhinfo[19]=1.0459;

      if(RI<=0) RI=2.0E-8;
```

```
      while (zi<=ZiFlag)
         {

                  double ratio;
                  double aw;
                  rsurf[zi]=RI;
                  co[zi]=NTotal/(sqrt(2.0*M_PI)*log(GRSigma)*rsurf[zi])
                  *exp(-
                  pow(log(rsurf[zi]/RMean),2.0)/(2.0*pow(log(GRSigma),2
                  .0)))*DR;
                  aw=log(RH_E)-2*0.072*1.7167E-
                  5/rsurf[zi]/8.3143/298.15;
                  ratio= mfalsi(0.0,1.0, 1E-7,exp(aw));
                  ratio=(1-ratio)*RHOW/(ratio*PHO_NH4SO4+(1-
                  ratio)*RHOW);
                  mini[zi]=4/3*M_PI*pow(rsurf[zi],3)*ratio;
                  mcond[zi]=4/3*M_PI*pow(rsurf[zi],3)-mini[zi];
                  mini[zi]=mini[zi]*PHO_NH4SO4;
                  mcond[zi]=mcond[zi]*RHOW;
                  mass[zi]=mcond[zi]+mini[zi];
#if RP_HOST
                  Message("%d\t%-7.5g\t%-7.5g\n ", zi, mini[zi],
                  mcond[zi]);
#endif
                  zi++;
                  RI=RI+DR;

         }

      nz=zi;
      zi=1;
      q=1;
      for(q=1; q<=nz; q++) Imini[q]=mini[q];
      w=1;
      zrsurf=dmatrix(1, ZONE_N, 1, nz);
      zmcond=dmatrix(1, ZONE_N, 1, nz);
      zmass=dmatrix(1, ZONE_N, 1, nz);
      srand((unsigned)time(NULL));
      for(w=1;w<=ZONE_N;w++) {
            RH=rhinfo[w]*100.0;
#if RP_HOST
            Message("%d\t%-8.5g\n ", w, RH );
#endif
#if RP_NODE
            thrd=Lookup_Thread(d, 22-w);
            begin_c_loop(ct,thrd){
            C_YI(ct,thrd,0)=RH/100*0.0167534;
            }
            end_c_loop(ct,thrd);
#endif
            for( i=1; i<=nz; i++) {
                  zrsurf[w][i]=rsurf[i];
                  zmcond[w][i]= mcond[i];
                  zmass[w][i] = mass[i];
```

```
            }

      }
#if !RP_NODE
      fp=fopen("output_total.txt","wrb");
      fp1=fopen("output_large.txt", "wrb");
      fprintf(fp1, "trance of RH and Temp of the large zone \n");
      fprintf (fp1, " time     RH,      TEM\n");
      fprintf(fp, "time  , radius ,       concent\n ");
      fp2=fopen("output_super.txt","wrb");
      fp3=fopen("output_temi.txt","wrb");
      fclose(fp);
      fclose(fp1);
      fclose(fp2);
      fclose(fp3);
#endif

}

double fx(double x, double aw) {
    double ffx;
    ffx= 1-0.2715*x+0.3113*pow(x,2)-2.336*pow(x,3)+1.412*pow(x,4)-aw;
    return ffx;
}

double f1x(double x) {
    double f1x;
    f1x=-0.2715+2*0.3113*x-3*2.336*pow(x,2)+4*1.412*pow(x,3);
    return f1x;
}


double newton(double a,double xtol, double aw){
    double error, fa, ga;
    do
    {
      fa=fx(a, aw);
      ga=f1x(a);
      a=a- fa/ga;
      error=fabs(a-ga);

    }
    while (error>xtol);

    return a;
}

double mfalsi (double a, double b, double xtol, double aw) {
    double fa, fb;
    double wn,wn1, fw, fw1;
    fa=fx(a, aw);
    fb=fx(b, aw);
    wn=a;
    fw=fx(wn, aw);
```

```
    do
    {
      wn1=(fb*a-fa*b)/(fb-fa);
      fw1=fx(wn1, aw);
      if(fa*fw1<=0) {
            b=wn1;
            fb=fw1;
            if ((fw*fw1)>0) fa=fa/2;
      }else {
            a=wn1;
            fa=fw1;
            if((fw*fw1)>0) fb=fb/2;
      }
      wn=wn1;
      fw=fx(wn,aw);
    }
    while (fabs(fw)>xtol);

    return wn;
}
////////////////////////////////////////////////////////////////////////
                                    Adjust.c
////////////////////////////////////////////////////////////////////////
#include "udf.h"
#include "stdio.h"
#include "stdlib.h"
#include "string.h"
#include "malloc.h"
#include "math.h"
#include "time.h"

#define NR_END 1
#define FREE_ARG char*

#define NBMAX 501
#define NGMAX 10001
#define NPTCS 201
#define NZMAX 100
#define NSMAX 100

#define M_PI    3.14159265358979323846
#define RHOG    1.205
#define CVG     720
#define CPG     1010
#define RHOW    1.0495E3
#define CVV     1463
#define CPV     1952
#define TDIFF   0.32
#define CL      4218
#define L       2.5E6
#define UGC     8.3143
#define MV      0.018016
#define ST      0.072
```

```
#define MDIFF   2.0e-5
#define MFP     6.8E-8
#define MSSUL   0.09808
#define MSNACL  0.05845
#define MSAMSU  0.13215
#define MNANO3  0.085
#define MNA2SO4 0.128
#define MNH4NO3 0.132
#define MNH4CL  0.054
#define PHO_NANO3 2261
#define PHO_NH4SO4 1769
#define ZONE_N 19


void free_vector(double *v, int nl, int nh);
void Initial(double NTotal, int nz, int nsp, double rsurf, double
*mcondi, double *mini, double *co, double RMean, double RSigma, int
*species, double *rsp,double *mass);
double *dvector(int nl,int nh);
int *ivector(int nl, int nh);
double **dmatrix(int nrl, int nrh, int ncl, int nch);
void tridag(double a[],double b[],double c[],double r[],double
u[],unsigned long n);
double psoft(double temp);
double pp(double mini, double mcond, double kelconst, double tem,
double rsurf, int choice);
void thomas(int n, double **g, double *b);

double *d_mass, *d_heat;
extern double *co, *rsurf;
extern double DR;
extern double *Imini;
extern double *mass, *mini, *mcond;
extern int nz;
extern double RSigma;
extern double RMean;
extern int ti;
extern double **zrsurf, **zmcond, **zmass;

DEFINE_ADJUST(comput_mass_heat,domain)
{
#if !RP_HOST
    Thread *thrd;
    cell_t ct;
#endif
#if RP_HOST
    FILE *fp,*fp0, *fp1, *fp2, *fp3;
#endif
    double super;
    double flux, tembc, rhobc, dmass;
    double *u, pva, *rho, *tem, dtemp;
    int    tt,i,index,m;
    double *rhol, *a, *b, *c, *r, *eta, *num, qo, so;
    double *inter, kelconst, const1, const2, *s, psat, dt;
```

```
double satrinf, delta, prho, qlrho, qrho, trho,bcqtem, ptem, qtem,
rtem, r1tem;
double dtem, rhoi, temi, deta, rinf=1.0E-4, kc,RHOG1;
double *kn,*beta,flag;
int timestep;

double tflag;
int    species;
int    ngrid=201, nb=201;
int    j, k,l;
double RI,MTemp;
double *RFinal, *NFinal;
double real_time;
int cell_number;
double Mass_Fraction, Temperature, Pressure;
int index_max;
double *co_total;

double con;
double RII;

int mm;
int v, xx, bb, jj;

real_time=CURRENT_TIME;
d_mass = dvector(1,ZONE_N+2);
d_heat = dvector(1, ZONE_N+2);
num= dvector(1, nb);
eta= dvector(1, ngrid);
s= dvector(1, nz);
inter= dvector(0, nb);
a= dvector(1, ngrid);
b= dvector(1, ngrid);
c= dvector(1, ngrid);
r= dvector(1, ngrid);
u= dvector(1, ngrid);
rho= dvector(1,ngrid);
tem= dvector(1,ngrid);
rhol= dvector(1, nz);
kn=dvector(1,nz);
beta=dvector(1,nz);
index_max=nz;
RII=0.0;

dt=2.E-5;
temi=0.0;
const1= 4.0*RHOW*M_PI/3.0;
kelconst= 2.0*MV*ST/(UGC*RHOW);
timestep=N_TIME;

if(ti==0){
  #if RP_HOST
  fp=fopen("output_total_0.txt","a");
  fprintf(fp, "t=0==================================\n");
```

```
      for(tt=0;tt<=nz;tt++) {

                  fprintf(fp, "%-2.2e\t %-2.6e\n ",rsurf[tt],co[tt]);
      }
      fprintf(fp, "\n");
      fclose(fp);

#endif

    }

    if(N_TIME>ti) {
    ti++;
    if((ti==1)||(ti==10)||(ti==20)||(ti==40)||(ti==70)||(ti==100)||(ti=
    =500)||(ti==1000)||(ti%2500==0)) {
      Temperature=0.0;
      Mass_Fraction=0.0;
      cell_number=0;
      Pressure=0.0;
#if RP_NODE
      thrd=Lookup_Thread(domain, 2);
      begin_c_loop(ct,thrd){
            cell_number++;
            Temperature+=C_T(ct,thrd);
            Mass_Fraction+=C_YI(ct,thrd,0);
            Pressure+=C_P(ct,thrd);
      }
      end_c_loop(ct,thrd);
      cell_number=PRF_GRSUM1(cell_number);
      Temperature=PRF_GRSUM1(Temperature);
      Mass_Fraction=PRF_GRSUM1(Mass_Fraction);
      Pressure=PRF_GRSUM1(Pressure);
      Temperature/=cell_number;
      Mass_Fraction/=cell_number;
      Pressure/=cell_number;
      super=Mass_Fraction*101325.0/1706.8;
      temi=Temperature;
#endif
      node_to_host_double_3(temi,super,Pressure);

#if RP_HOST
      fp1=fopen("output_large.txt","a");
      fprintf(fp1, "%d\t%-7.5g\t%-7.5g\n ", ti, super, temi );
      fclose(fp1);

#endif
    }
    for(k=1;k<=ZONE_N; k++) {
      d_mass[k]=0.0;
      d_heat[k]=0.0;
      Temperature=0.0;
      Mass_Fraction=0.0;
      cell_number=0;
      Pressure=0.0;
```

```
#if RP_NODE
      thrd=Lookup_Thread(domain, 22-k);
      begin_c_loop(ct,thrd){
            cell_number++;
            Temperature+=C_T(ct,thrd);
            Mass_Fraction+=C_YI(ct,thrd,0);
            Pressure+=C_P(ct,thrd);
      }
      end_c_loop(ct,thrd);
      cell_number=PRF_GRSUM1(cell_number);
      Temperature=PRF_GRSUM1(Temperature);
      Mass_Fraction=PRF_GRSUM1(Mass_Fraction);
      Pressure=PRF_GRSUM1(Pressure);
      Temperature/=cell_number;
      Mass_Fraction/=cell_number;
      Pressure/=cell_number;
      super=Mass_Fraction*101325.0/1706.8;
      temi=Temperature;
#endif
      node_to_host_double_3(temi, super, Pressure);
#if RP_HOST
      if((ti==1)||(ti%1250==0)) {
            fp2=fopen("output_super.txt","a");
            fp3=fopen("output_temi.txt","a");
            fprintf(fp2,"%-7.5g\t", super);
            fprintf(fp3,"%-7.5g\t", temi);
            if(k==ZONE_N){
                  fprintf(fp2, "\n");
                  fprintf(fp3, "\n");
            }
            fclose(fp2);
            fclose(fp3);
      }
#endif
      RII=RMean-3*RSigma;
      if(RII<=0) RII=5E-9;
      flag=1;
      satrinf= super;
      psat= psoft(temi);
      RHOG1=RHOG;
      rhoi= MV*satrinf*psat/(UGC*temi);
      tembc= temi;
      rhobc= rhoi;
      const2=RHOG1*CPG+rhoi*CPV;
      psat= psoft(tembc);
      species=3;
      j=1;
      for(j=1;j<=ngrid;j++) {
                  rho[j]=rhobc;
                  tem[j]=tembc;
      }
      l=1;

      for(l=1; l<nz; l++) {
```

```
            dmass=0.0;
            dtemp=0.0;
            RI=zrsurf[k][l];
            con=co[l];
            deta = 1.0/(ngrid-1);
            for(i=1; i<=ngrid;i++) eta[i]=(i-1)*deta;
            so= 0.0;
            qo=0.0;
            pva = pp(mini[l],zmcond[k][l],kelconst, tem[1],
RI,species);
            delta= rinf-RI;
            if(RI/rinf >1.2) exit(0);
            rho[1]= MV*pva/(UGC*tem[1]);

            a[1]= 0.0;
            b[1]= 1.0;
            c[1]=0.0;
            c[ngrid]= 0.0;
            b[ngrid]= 1.0;
            c[ngrid]= 0.0;
            r[1]=rho[1];
            r[ngrid]= rhobc;
            qlrho= MDIFF*dt/(delta*deta);
            prho= qlrho/(delta*deta);
            v=2;
            for(v=2;v<ngrid;v++) {
                  qrho=qlrho/(eta[v]*delta+RI);
                  trho= prho/tem[v];
                  a[v]= -prho+qrho+0.25*trho*(tem[v+1]-tem[v-1]);
                  b[v]=1.0+2.0*prho-trho*(tem[v+1]-2.0*tem[v]+tem[v-
1]);
                  c[v]= -prho-qrho-0.25*trho*(tem[v+1]-tem[v-1]);
                  r[v]= rho[v]+qrho*(tem[v+1]-tem[v-1])/tem[v];
            }
            tridag(a,b,c,r,u,ngrid);
            xx=1;
            for(xx=1; xx<ngrid; xx++) rho[xx]=u[xx];
            flux= (rho[2]-rho[1])*dt/(delta*deta);
            dmass= 4.0*M_PI*MDIFF*flux*RI*RI;
            zmcond[k][l]+=dmass;
            zmass[k][l]+=dmass;

            if(zmass[k][l]<=Imini[l]) {
                  dmass=0.0;
                  dtemp=0.0;
                  zmass[k][l]=Imini[l];
                  mini[l]=Imini[l];
                  zmcond[k][l]=0.05*Imini[l];
                  dmass=zmass[k][l]-Imini[l];
                  flag=0;
            }

            RI= pow(3.0*(zmcond[k][l]/RHOW+mini[l]/PHO_NH4SO4)/4/M_PI,
1.0/3.0);
```

```
            bcqtem= 3.0*dt/ (RI*RHOW*CL*delta*deta);
            a[1]=0.0;
            b[1]=1.0+TDIFF*bcqtem;
            c[1]=-TDIFF*bcqtem;
            a[ngrid]=0.0;
            b[ngrid]=1.0;
            c[ngrid]=0.0;
            r[1] = tem[1] + L*MDIFF*bcqtem* (rho[2]- rho[1]);
            r[ngrid] = tembc;
            r1tem= dt/(delta*deta);
            dtem = MDIFF*CPV*r1tem;
            bb=2;
            for(bb=2; bb<ngrid; bb++) {
                  kc= TDIFF+MDIFF*CPV*rho[bb];
                  rtem= kc*r1tem;
                  ptem= rtem/(delta*deta);
                  qtem= rtem/(eta[bb]*delta+ RI);
                  a[bb]= -ptem+qtem;
                  b[bb]= CVV*rho[bb]+RHOG1*CVG+2.0*ptem;
                  c[bb]= -ptem-qtem;
                  r[bb]= tem[bb]*(CVV*rho[bb]+RHOG1*CVG);
                  a[bb]/=(CVV*rho[bb]+RHOG1*CVG);
                  b[bb]/=(CVV*rho[bb]+RHOG1*CVG);
                  c[bb]/=(CVV*rho[bb]+RHOG1*CVG);
                  r[bb]/=(CVV*rho[bb]+RHOG1*CVG);

            }
            tridag(a,b,c,r,u,ngrid);
            dtemp= u[1]-tem[1];

            jj=1;
            for(jj=1;jj<ngrid;jj++) tem[jj]=u[jj];

            so=co[l]*dmass;
            qo=co[l]*(L*dmass-CL*zmass[k][l]*dtemp);

            MTemp=zmcond[k][l];

            d_mass[k]=d_mass[k]+so;
            d_heat[k]=d_heat[k]+qo;
            zrsurf[k][l]=RI;

      }
      tflag=real_time*2.0E5 ;
    }


#if RP_HOST
    if((ti==15000)||(ti%25000==0)||(ti==149999)){
    index_max=nz;
    for(k=1; k<=ZONE_N;k++){
      for(tt=1;tt<=nz-1;tt++) {
            index=(int)(zrsurf[k][tt]/DR);
            if(index>index_max) index_max=index;
```

```
      }
    }
    Message( "before dvector");
    NFinal= dvector(0,index_max+1);
    RFinal= dvector(0,index_max+1);
    Message("After dvector\n");
    RFinal[0]=0.0;
    NFinal[0]=0.0;
    for(mm=1;mm<=index_max;mm++){
      NFinal[mm]=0.0;
      RFinal[mm]=RFinal[mm-1]+DR ;
    }
    for(k=1;k<=ZONE_N;k++) {

      for(tt=1;tt<=nz;tt++){
            index=(int)(zrsurf[k][tt]/DR);
            NFinal[index]=NFinal[index]+co[tt];
      }
    }
    if(ti==15000) fp=fopen("output_total_0.3s.txt","a");
    if(ti==25000) fp=fopen("output_total_0.5s.txt","a");
    if(ti==50000) fp=fopen("output_total_1s.txt","a");
    if(ti==75000) fp=fopen("output_total_1.5s.txt","a");
    if(ti==100000) fp=fopen("output_total_2s.txt","a");
    if(ti==125000) fp=fopen("output_total_2.5s.txt","a");
    if(ti==149999) fp=fopen("output_total_2.9s.txt","a");
    if(ti==150000) fp=fopen("output_total_3.0s.txt","a");
    fprintf(fp, "time=%d\n",ti);
    fprintf(fp, "////////////////////////////////////////////////
    \n");
      for(m=0;m<=index_max;m++) {
            NFinal[m]=NFinal[m]/ZONE_N;
            fprintf(fp, "%-2.2e\t %-2.6e\t ", RFinal[m],NFinal[m]);
            fprintf(fp, "\n");
      }
    fclose(fp);
      free(NFinal);
    free(RFinal);
    }
#endif
    }else {
      for(i=1;i<=ZONE_N+2;i++){
            d_heat[i]=0.0;
            d_mass[i]=0.0;
      }
    }
}


void free_vector(double *v, int nl, int nh)

{
    free((FREE_ARG) (v+nl-NR_END));
}
```

```
double *dvector(int nl,int nh)

{
    double *v;

    v=(double *)malloc((unsigned int) ((nh-
nl+1+NR_END)*sizeof(double)));
    if (!v) printf("allocation failure in dvector()");
    return v-nl+NR_END;
}

int *ivector(int nl, int nh)

{
    int *v;

    v=(int *)malloc((int) ((nh-nl+1+NR_END)*sizeof(int)));
    if (!v) printf("allocation failure in ivector()");
    return v-nl+NR_END;
}

unsigned char *cvector(int nl, int nh)

{
    unsigned char *v;

    v=(unsigned char *)malloc((unsigned int) ((nh-
    nl+1+NR_END)*sizeof(unsigned char)));
    if (!v) printf("allocation failure in cvector()");
    return v-nl+NR_END;

}

double **dmatrix(int nrl, int nrh, int ncl, int nch)

{
    long i, nrow=nrh-nrl+1,ncol=nch-ncl+1;
    double **m;


    m=(double **) malloc((unsigned
    int)((nrow+NR_END)*sizeof(double*)));
    if (!m) printf("allocation failure 1 in matrix()");
    m += NR_END;
    m -= nrl;


    m[nrl]=(double *) malloc((unsigned
    int)((nrow*ncol+NR_END)*sizeof(double)));
    if (!m[nrl]) printf("allocation failure 2 in matrix()");
    m[nrl] += NR_END;
    m[nrl] -= ncl;
```

```
    for(i=nrl+1;i<=nrh;i++) m[i]=m[i-1]+ncol;

    return m;
}

void tridag(double a[],double b[],double c[],double r[],double
u[],unsigned long n)
{
    unsigned long j;
    double bet,*gam;

    gam=dvector(1,n);
    if (b[1] == 0.0) printf("Error 1 in tridag");
    u[1]=r[1]/(bet=b[1]);
    for (j=2;j<=n;j++) {
      gam[j]=c[j-1]/bet;
      bet=b[j]-a[j]*gam[j];
      if (bet == 0.0)   printf("Error 2 in tridag");
      u[j]=(r[j]-a[j]*u[j-1])/bet;
    }
          for (j=(n-1);j>=1;j--)
            u[j] -= gam[j+1]*u[j+1];

    free_vector(gam,1,n);
}

double psoft(double temp)
{

 return(exp(77.34-7235.42/temp-8.20*log(temp)+0.0057*temp));

}


void thomas(int n, double **g, double *b)
{
    int i;
    g[1][3] = -g[1][3]/g[1][2];
    b[1] = b[1] / g[1][2];
    for ( i=2; i<=n; i++) {
      g[i][3] = -g[i][3]/(g[i][2]+g[i][1]*g[i-1][3]);
      b[i] = ( b[i]-g[i][1]*b[i-1]) / (g[i][2]+g[i][1]*g[i-1][3]);
    }
    for ( i=n-1; i>=1; i--) b[i]+=g[i][3]*b[i+1];
    return;
}

double pp(double mini, double mcond, double kelconst, double tem,
double rsurf, int choice)
{
  double x,aw;
  double pva;
  if(choice==1) {
```

```
x=3.0*MV*mini/(MSSUL*mcond);
aw=exp(x);
pva=aw*(exp(kelconst/(tem*rsurf)))*(psoft(tem));
}else if(choice==2) {

x=mini/(mini+mcond);

aw=1.0-0.6366*x+0.8624*pow(x,2)-11.58*pow(x,3)+15.18*pow(x,4);

pva=aw*(exp(kelconst/(tem*rsurf)))*(psoft(tem));

}else if (choice==3) {
x=mini/(mini+mcond);

aw=1.0-0.2715*x+0.3113*pow(x,2)-2.336*pow(x,3)+1.412*pow(x,4);
pva=aw*(exp(kelconst/(tem*rsurf)))*(psoft(tem));
}else if (choice==0){
pva=(exp(-kelconst/(tem*rsurf)))*(psoft(tem));
}else if (choice==4)
{
    x=mini/(mini+mcond);
    aw=1.0-0.552*x+1.286*pow(x,2)-3.496*pow(x,3)+1.843*pow(x,4);
    pva=aw*(exp(kelconst/(tem*rsurf)))*(psoft(tem));
}else if (choice==5)
{
    x=mini/(mini+mcond);
    aw=1.025461-1.91093*x+4.720573*pow(x,2)-
    4.44043*pow(x,3)+0.491025*pow(x,4);
    pva=aw*(exp(kelconst/(tem*rsurf)))*(psoft(tem));
}else if (choice==6)
{
    x=mini/(MNH4CL*(mini+mcond));
    aw=0.9968-0.02611*x-0.001599*pow(x,2)+1.355E-4*pow(x,3)-2.317E-
    6*pow(x,4)-1.113E-8*pow(x,5);
    pva=aw*(exp(kelconst/(tem*rsurf)))*(psoft(tem));

}else if (choice==7)
{
    x=mini/(mini+mcond);

    if (mini/(mini+mcond)<=0.4)
    {
      aw=1.0-0.00355*x+9.63E-5*x*x-2.97E-6*pow(x,3);
    }else if (x<=0.67)
    {
      aw=1.557-0.0199*x-1.92E-5*x*x+1.47E-6*pow(x,3);
   }
    x=mini/(mini+mcond);
    pva=aw*(exp(kelconst/(tem*rsurf)))*(psoft(tem));
}else  printf("Warning: Error in Double PP");

return pva;
}
```

```
////////////////////////////////////////////////////////////////////////
                                Heat_Source.c
////////////////////////////////////////////////////////////////////////

#include <stdio.h>
#include "udf.h"

extern double *d_heat;

DEFINE_SOURCE(heat_source, c, t ,ds, eqn)
{
    double heat_source;
    int zone_ID = THREAD_ID(t);
    heat_source=d_heat[22-zone_ID]*1E5;
    return heat_source;
}
////////////////////////////////////////////////////////////////////////
                                Mass_Source.c
////////////////////////////////////////////////////////////////////////

#include <stdio.h>
#include "udf.h"
extern double *d_mass;

DEFINE_SOURCE(mass_source, c,t,ds,eqn)
{   double mass_source;
    int zone_ID = THREAD_ID(t);
    mass_source=-d_mass[22-zone_ID]*1E5;
    return mass_source;
}
```

VITA

Name: Jun Geng

Address: Department of Nuclear Engineering
Texas A&M University
3133 TAMU
College Station, TX 77843-3133

Email Address: Jovigeng0729@hotmail.com

Education: B.S., Thermodynamic Energy Engineering,
HuaZhong University of Science and Technology,
Wuhan, China , 2002

M.S., Heat Energy Engineering,
HuaZhong University of Science and Technology,
Wuhan, China, 2005

M.S., Health Physics,
Texas A&M University,
College Station, TX USA, 2007